# ELECTROCHEMICAL ALTOMIC LAYER DEPOSITION (E-ALD) OF PHOTOVOLTAIC (PV) MATERIALS

by

BRIAN ROBERT PERDUE

(Under the advisement of John Stickney)

## ABSTRACT

This dissertation investigates the layer-by-layer deposition of CdS and CdTe, two materials used to form photovoltaics (PV) by electrochemical atomic layer deposition (E-ALD). Like atomic layer deposition (ALD) E-ALD achieves compound growth by alternating the deposition of atomic layers of each component element using surface limited reactions, however, unlike ALD, E-ALD does this in the condensed phase. The electrochemical surface limited reactions used for compound formation using E-ALD are known as underpotential deposition (UPD). In E-ALD, compounds are formed by the alternating the UPD of one element onto another element. E-ALD allows for the optimization of solution composition, pH, and deposition potential for each element used in the E-ALD cycle. In this report, 100 cycle deposits of CdTe were grown using E-ALD, which were then analyzed using electron probe microanalysis (EPMA), X-ray diffraction (XRD), spectroscopic ellipsometry (SE) and photoelectrochemistry (PEC), to ascertain film quality. Results indicate that the E-ALD grown CdTe was essentially stoichiometric, crystalline, has the proper bandgap, optical constants, has an external quantum efficiency of 10%, and is p-type, without the need of a post deposition anneal step. CdS was grown by three different condensed phase deposition techniques, chemical bath deposition (CBD), successive ionic layer absorption and reaction (SILAR), and E-ALD. Deposits were then analyzed with the same thin film characterization techniques. Analysis indicates that the deposited CdS films were stoichiometric. E-ALD and SILAR produce crystalline films, which were n-type and had the proper bandgap and optical constants. PEC results showed that E-ALD of CdS was the most photosensitive while CBD was the least, prior to a post deposition anneal.

CdS and CdTe are two II-VI compound semiconductors that form a PV ideally suited for terrestrial solar absorption. PV devices using these materials can be fabricated either using the superstrate configuration and the substrate configuration. In this study, PV devices fabricated in the superstrate configuration exhibited excessive stress between the layers and delaminated from the substrate. PV devices made in the substrate configuration produced current densities comparable to modern PV devices with 1/10th the material, however, they appeared to suffer from shunts.

INDEX WORDS: E-ALD, ALD, SOLAR, PHOTOVOLTAICS ELECTROCHEMISTRY, UPD, XRD, EPMA, CdTe, CdS, thin film, spectroscopic ellipsometry, nanofilm, photoelectrochemistry, electrochemical atomic layer deposition, underpotential deposition

# ELECTROCHEMICAL ALTOMIC LAYER DEPOSITION (E-ALD) OF PHOTOVOLTAIC (PV) MATERIALS

by

BRIAN ROBERT PERDUE

BS, University of California Santa Barbara, 2004

A Dissertation Submitted to the Graduate Facility of The University of Georgia in Partial
Fulfillment of the Requirements for the Degree

DOCTOR OF PHILOSOPHY

ATHENS GA
2013

# ELECTROCHEMICAL ALTOMIC LAYER DEPOSITION (E-ALD) OF PHOTOVOLTAIC (PV) MATERIALS

by

BRIAN ROBERT PERDUE

| | |
|---|---|
| Major Professor: | John L Stickney |
| Committee: | Richard Dluhy |
| | Gary Douberly |

Electronic Version Approved

Maureen Grasso
Dean of the Graduate School
The University of Georgia
December 2013

# DEDICATION

I would like to dedicate my work to the love of my life Stephanie Perdue for keeping me sane and grounded thought what will arguably one of be the most difficult times in our marriage, and to my mother Jan Perdue, who was always there to hold me up whenever I needed it. Without their love and support I would not have been able to do this.

# ACKNOWLEDGEMENTS

I would like to thank John Stickney for being not only a great mentor, but one of the best bosses I have ever had.  He was always there to help tutor and challenge and cultivated an excellent learning environment.  I would also like to thank the past and present members of Stickney group for their help and support through the years.

## TABLE OF CONTENTS

CHAPTER

# CHAPTER 1

# INTRODUCTION AND LITERATURE REVIEW

The photovoltaic effect was discovered in 1839 by Edmond Becquerel. After the introduction of silicon as the prime semiconductor material in the late 1950s, silicon photovoltaic (PV) diodes became available. The oil crisis of 1973 led to the public awareness of the limitation of fossil fuels, and as a result many programs were commissioned to search for alternative energy sources, including PV solar energy[1,2].

The rise of oil prices caused the reevaluation of the issues dealing with energy supply and demand. In the 20th century, the population quadrupled, causing the demand for energy to increase 16 fold. The exponential increase in energy demand is exhausting nonrenewable fossil fuel supplies. About 13 terawatts (TW)/year of energy are currently needed to sustain the present lifestyle of 6.5 billion people in the world[3].

In order to meet the increasing demand for energy in the near future, we are forced to seek environmentally clean alternatives Renewable energy can be tapped from the available resources to help combat this problem. Solar energy striking the earth (120,000 TW) stands out as the only viable means of meeting our future energy demands[3]. Covering 0.1% of the earth's surface with solar cells at 10% efficiency would satisfy our current energy needs[4].

A PV solar cell is a semiconductor diode comprised of a n-type window material and a p-type absorber material. When forming a PN junction, the initial Fermi levels of these materials are different and must equilibrate at the junction (interface). The equilibration of the two Fermi levels (or chemical potentials) occurs by transfer of electrons and holes from one semiconductor to another. The result is a depletion layer were the concentrations of majority carriers have dropped, causing the conduction and valence band edges to bend, such that a potential barrier is established against further electron transfer[5]. This potential barrier, or electric field, is also the driving force for the separation of charges which are produced by light absorption. PV absorb incoming light and convert it into electron-hole pairs. Ideally photons with an energy ($h\nu$) less than the bandgap ($E_{gap}$) will not contribute to photogeneration, whereas all photons with an energy $h\nu$ greater than $E_{gap}$ will each contribute energy equivalent to the energy $E_{gap}$ to the photogeneration of an electron-hole pair. The excess energy ($h\nu$ - $E_{gap}$) is rapidly lost as heat to the environment[1,5]. After being created, the electron-hole pairs separate, due to the internal electric field, with electrons drifting to one of the electrodes and holes drifting to the other[1,5].

PV materials are typically inorganic semiconductors, which form suitable junctions which exhibit a PV effect when exposed to light. If possible, the absorber material of an efficient single junction terrestrial thin film solar cell should be a direct bandgap semiconductor with a bandgap of about 1.5 eV (826 nm)[2,6-10], with a high solar optical absorption and quantum efficiency. In the simplest case, a pure elemental PV would be desirable because pure elements are easier to work with than compounds, for example Si PV. However there are no elemental semiconductors with a direct bandgap close to 1.5 eV. Silicon is an indirect band gap material with a bandgap of 1.1 eV. However, silicon is presently the most important PV material, despite its drawbacks.

When multiple elements are considered, a wide array of possibilities are present. There are many two element (binary), three element (ternary), and even four element (quaternary) systems to consider. The most important binary systems are presently the III-V and II-VI compounds. Examples of binary compounds include GaAs (III-V), InP (III-V), CdTe (II-VI) and

CdS (II-VI) and $Cu_2S$. $Cu_2S$ is not a III-VI or II-VI compound, but rather a chalcocite compound. $CuInSe_2$ (CIS) and $Cu(In_{1-x}Ga_x)Se_2$ (CIGS) are both I-III-VI chalcopyright compounds with CIS being a ternary compound and CIGS being quaternary compound. All of the above mentioned compounds (excluding CdS) are possible candidates for PV because they have band gap energies near the optimal 1.5 eV, and thus have a theoretical efficiency limit of 30% [1,2,6,8,10].

CdTe ($E_{gap}$ =1.5 eV) and CdS ($E_{gap}$ =2.4 eV) are II-VI compound semiconductors of opposite type and form a diode heterojunction PV. II-VI compounds are typically direct gap semiconductors with sharp optical absorption edges and large absorption coefficients at wavelengths above the bandgap. Because of their large absorption coefficients, a II-VI semiconductor of about 1 μm thickness can absorb close to 99% of the impinging radiation with energies in excess of the bandgap[6,9], allowing the formation of thin film PV, relative to say the indirect band gap material Si, which requires 10 mm because of its much lower absorption coefficient. CdTe is used as a p-type absorber, while CdS is used as an n-type window. The radiation is incident on the surface of the window, generating electron hole pairs, or excitons, in the CdTe absorber[1,2,6-10]. The primary function of the CdS window is to form a junction with the CdTe absorber layer while admitting a maximum amount of light to the junction region and absorber layer. Ideally no photocurrent generation occurs in the window layer however it is a possibility. Between CdTe ⟨111⟩ and CdS ⟨001⟩, the hexagonal faces, the lattice mismatch is 9.7%.[6,10] In spite of that large lattice mismatch, CdS remains a good heterojunction partner for CdTe, possibly because in high-efficiency devices the lattice mismatch is reduced by forming an interfacial $CdS_{1-x}Te_x$ alloy layer, and because the role of the lattice mismatch in a submicrometer-grained polycrystalline films is not as significant[10]. Device quality polycrystalline films of II-VI compounds can be prepared from inexpensive raw materials by a number of low-cost methods[2,7-10]. They are well-suited for thin film solar cells and provide an economically viable approach to the terrestrial utilization of solar energy.

Spray pyrolysis is a technique well-suited for large scale applications, where a precursor solution is pulverized by means of a neutral gas (e.g. nitrogen) so that it arrives at the substrate in the form of very fine droplets. The constituents react forming the compound on the substrate. The reactants are selected such that the products, other than the desired compound, are volatile at the temperature of deposition[11]. Devices fabricated by this method have shown efficiencies in the range of 8-10.5%[12]. This deposition method is simple, low cost, and results in comparatively large polycrystalline grained films, that do not require post-deposition annealing[6,9,11,12].

Magnetron sputtering is a popular technique for II-VI compound deposition, popular because the plasma can be sustained at much lower pressures and/or higher current densities than a glow discharge without magnetic assistance[13]. PV fabricated with this method have reached efficiencies of 14%[14]. This method is useful because it involves a low substrate temperatures, high deposition rate, is relatively cheap and is applicable to the formation of large deposit areas[13,14].

In Close-Spaced Sublimation (CSS) both CdS and CdTe are sublimed from a solid source. Film deposition using CSS is based on the reversible deposition of these elements at high temperatures in an inert gas at a pressure of 1-100 mbar. The source dissociates into its elements, which recombine on the substrate surface, forming CdS or CdTe films. Since the rate of sublimation depends strongly on the source temperature and the gas pressure in the reaction tube, the rate of deposition varies similarly. The most critical CSS process parameters for the deposition of the film are the substrate/source temperature and the ambient conditions[6,9,15-17]. CSS seems to be the method of choice when fabricating CdS-CdTe solar cells[1,2,6-10]. PV made by this method generally reach efficiencies of >8%[16], though they can reach efficiencies of 16% or higher[2,6,17].

In molecular beam epitaxy (MBE) atomic or molecular beams are generated from Knudsen effusion cells and are directed toward a heated substrate under ultrahigh vacuum conditions. When the conditions are right, growth of a single crystal epitaxial film on the substrate can be achieved[18]. Cells fabricated from this method can achieve efficiencies greater than 10%[19]. MBE was used to form the highest efficiency triple junction solar cell on record for NASA[8]. Despite its ability to produce high quality crystalline deposits, is suffers from high production costs and the inability to scale up.

Metalorganic vapor phase epitaxy (MOVPE) is a very complex procedure which includes thermodynamic, hydrodynamic, and kinetic control of reactions from the gas phase on a surface[20]. This process can result in the formation of atomically controlled surfaces and epitaxial growth. This process results in the elimination of pinholes, and conformal coating as well as thickness uniformity and homogeneity [21]. Efficiencies for cells fabricated from this method range from 4% to 11.8%[9,22]. The main benefits of this technique are conformal growth and the elimination of pinholes, however the deposition methodology is very complex and uses high temperatures so the substrates which can be used are limited.

Atomic layer deposition (ALD) is another technique that allows for uniform conformal deposition. Suntola developed a technique called atomic layer epitaxy (ALE)[21] which is the forefather to most gas based ALD techniques. ALD techniques are high temperature gas phase deposition processes in which gaseous precursors are introduced to a heated substrate and the desired compound is grown one atomic layer at a time. The technique uses a series of surface limited reactions for which deposition is limited to the top layer of a surface and stops once the surface is covered, resulting in formation of an atomic layer. An atomic layer is defined as a monolayer (ML) or less that is no more than one atom thick. A ML, which is a unit of coverage, is defined as one adsorbate per substrate surface atom. This process is driven by the stability gained by forming a compound compared to the element alone. Excess element is sublimed off the surface because it is not stabilized by compound formation. Once the process is complete for one element a different element is introduced into the chamber and the process repeats. Upon completion of an ALD cycle, the deposition of one compound bilayer has been performed.

The techniques discussed above have a few drawbacks. Spray pyrolysis, CSS, and sputtering are all line of sight deposition techniques. Line of sight suffer from two fundamental flaws, they cannot conformally coat surfaces and are prone to pinholes[22]. Other drawbacks that are the use of high temperatures and vacuum. This is a problem for two reasons, the first is that it increases the average cost of production of the compounds and the second is that high temperatures can cause the interdiffusion between the layers of the PV, causing decreased performance. Increased temperatures are also not compatible with flexible substrates. Deposition of these materials in a condensed phase eliminates these problems, by removing vacuum and operating at room temperature[23].

CBD or solution growth of CdS is very popular because it is a low-cost simple technique for achieving good quality CdS films, suitable for obtaining high efficiency CdTe/CdS based solar cells [1,2,6-10]. In CBD, CdS films can be prepared by exploiting the decomposition of thiourea in an alkaline solution of a cadmium salt. This implies that the growth of CdS films can occur either by ion-by-ion condensation of $Cd^{2+}$ and $S^{2-}$ ions on the surface of the substrate or by adsorption of colloidal particles of CdS[6]. This method has been highly developed and studied[24-27] and is used in conjunction with other deposition techniques[12,14-17,22,28].

Electrodeposition holds promise as a low cost, flexible room temperature technique for the production of II-VI compound semiconductors. CdTe can be electrodeposited on to the CdS layer in an aqueous bath of $CdSO_4$ and $TeO_2$ (the Te concentration usually being much lower). This process was developed by Kroger[29,30] in the 1970s and has since been extensively studied[31-35]. The critical variables for this deposition method are the electroactive salts used, their concentration, the design of the deposition system, the solution temperature and the flow geometry. In order to produce high photoelectronic quality films, a thermal annealing at high temperature for several minutes is needed. Even though electrodeposition uses relatively cheap equipment the low deposition rate and the health hazards of the toxic components used are aspects that do not correspond to the industrial criteria for large area production[6]. Despite its drawbacks this method affords conformal uniform growth with the elimination of pinholes. Efficiencies for this method range from 10-14%[6,28].

Electrochemical atomic layer deposition (E-ALD) was pioneered by this group and is a form of condensed phase ALD or ALE[23,36]. This technique is being developed to improve electrodeposit morphology, crystallinity and stoichiometry and prevent 3D growth. As with ALD, E-ALD uses surfaces limited reactions to grow compounds one atomic layer at a time. Electrochemical surface limited reactions are known as underpotential deposition (UPD). In UPD, one element can deposit onto a second at a potential prior to its formal reduction potential. This occurs because it is more thermodynamically stable to deposit onto another element than it is to deposit onto itself. In a typical E-ALD cycle, a solution containing a reactant's electrochemical precursor is introduced to the substrate at a UPD potential. After the reaction is completed the solution is rinsed away using a blank solution, and a new solution containing a precursor for the next element is introduced at its UPD potential. After the reaction is complete, and the solution is rinsed from the cell, one cycle has been completed resulting in the formation of one compound bilayer. The thickness of the deposited is determined by the number of E-ALD cycles performed. This layer by layer Frank-van der Merwe growth affords superior control over thickness, homogeneity, crystallinity, and the overall quality of the deposit.

. This dissertation involves the growth and characterization of CdS and CdTe thin films and the fabrication of CdS/CdTe photovoltaic. In these studies the films were grown using an automated flow cell system using a three electrode cell using a Ag/AgCl reference electrode controlled by a potentiostat. The basic setup for this procedure has the bottles containing the precursor solutions incased in a box so that the solution and the box can be purged of oxygen by nitrogen bubbling, with the $N_2$ box helping minimizing $O_2$ in the system. These bottles are hooked up to a valve block, with its outlet connected to the electrochemical flow cell. The outlet of the cell is attached to a peristaltic pump, which facilitates sucking solutions through the cell. The potentiostat, valves and the pump are controlled by a PC running SEQUENCER 4 software (Electrochemical ALD L.C., Athens GA). More details can be found on this flow cell in following publications[37-41].

Chapter 2 of this dissertation presents the optimization of the E-ALD deposition of CdTe for use in PV devices. Deposits of 100 E-ALD cycles were grown with three different deposition chemistries, acidic Te, basic Te, and with and without stripping. These films were then analyzed with a variety of thin film characterization techniques including electron probe microanalysis (EPMA) X-ray diffraction (XRD) spectroscopic ellipsometry (SE) and photoelectrochemistry (PEC) to probe various aspects of the films. The deposited films are stoichiometric, crystalline, have the proper bandgap, optical constants, as well as p-type conductivity without the need of a post deposition anneal step. The growth rate of the film can be adjusted by altering the Te deposition potential, and the film thickness increases as a function of the number of cycles run constant with layer-by-layer Frank van der Merwe type growth.

Chapter 3 of this dissertation outlines the work done on a comparison of CdS grown by three different methods. CdS was synthesized by E-ALD, successive ionic layer absorption and reaction (SILAR), and CBD. In the SLIAR deposition process, ions of one element are introduced to a substrate and adsorb onto the surface of the substrate, the excess ions are rinsed away. Then ions of the next element are introduced to the cell, these ions react with the adsorbed layer precipitating the desired compound, finally the remaining ions are rinsed away. The CBD of CdS is based on the thermal decomposition of thiourea to free sulfide and the subsequent reaction with Cd ions. Thin films of CdS were fabricated with each condensed phase deposition technique and analyzed with EPMA, XRD, SE, and PEC. CdS films produced by each deposition technique were essentially stoichiometric, SILAR and ALD produced crystalline deposits while CBD did not. All deposition techniques produced n-type conductivity, however, E-ALD CdS was the most photosensitive and CBD CdS was the least. Based on this work it is inferred that SILAR and E-ALD produce almost identical deposits.

Chapter 4 of this dissertation involves the fabrication and testing of E-ALD PV devices. PV were fabricated in the substrate and superstrate configurations. When devices were fabricated in the superstrate configuration, devices were delaminated from the glass most likely do to strain across the CdS/CdTe layers. PV fabricated in the substrate configuration with Au on glass serving as the back contact had 200 nm (~600cycles) of E-ALD grown CdTe, 80 nm of CBD grown CdS, and 100 nm magnetron sputtered ITO to serve as to front contact. Cells achieve a maximum current density of 0.65 mA/cm2 when exposed to AM1.5 light; however, appear to suffer from shunts. Work on these defects is underway

Chapter 5 of this dissertation is related to Chapter 2 in that it used the optimized E-ALD CdTe chemistries on Au to investigate the compatibilities of other substrates. The scope of this work was to investigate the influence substrate chemistry plays on the deposition process. The substrates used in this study were Au, Ni, Cu, Ag, Ge, and Mo, as was the case in Chapter 2 100 cycle deposits of E-ALD CdTe were grown onto each substrate and analyzed with EPMA, XRD and SE. Results indicate that substrates that can oxidatively dissolve and produce ions (Ni Cu Ag) hinder the E-ALD deposition process and decrease the quality of the film grown. It is proposed that competing compound formation reactions can occur when ions produced by the oxidative dissolution of the substrate are present with the E-ALD solution. These reactions could potentially short circuit the E-ALD process in the early cycles. Substrates that did not produce ions (Au Ge Mo) did not seem to affect the process and grew CdTe films of good quality, however, a surface pretreatment was required in some cases for successful electrodeposition.

Finally Chapters 6, 7 and 8 involve work unrelated to PV formation rather examine different applications of E-ALD. Chapter 6 investigates the possibility of utilizing lithography patterned nanowire electrodeposition (LPNE) as a means to fabricate high quality CdTe nanowires. LPNE is a 7 step process that allows for the low cost fabrication of nanowires and structures which involves electrodeposition of the desired material onto a sacrificial metal trench electrode shielded by photoresist. E-ALD LPNE nanowires were fabricated and examined with scanning electron microscopy (SEM) and atomic force microscopy (AFM). The nanowire produced were an order of magnitude too large. We suspect that the cause for this was insufficient rinsing under the trench. E-ALD was able to conformally coat Au LPNE nanowires with CdTe.

Chapter 7 is a reevaluation of previous work done by this group. Germanene a 2D allotrope of germanium (similar to graphene) was possibly formed by E-ALD. The Ge work done by this group was reinvestigated assuming that germanene was being formed rather than germanium. Films were probed with micro-Raman and scanning tunneling microscopy (STM). STM images show a large atomically flat terrace with a Moiré pattern. Bond distances calculated from these images suggest the presence of an adsorbed germanene monolayer. Micro-Raman analysis shows a strong Raman shift consistent with Raman shifts predicted by *Ab Initio* calculations.

Chapter 8 is the proof of concept work in the formation of $Cu_2Se$ by electrochemical pulse deposition. Results show that $Cu_{2.1}Se$ is the predominate species formed despite the sequence used. The slight Cu excess is most likely due to the excess of $Cu^{2+}$ ions created at the surface of the electrode during the anodic pulse which do not have time to completely diffuse away. XRD results indicate crystalline $Cu_2Se$ with a preferred (111) orientation. Excess selenium observed with the optical microscope is confirmed with XRD as well. SE results show an index of refraction of 1.9 as well as an average growth rate of 0.2mL per pulse and a direct bandgap of 1.7eV. The process appears to grow linearly with pulse number

# References

(1) Shah, A.; Torres, P.; Tscharner, R.; Wyrsch, N.; Keppner, H. *Science* **1999**, *285*, 692.

(2) Birkmire, R. W.; Eser, E. *Annual Review of Materials Science* **1997**, *27*, 625.

(3) Kamat, P. V. *Journal of Physical Chemistry C* **2007**, *111*, 2834.

(4) Yu, K. H.; Chen, J. H. *Nanoscale Res. Lett.* **2009**, *4*, 1.

(5) Nozik, A. J. *Annu. Rev. Phys. Chem.* **1978**, *29*, 189.

(6) Bosio, A.; Romeo, N.; Mazzamuto, S.; Canevari, V. *Progress in Crystal Growth and Characterization of Materials* **2006**, *52*, 247.

(7) Omura, K.; Hanahusa, A.; Arita, T.; Higuchi, H.; Aramoto, T.; Nishio, T.; Sibutani, S.; Kumazawa, S.; Murozono, M.; Yabuuchi, Y.; Takakura, H. *Renewable Energy* **1996**, *8*, 405.

(8) Kazmerski, L. L. *Journal of Electron Spectroscopy and Related Phenomena* **2006**, *150*, 105.

(9) Chu, T. L.; Chu, S. S. *Solid-State Electronics* **1995**, *38*, 533.

(10) Chopra, K. L.; Paulson, P. D.; Dutta, V. *Progress in Photovoltaics* **2004**, *12*, 69.

(11) Patil, P. S. *Materials Chemistry and Physics* **1999**, *59*, 185.

(12) Sharma, R. K.; Jain, K.; Rastogi, A. C. *Current Applied Physics* **2003**, *3*, 199.

(13) Ellmer, K. *J. Phys. D-Appl. Phys.* **2000**, *33*, R17.

(14) Compaan, A. D.; Gupta, A.; Lee, S.; Wang, S.; Drayton, J. *Solar Energy* **2004**, *77*, 815.

(15) Dhere, R. G.; Al-Jassim, M. M.; Yan, Y.; Jones, K. M.; Moutinho, H. R.; Gessert, T. A.; Sheldon, P.; Kazmerski, L. L. *J. Vac. Sci. Technol. A-Vac. Surf. Films* **2000**, *18*, 1604.

(16) Paulson, P. D.; Dutta, V. *Thin Solid Films* **2000**, *370*, 299.

(17) Britt, J.; Ferekides, C. *Appl. Phys. Lett.* **1993**, *62*, 2851.

(18) Joyce, B. A. *Contemporary Physics* **1991**, *32*, 21.

(19) Ringel, S. A.; Smith, A. W.; Macdougal, M. H.; Rohatgi, A. *J. Appl. Phys.* **1991**, *70*, 881.

(20) Stringfellow, G. B. *Materials Science and Engineering B* **2001**, *87*, 97.

(21) Suntola, T. *Thin Solid Films* **1992**, *216*, 84.

(22) Jones, E. W.; Barrioz, V.; Irvine, S. J. C.; Lamb, D. *Thin Solid Films* **2009**, *517*, 2226.

(23) Gregory, B. W.; Stickney, J. L. *Journal of Electroanalytical Chemistry* **1991**, *300*, 543.

(24) Mane, R. S.; Lokhande, C. D. *Materials Chemistry and Physics* **2000**, *65*, 1.

(25) Calixto, M. E.; Tufiño-Velázquez, M.; Contreras-Puente, G.; Vigil-Galán, O.; Jiménez-Escamilla, M.; Mendoza-Perez, R.; Sastré-Hernández, J.; Morales-Acevedo, A. *Thin Solid Films* **2008**, *516*, 7004.

(26) Lincot, D.; Borges, R. O. *Journal of the Electrochemical Society* **1992**, *139*, 1880.

(27) Ortegaborges, R.; Lincot, D. *Journal of the Electrochemical Society* **1993**, *140*, 3464.

(28) Rakhshani, A. E. *J. Appl. Phys.* **2001**, *90*, 4265.

(29) Kroger, F. A. *Journal of the Electrochemical Society* **1978**, *125*, 2028.

(30) Panicker, M. P. R.; Knaster, M.; Kroger, F. A. *Journal of the Electrochemical Society* **1978**, *125*, 566.

(31) Kampmann, A.; Cowache, P.; Vedel, J.; Lincot, D. *Journal of Electroanalytical Chemistry* **1995**, *387*, 53.

(32) Kampmann, A.; Lincot, D. *Journal of Electroanalytical Chemistry* **1996**, *418*, 73.

(33) Lepiller, C.; Lincot, D. *Journal of the Electrochemical Society* **2004**, *151*, C348.

(34) Lincot, D. *Thin Solid Films* **2005**, *487*, 40.

(35) Josell, D.; Beauchamp, C. R.; Jung, S.; Hamadani, B. H.; Motayed, A.; Richter, L. J.; Williams, M.; Bonevich, J. E.; Shapiro, A.; Zhitenev, N.; Moffat, T. P. *Journal of the Electrochemical Society* **2009**, *156*, H654.

(36) Gregory, B. W.; Suggs, D. W.; Stickney, J. L. *Journal of the Electrochemical Society* **1991**, *138*, 1279.

(37) Colletti, L. P.; Flowers, B. H.; Stickney, J. L. *Journal of the Electrochemical Society* **1998**, *145*, 1442.

(38) Colletti, L. P.; Stickney, J. L. *Journal of the Electrochemical Society* **1998**, *145*, 3594.

(39) Flowers, B. H.; Wade, T. L.; Garvey, J. W.; Lay, M.; Happek, U.; Stickney, J. L. *Journal of Electroanalytical Chemistry* **2002**, *524-525*, 273.

(40) Huang, B. M.; Colletti, L. P.; Gregory, B. W.; Anderson, J. L.; Stickney, J. L. *Journal of the Electrochemical Society* **1995**, *142*, 3007.

(41) Lay, M. D.; Stickney, J. L. *Journal of the Electrochemical Society* **2004**, *151*, C431.

# CHAPTER 2

# LOW COST HIGH QUALIT GROWTH OF CDTE USING ELECTROCHEMICAL ATOMIC LAYER DEPOSITION (E-ALD) FOR USE IN PHOTOVOLTAICS[1]

---

[1] B. Perdue, J Czerniawski, M. Stickney, J. L. Stickney, To be submitted to *Journal of the Electrochemical Society*

# Abstract

The E-ALD growth CdTe by different as a function of the Te solution chemistry is discussed. Like atomic layer deposition (ALD), E-ALD involves the growth of compounds one atomic layer at a time using surface limited reactions. However, in E-ALD the reactions are carried out in the condensed phase (aqueous solutions) rather than the gas phase. Electrochemical surface limited reactions are generally referred to as under potential deposition (UPD). In E-ALD, compounds are formed by alternating the UPD of one element onto another element. CdTe deposits formed using 100 E-ALD cycles were examined, using an acidic Te solution, a basic Te solution, and with and without a Te reductive stripping step. The resulting films were examined using various thin film characterization techniques including electron probe microanalysis (EPMA), X-ray diffraction (XRD), spectroscopic ellipsometry (SE), and photoelectrochemistry (PEC). EPMA results indicated that the E-ALD CdTe was stoichiometric within the uncertainty of the instrument, for all deposition chemistries. XRD results show that E-ALD grown CdTe has a strong (111) preferred orientation and deposits epitaxially onto an Au(111) single crystal substrate. SE results showed that E-ALD CdTe had an index of refraction of 2.98 and that the growth rate could be adjusted using the Te deposition potential. Both EPMA and SE show that the growth of E-ALD CdTe was linear, with the number of cycles run, consistent with a Frank-van der Merwe layer-by-layer growth mode. PEC results indicated that the 100 cycle E-ALD grown CdTe deposits (40 nm thick) were p-type, has an external quantum efficiency of 10% and had a direct bandgap of 1.5 eV. That is, E-ALD is capable of growing high quality deposits without the need of a post deposition anneal step.

# Introduction

Cadmium Telluride CdTe is a versatile II-IV compound which has uses in many different optoelectronic fields[1]. One of the applications where CdTe excels is as a terrestrial solar absorber. CdTe is a direct gap semiconductor with a sharp optical absorption edge and large absorption coefficient at above bandgap wavelengths[2]. As a result about 1 μm of CdTe is sufficient to absorb 99% of the impinging radiation with photon energy higher than the bandgap energy[2,3]. The bandgap of CdTe is 1.5eV which is ideally for a single junction photovoltaic for terrestrial absorption, allowing 95% conversion of the theoretical maximum[4,5]. CdTe is not without issues. Cd is toxic and both Cd and Te are not earth abundant, so it is imperative that the amount used in photovoltaics (PV) be minimized.

CdTe based PV devices are what are known as second generation or thin film based PV[6]. Thin film based PV also include other chalcogenide based absorbers such as $CuInSe_2$ (CIS) and $Cu(InGa)Se_2$ (CIGS). There are several reviews outlining the development of second generation or thin film based PV[2,3,7-9]. In recent years there have been new developments in the field of PV and it is entering what is being called the third generation. Some of the strategies employed in the 3rd generation are the use of nanostructures and nanomaterials. Different strategies and materials are discussed in the following works[10-13]. An offshoot of that work is the addition of plasmonics to photovoltaics[14,15]. All of these strategies involve the reduction of cost via the use of less material and increased performance due to advanced nanostructures. Using less material is an important strategy when considering toxic and non-earth abundant elements such as Cd and Te.

Execution of these strategies poses a unique set of problems. Line of sight deposition techniques such as close-space sublimation (CSS) and chemical vapor deposition (CVD) may have trouble conformally coating the nanostructures. Thus a deposition technique is needed which can provide uniform conformal deposition. One such technique was developed by Suntola called atomic layer epitaxy (ALE)[16]. ALE is the forefather to most gas based atomic layer deposition (ALD) techniques. ALD techniques are high temperature gas phase deposition processes in which gaseous precursors are introduced to a heated substrate and the desired compound is grown one atomic layer at a time. The technique uses a series of surface limited reactions which results in the deposition of an atomic layer. A surface limited reaction is a reaction which self terminates after the substrate atoms have been covered by the depositing atoms. The result of this process is an atomic layer. This process is driven by the stability gained by forming a compound compared to the element alone. Excess element is sublimed off the surface because it is not stabilized by compound formation. Once the process is complete for one element the next element is introduced into the chamber and the process repeats, completing one ALD cycle of deposition, and formation of a compound bilayer.

Electrodeposition is technique which allows for uniform conformal deposits. Electrodeposition holds promise as a low cost, flexible room temperature technique for the production compound semiconductors. This technique has been applied to many II-IV compounds as well as CIS and CIGS[1,17]. A process was developed by Kroger[18] and Panicker[19] in which near stoichiometric CdTe was reductively deposited from on bath containing precursors for both Cd and Te. This process showed such promise that is was eventually commercialized by BP[20]. Unfortunately deposits fabricated by this method require annealing to produce PV grade material due to its poor crystallinity and to cover it from n-type, as deposited, to p-type as used in PV.

Electrochemical atomic layer deposition (E-ALD) was pioneered by this group and is a form of condensed phase ALD or ALE[21,22]. This technique is being developed to improve electrodeposit morphology, crystallinity and stoichiometry and prevent 3D growth. As with ALD, E-ALD uses surfaces limited reactions to grow compounds one atomic layer at a time. Electrochemical surfaces limited reactions are known as underpotential deposition (UPD). In UPD, and one element can deposit onto a second at a potential prior to its formal reduction potential. This occurs because it is more thermodynamically stable to deposit onto another element than it is to deposit onto itself. In a typical E-ALD cycle, a solution containing a reactant's electrochemical precursor is introduced to the substrate at a UPD potential. After the reaction is completed the solution is rinsed away using a blank solution, and a new solution containing a precursor for the next element is introduced at its UPD potential. After the reaction is complete, and the solution is rinsed from the cell, one cycle has been completed resulting in the formation of one compound bilayer. The thickness of the deposited is determined by the number of E-ALD cycles performed. This layer-by-layer Frank-van der Merwe growth affords superior control over thickness, homogeneity, crystallinity, and the overall quality of the deposit. E-ALD deposition of CdTe has been studied by this group[22-31] and Foresti[32] so much is known about this system. The goal of this work is to optimize the E-ALD cycle chemistry of the deposition of CdTe, for use in PV. The CdTe deposits will be analyzed with a primary emphasis on their optical properties, film morphology and crystallinity.

## Experimental

In these studies the films were grown using an automated flow cell system using a three electrode cell using a Ag/AgCl reference electrode controlled by a potentiostat. The basic setup for this procedure has the bottles containing the precursor solutions incased in a box so that the solution and the box can be purged of oxygen by nitrogen bubbling, with the $N_2$ box helping minimizing $O_2$ in the system. These bottles are hooked up to a valve block, with its outlet connected to the electrochemical flow cell. The outlet of the cell is attached to a peristaltic pump, which facilitates sucking solutions through the cell. The potentiostat, valves and the pump are controlled by a PC running SEQUENCER 4 software (Electrochemical ALD L.C., Athens GA). More details on the flow cell can be found in previous publications[23-26,28]. The electrodes used in these studies were polycrystalline Au on glass, with a 50 nm Ti adhesion layer, purchased from Evaporated Metal Films.

Cd was electrodeposited from a solution containing 0.5 mM $CdSO_4$ in 0.5 M $NaClO_4$, pH 3. Te was electrodeposited from one of two solutions. The first being 0.1mM $TeO_2$ in 0.5 M $NaClO_4$, pH 3, or 0.1 mM $TeO_2$ in 0.5M $NaClO_4$ buffered with 50 mM sodium borate pH 9. Due to the limited solubility of $TeO_2$ in water, it needs to be first dissolved in concentrated $H_2SO_4$ or NaOH, before diluting to the final volume and pH. The blank consisted of 0.5 M $NaClO_4$, pH 3 and its purpose was to rinse out the cell of any precursors from previous solutions. All solutions were made with 18 MΩ water supplied from a Millipore water flirtation system. The electrochemical precursors were purchased from Alfa Æsar with a purity of 99.999%

Three different cycles were examined in this work: one using an acidic Te solution, one using an acidic Te solution together with a reductive Te stripping step, and one using a basic Te solution, no stripping step. A visual representation of a typical E-ALD cycle can be found in Figure 2.1. For the E-ALD deposition of CdTe with acidic Te chemistry, the cycle can be broken down into 2 steps. The first step involved $Cd^{2+}$ ions being pumped into the cell at 18 $\frac{mL}{min}$ for 5 seconds at a potential of -550mV. That was followed by holding the solution without flowing for 15 seconds of deposition, at the same potential, and allowing the system to come to equilibrium. The $Cd^{2+}$ ions were then rinsed from the cell with the blank solution for 15 seconds, concluding Cd deposition. For the Te step, a solution of $HTeO_2^+$ ions are pumped into the cell for 5 seconds at a potential of -200mV. This is followed by a quiescent deposition for 15 seconds, at the same potential. The $HTeO_2^+$ ions are then rinsed from the cell, using the blank solution, for 15 seconds, completing this E-ALD cycle for CdTe. Upon completion of an E-ALD cycle, approximately one compound bilayer of CdTe should have been electrodeposited. Some minor variations to this cycle are made, depending on the Te chemistry used. If a stripping steps is included at the end of the cycle, the Te deposition was shifted 100 mV more negative. The stripping step involves first rinsing with blank and then stepping the potential to -900mV for 15 seconds, where Te atoms in excess of an atomic layer are reduced to a soluble telluride species, which diffuse away. This is followed by rinsing again with blank for 15 seconds at the same potential to remove the telluride products. When using the basic Te chemistry the only difference is that the Te deposition potentials changes to -800 mV.

100 E-ALD cycle deposits were performed using the three different deposition chemistries, and the resulting deposits were analyzed using a variety of thin film characterization techniques. The stoichiometry of the deposits were investigated using EPMA on a JEOL 8600 SUPERPROBE with a 10 KeV accelerating voltage 15 nA beam current and a 10 um beam diameter. Using the large beam helped to average slight sample inhomogeneities. Deposit crystallinity was examined on a PANanalytical X'PERT Pro with an open eulerian cradle utilizing a 1.54 nm Cu $K\alpha_1$ source and a parallel plate collimator. When preforming grazing incidence scans the x-ray tube was in line focus and used a Göbel mirror. Texture measurements were made with the X-ray tube in point focus with a polycapillary lens. Optical properties of the deposits were analyzed using a spectroscopic ellipsometer (SE), JA Woolam M-2000V.

Photoelectrochemical measurements were performed based on methodologies described by Lincot[33,34] et al.. The liquid electrolyte used was 0.1M acetic acid, 0.1M sodium acetate and 0.2 M $Na_2SO_3$, pH 4.6.

## Results and Discussion

The UPD behavior of Cd and Te have been studied by is group[21-31,35,36]. Cd UPD can occurs reductively from $Cd^{2+}$ ions, resulting in a coverage of between 0.3 and 1 monolayers (ML). A monolayer is defined in this report relative to the number of surface atom in the substrate. Assuming the Au on glass substrates resemble a Au(111) surface, that would be about $1.35 \times 10^{15}$ atom/$cm^2$. As the potential approaches the $E^{o\prime}$ for bulk Cd deposition, Cd can create a surface alloy with the underlying Au substrate. Due to reactive nature of Cd it is unstable at more positive potentials which presents a challenge when trying to deposit more noble elements onto it. Formation of Te monolayers onto Cd can be done in a few different ways. The first is to exploit the irreversibility of Te. Te has very slow deposition kinetics, as a result, all features observed in Te cyclic voltammetry are seen at overpotentials. When constructing an E-ALD cycle the proper overpotetial and deposition time must be chosen to obtain the desired atomic layer. This Te overpotential must also be at a potential which the Cd atomic layer will be stable and not oxidatively dissolve. Another strategy for depositing a Te monolayer is to deposit bulk Te then reductively strip the bulk Te to $Te^{2-}$, which is a water soluble species that diffuses away, leaving behind a Te monolayer that has been stabilized by compound formation. This method is desirable because a Te deposition potential can be chosen such that the Cd monolayer is stable and the bulk Te can be removed afterwards. The drawback to this methodology is that it results in increased cycle times due to the fact that 2 extra steps in the cycle must be added. The final method is to change the Te solution chemistry. The $E^{o\prime}$for Te deposition shifts more negative as the pH increases[28]. This occurs because $H^+$ ions are involved in the electrodeposition of $HTeO_2^+$. The shifting of the reduction potential of Te to more negative potentials allows for better overlap between the Cd deposition potential and the Te deposition potential. E-ALD CdTe deposits of 100 cycles were grown using the three different deposition chemistries and used for analysis. The deposits were approximately 1.82 $cm^2$ in size.

The stoichiometry of the resulting deposits made from the different deposition chemistries were evaluated with EPMA. EPMA has two distinct advantages over energy dispersive x-ray spectrometry (EDX), the first is that is more quantitative and the second is that it is more sensitive. The stoichiometry was measured in 5 spots in various positions across the deposits. This was done to probe the uniformity of the deposit. Results from EPMA are shown in Table 2.1. The Cd/Te ratios for each of the deposits are 1.02, 1.02 and 0.98 for the acidic Te chemistry, stripping chemistry, and basic Te chemistry. This suggests that deposits produced by E-ALD are stoichiometric. To investigate this further a single crystal of CdTe purchased and was used as an internal standard to develop a better understanding of the instrument variability. The CdTe single crystal results show that with a similar sample size $\eta$=5, the standard deviation of the CdTe single crystal is on the same order of magnitude as the standard deviation obtained by E-ALD deposits. This implies that the CdTe deposits produced by E-ALD appear stoichiometric within the variability of the instrument.

The crystallinity of the deposits was analyzed using grazing incidence XRD. A typical XRD spectrum of a CdTe deposit made by any of the deposition chemistries can be shown in Figure 2.2. The substrate was a polycrystalline Au on glass as such the three major reflections of the Au low index plane are expected. There are minor peaks occurring at 2θ positions 38.1° and 44.4° these in junction with the major peak at 64.5° account for the Au (111), (200), and (220) reflections according to card number 04-0784. The major peak at 2θ of 23.7° as well as the minor peaks at 39.3° and 46.2° can be assigned to CdTe (111),(220) and (311) according to card number 12-0770 for cubic $F\bar{4}3m$ CdTe. The spectrum in Figure 2.2 shows two important pieces of information, the first being that without annealing, E-ALD grown CdTe has a strong preferred (111) orientation consistent with the literature[1,21-31,33-38], and the second is that the CdTe film prefers hexagonal growth despite the crystallinity of the substrate. It is important to note that bulk crystallinity of the Au electrode may not reflect the structure at the surface of the electrode. That is to say that the gold electrode may have a (110) crystal but (111) planes are exposed at the surface of the electrode.

XRD Pole figures were collected in order to investigate the orientation of the CdTe film with respect to a Au(111) single crystal . An initial θ-θ was collected to determine the optimal geometry for the CdTe film as well as the Au substrate then pole figures were collected. The pole figures for Au and CdTe are represented in Figure 2.3. The Au (111) substrate pole figure is depicted in Figure 2.3 a). It has a series of three reflections at a ψ of 70° which is the reflection off of the $(\bar{1}11), (1\bar{1}1)$ and $(11\bar{1})$ planes. Figure 2.3 b) is the pole figure for the E-ALD CdTe. This shows a series of 6 major reflections each three fold symmetric consistent with a (111) single crystal. The outer most reflections in Figure 2.3 b) (ψ of 70°) are superimposable with the Au peaks in Figure 2.3a). This is an indication that the (111) crystal planes in the CdTe film have the same orientation as the underlying Au crystal. This may suggest an epitaxial deposit which is consistent with the literature[21,22,27-29,36]. The next series of major reflections occur at a ψ of 55°, the angle at which (100) planes should occur. When examining the $F\bar{4}3m$ space group the angular difference between the (111) scattering vector and the (100) is about 60° ϕ which accounts for the difference in position between the ψ 70° corresponding to the (111) reflections and the ψ 55° corresponding to the (100) reflections. These peaks suggest that CdTe may be depositing onto Au (100) step faces with (111) orientation.

Optical constants and thickness for the three different growing chemistries were measured by variable angle SE. A typical spectrum can be found in Figure 2.4. The data was collected below, at, and above the Brewster angle for Au at 682.8 nm in order to obtain the maximum amount of information about the film. The data was then fitted with the Cauchy equation which relates thickness and optical constants, two very valuable pieces of information. The index of refraction at 632.8 nm and the thickness were calculated from the model. The index of refraction for CdTe at 632.8 nm reported in the literature is 2.98[39-41], the calculated index of refraction for E-ALD CdTe was 3.02, 2.85 and 2.91 for acidic, stripping, and basic deposition chemistries showing good agreement. Growth rates can be estimated from this information as well. The XRD in Figure 2.2 indicates that E-ALD CdTe has a strong preferred (111) orientation and $F\bar{4}3m$ symetry. In this crystal structue the Cd and Te atoms are tetrahedrally bonded to one and other. Using geometry, and the CdTe lattice constant a=0.648 nm the distance between compound bilayers in the (111) direction can be calculated. With this orientation and crystal structure the calculation simplifies to finding the height of a tetrahedron. Using geometry it is found that the height of a CdTe compound bilayer in the (111) direction is equal to $\sqrt{\frac{a^2}{2}-\frac{a^2}{6}}=\frac{a}{\sqrt{3}}$. To calculate a growth rate the assumption is made that all thickness contributions will be from growth in the (111) direction. The thickness calculated from the model in Figure 2.4 was 41.7 nm so the growth rate can be estimated by $\frac{41.7\ nm}{200\ cycles*0.374\frac{ML}{cycle}}=$ $0.6\frac{ML}{cycle}$ consistent with an E-ALD process. This was investigated further by altering the Te deposition potential to show how the properties of the material grown changed. These results can be found in Figure 2.5. Figure 2.5 shows by changing the Te deposition potential the growth rate of CdTe can be altered from $0.1\frac{ML}{cycle}$ to $1.2\frac{ML}{cycle}$, however, once the growth rate is pushed outside of submonolayer growth per cycle the properties of the compound changes and begins to deviate from CdTe behavior as shown by the change in optical constant.

The suggested layer-by-layer growth mechanics of E-ALD was investigated with EPMA and SE. A series of deposits were made using the same chemistry just running a different number of cycles and the deposits were analyzed with SE and EPMA the results can be found in Figure 2.6. Figure 2.6 shows that the thickness calculated from SE as well as the Te signal from EPMA increase linearly as a function of number of cycles. This is a strong indication of layer-by-layer Frank-Van Der Merwe type growth.

Conductivity type band gap and external quantum efficiency (EQE) were measured using photoelectrochemistry. The photoelectrochemical behavior of thin films of CdTe have been previously studied by Lincot[33,34]. A typical photoelectrochemical cyclic voltammogram is shown in Figure 2.7. By forcing the semiconductor into depletion mode, the conductivity type of the semiconductor can be determined. The assumption made is that when the semiconductor is depleted of its majority carrier any current produced will be due to exciton creation[42]. By scanning the potential negative an increase in photocurrent is observed, thus the majority carriers are holes making the semiconductor p-type. This is important because most electrodeposited CdTe is n-type and type converts to p-type by annealing. E-ALD is able to produce p-type CdTe without the need of a post deposition anneal step. By poising the potential at a point where maximum photocurrent occurs, the external quantum efficiency (EQE) can be calculated. The EQE was calculated using the following formula $EQE = \frac{I_p}{I_d} * \frac{hc}{e\lambda} * SR(\lambda)$. Where $I_p$is the measured photocurrent, $I_d$is the current measured by calibrated Si detector, $h$ is planks constant,

$c$ is the speed of light in vacuum, $e$ is the fundamental charge of an electron, $\lambda$ is the wavelength, and $SR(\lambda)$ is the spectral response of the Si detector with the units of $\left(\frac{A}{W}\right)$. When this is done the maximum EQE for a thin film of CdTe is 10%. This is for a sample that is only 40 nm thick, at this efficiency a sample of about 1μm thick would absorb 95% of the light consistent with literature.

Bandgap measurements were made with both reflectance and photoelectrochemial measurements. Estimation of the band gap in semiconductors was proposed by Davis and Mott[43]. If the semiconductor has a direct band gap plotting the absorption coefficient squared vs photon energy in eV and extrapolating a line on the most linear portion of the graph to the x axis will yield an approximation of the bandgap. This measurement was done both with reflectance measurements and photoelectrochemial measurements. These results can be shown in Figure 2.8. Two orthogonal techniques both confirm that thin films of CdTe grown by E-ALD have a direct bandgap of 1.5 eV consistent with the values in the literature.

## Conclusion

CdTe deposits were grown with E-ALD. Different deposition chemistries were investigated and analyzed with various thin film techniques. EPMA results indicate that E-ALD CdTe seems stoichiometric within the uncertainty of the instrument for all deposition chemistries. XRD results show that E-ALD grown CdTe has a strong (111) preferred orientation and deposits epitaxially onto a single crystal Au substrate. SE results show that E-ALD CdTe has an index of refraction of 2.98 and the growth rate can be adjusted by adjusting the Te deposition potential. Both EPMA and Se show that the growth of E-ALD CdTe is linear with number of cycles run consistent with Frank-van der Merwe layer by layer growth. PEC results indicate that E-ALD grown CdTe is p-type, has an external quantum efficiency of 10% and has a direct bandgap of 1.5eV. In summation E-ALD is capable of growing a high quality CdTe deposit without the need of a post deposition anneal step.

# References

(1) Pauporte, T.; Lincot, D. *Electrochimica Acta* **2000**, *45*, 3345.

(2) Chu, T. L.; Chu, S. S. *Solid-State Electronics* **1995**, *38*, 533.

(3) Bosio, A.; Romeo, N.; Mazzamuto, S.; Canevari, V. *Progress in Crystal Growth and Characterization of Materials* **2006**, *52*, 247.

(4) Henry, C. H. *J. Appl. Phys.* **1980**, *51*, 4494.

(5) Shockley, W.; Queisser, H. J. *J. Appl. Phys.* **1961**, *32*, 510.

(6) Ginley, D.; Green, M. A.; Collins, R. *MRS Bull.* **2008**, *33*, 355.

(7) Birkmire, R. W.; Eser, E. *Annual Review of Materials Science* **1997**, *27*, 625.

(8) Nozik, A. J. *Nano Letters* **2010**, *10*, 2735.

(9) Shah, A.; Torres, P.; Tscharner, R.; Wyrsch, N.; Keppner, H. *Science* **1999**, *285*, 692.

(10) Kamat, P. V. *Journal of Physical Chemistry C* **2007**, *111*, 2834.

(11) Yu, K. H.; Chen, J. H. *Nanoscale Res. Lett.* **2009**, *4*, 1.

(12) Tsakalakos, L. *Materials Science & Engineering R-Reports* **2008**, *62*, 175.

(13) Cao, L. Y.; Fan, P. Y.; Vasudev, A. P.; White, J. S.; Yu, Z. F.; Cai, W. S.; Schuller, J. A.; Fan, S. H.; Brongersma, M. L. *Nano Letters* **2010**, *10*, 439.

(14) Atwater, H. A.; Polman, A. *Nat. Mater.* **2010**, *9*, 205.

(15) Ferry, V. E.; Munday, J. N.; Atwater, H. A. *Advanced Materials* **2010**, *22*, 4794.

(16) Suntola, T. *Thin Solid Films* **1992**, *216*, 84.

(17) Lincot, D. *Thin Solid Films* **2005**, *487*, 40.

(18) Kroger, F. A. *Journal of the Electrochemical Society* **1978**, *125*, 2028.

(19) Panicker, M. P. R.; Knaster, M.; Kroger, F. A. *Journal of the Electrochemical Society* **1978**, *125*, 566.

(20) Cunningham, D.; Rubcich, M.; Skinner, D. *Progress in Photovoltaics* **2002**, *10*, 159.

(21) Gregory, B. W.; Stickney, J. L. *Journal of Electroanalytical Chemistry* **1991**, *300*, 543.

(22) Gregory, B. W.; Suggs, D. W.; Stickney, J. L. *Journal of the Electrochemical Society* **1991**, *138*, 1279.

(23) Colletti, L. P.; Flowers, B. H.; Stickney, J. L. *Journal of the Electrochemical Society* **1998**, *145*, 1442.

(24) Colletti, L. P.; Stickney, J. L. *Journal of the Electrochemical Society* **1998**, *145*, 3594.

(25) Flowers, B. H.; Wade, T. L.; Garvey, J. W.; Lay, M.; Happek, U.; Stickney, J. L. *Journal of Electroanalytical Chemistry* **2002**, *524-525*, 273.

(26) Huang, B. M.; Colletti, L. P.; Gregory, B. W.; Anderson, J. L.; Stickney, J. L. *Journal of the Electrochemical Society* **1995**, *142*, 3007.

(27) Lay, M. D.; Sorenson, T. A.; Stickney, J. L. *J. Phys. Chem. B* **2003**, *107*, 10598.

(28) Lay, M. D.; Stickney, J. L. *Journal of the Electrochemical Society* **2004**, *151*, C431.

(29) Varazo, K.; Lay, M. D.; Sorenson, T. A.; Stickney, J. L. *Journal of Electroanalytical Chemistry* **2002**, *522*, 104.

(30) Venkatasamy, V.; Jayaraju, N.; Cox, S. M.; Thambidurai, C.; Happek, U.; Stickney, J. L. *J. Appl. Electrochem.* **2006**, *36*, 1223.

(31) Villegas, I.; Stickney, J. L. *Journal of the Electrochemical Society* **1991**, *138*, 1310.

(32) Forni, F.; Innocenti, M.; Pezzatini, G.; Foresti, M. L. *Electrochimica Acta* **2000**, *45*, 3225.

(33) Kampmann, A.; Cowache, P.; Vedel, J.; Lincot, D. *Journal of Electroanalytical Chemistry* **1995**, *387*, 53.

(34) Kampmann, A.; Lincot, D. *Journal of Electroanalytical Chemistry* **1996**, *418*, 73.

(35) Gregory, B. W.; Norton, M. L.; Stickney, J. L. *Journal of Electroanalytical Chemistry* **1990**, *293*, 85.

(36) Suggs, D. W.; Stickney, J. L. *Surface Science* **1993**, *290*, 375.

(37) Josell, D.; Beauchamp, C. R.; Jung, S.; Hamadani, B. H.; Motayed, A.; Richter, L. J.; Williams, M.; Bonevich, J. E.; Shapiro, A.; Zhitenev, N.; Moffat, T. P. *Journal of the Electrochemical Society* **2009**, *156*, H654.

(38) Lepiller, C.; Lincot, D. *Journal of the Electrochemical Society* **2004**, *151*, C348.

(39) Adachi, S.; Kimura, T.; Suzuki, N. *J. Appl. Phys.* **1993**, *74*, 3435.

(40) D, P. E. *Handbook of Optical Constants of Solids*; Academic Press: Orlando, 1985.

(41) D, P. E. *Handbook of Optical Constants of Solids II*; Academic Press: Academic Press, 1991.

(42) Bard, A. J. *Electrochemical methods : fundamentals and applications*; 2nd ed. ed.; New York: Wiley, 2001.

(43) Davis, E. A.; Mott, N. F. *Philosophical Magazine* **1970**, *22*, 903.

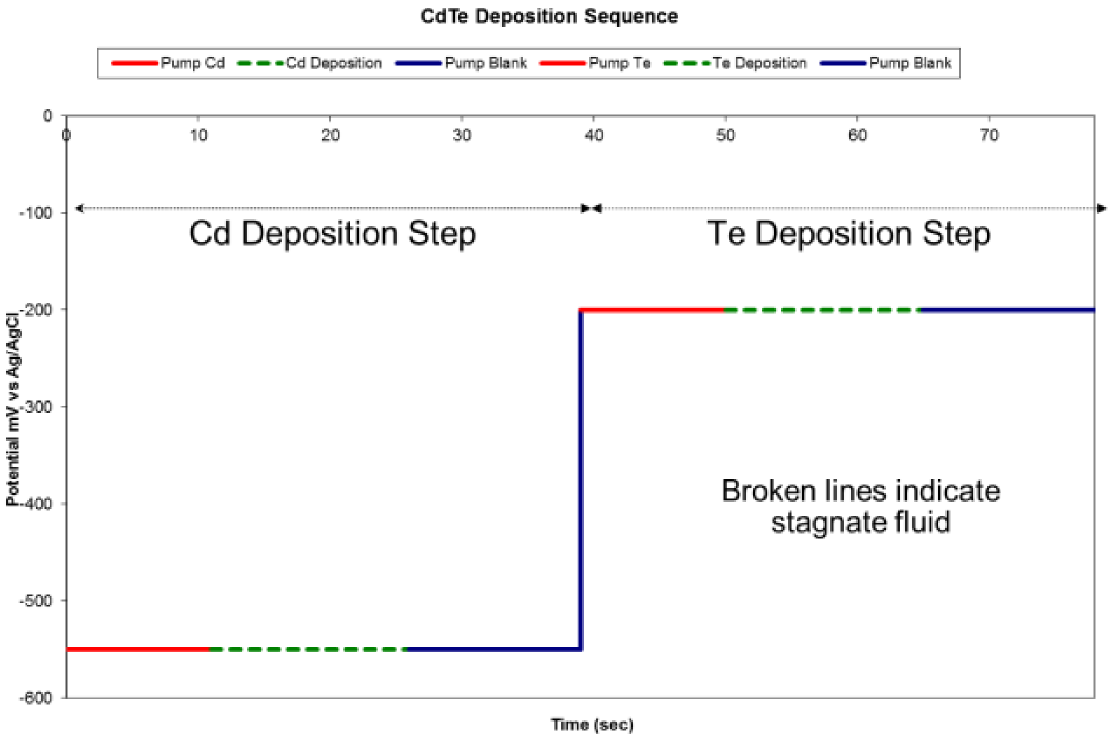

**Figure 2.1**: CdTe deposition sequence diagram. The above is the sequenced used with acidic Te deposition chemistry

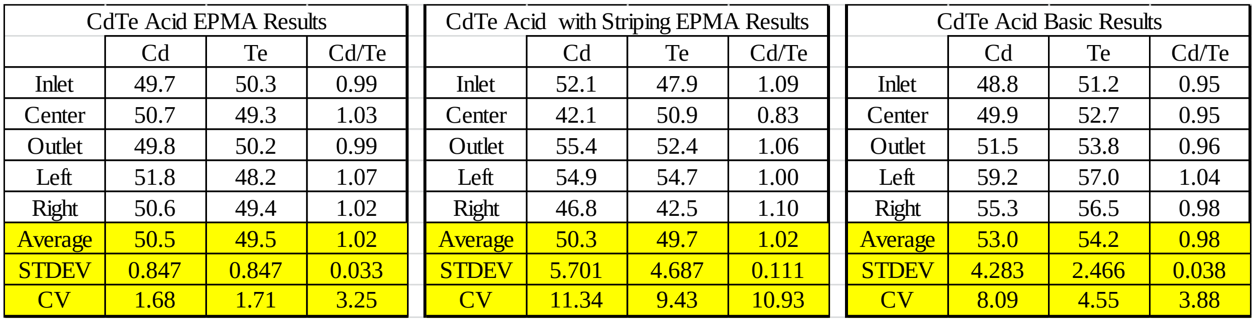

| CdTe Acid EPMA Results | | | |
|---|---|---|---|
| | Cd | Te | Cd/Te |
| Inlet | 49.7 | 50.3 | 0.99 |
| Center | 50.7 | 49.3 | 1.03 |
| Outlet | 49.8 | 50.2 | 0.99 |
| Left | 51.8 | 48.2 | 1.07 |
| Right | 50.6 | 49.4 | 1.02 |
| Average | 50.5 | 49.5 | 1.02 |
| STDEV | 0.847 | 0.847 | 0.033 |
| CV | 1.68 | 1.71 | 3.25 |

| CdTe Acid with Striping EPMA Results | | | |
|---|---|---|---|
| | Cd | Te | Cd/Te |
| Inlet | 52.1 | 47.9 | 1.09 |
| Center | 42.1 | 50.9 | 0.83 |
| Outlet | 55.4 | 52.4 | 1.06 |
| Left | 54.9 | 54.7 | 1.00 |
| Right | 46.8 | 42.5 | 1.10 |
| Average | 50.3 | 49.7 | 1.02 |
| STDEV | 5.701 | 4.687 | 0.111 |
| CV | 11.34 | 9.43 | 10.93 |

| CdTe Acid Basic Results | | | |
|---|---|---|---|
| | Cd | Te | Cd/Te |
| Inlet | 48.8 | 51.2 | 0.95 |
| Center | 49.9 | 52.7 | 0.95 |
| Outlet | 51.5 | 53.8 | 0.96 |
| Left | 59.2 | 57.0 | 1.04 |
| Right | 55.3 | 56.5 | 0.98 |
| Average | 53.0 | 54.2 | 0.98 |
| STDEV | 4.283 | 2.466 | 0.038 |
| CV | 8.09 | 4.55 | 3.88 |

**Table 2.1**: EPMA results of the three different deposition chemistries in relative percentages.

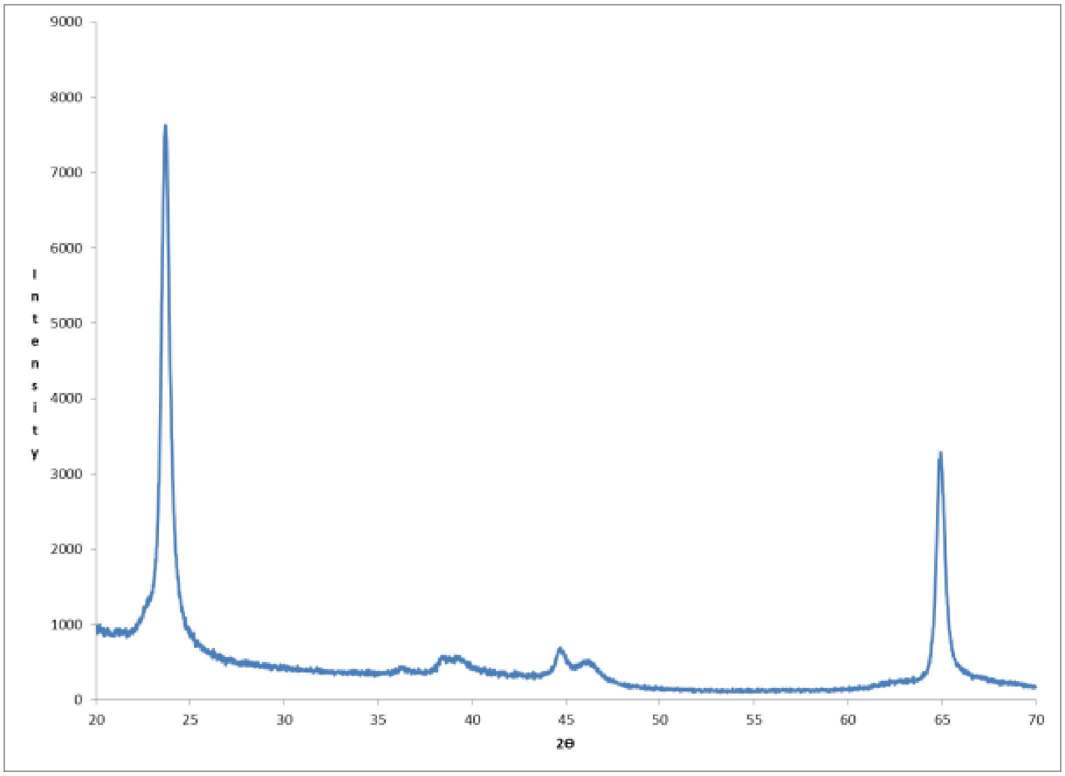

**Figure 2.2**: XRD spectrum of E-ALD grown CdTe on polycrystalline Au. The incident angle used is 0.5° with Cu $K_{\alpha 1}$ source.

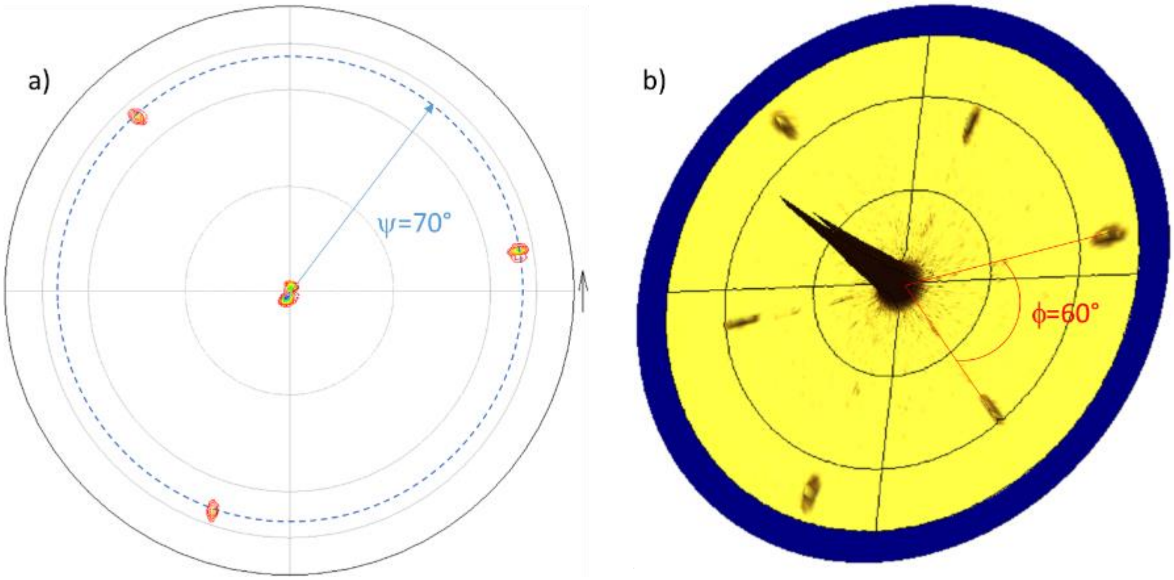

**Figure 2.3:** a) XRD pole pattern of Au single crystal substrate b) XRD pole pattern of E-ALD CdTe grown on Au single crystal substrate.

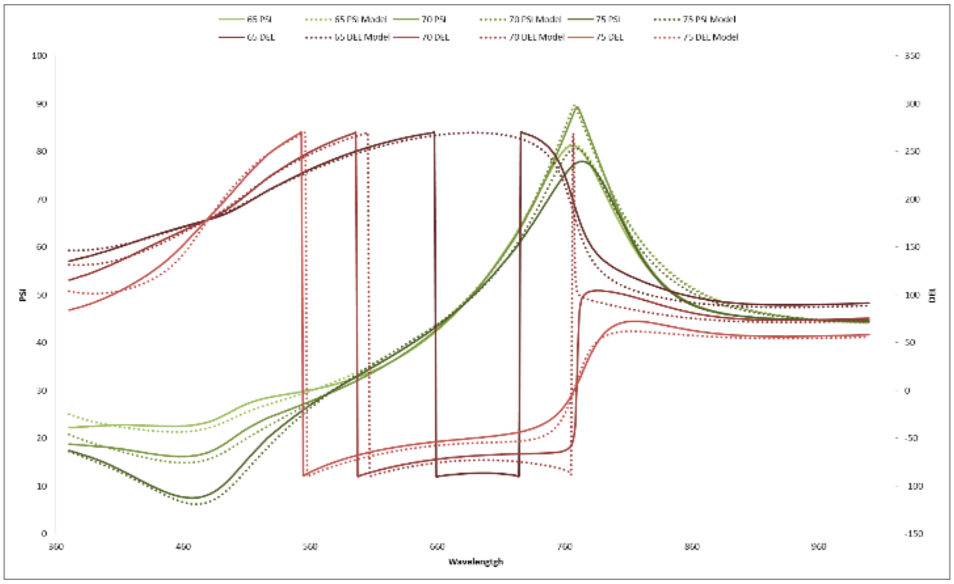

**Figure 2.4:** SE data collected of E-ALD CdTe grown onto polycrystalline Au. Solid lines indicate collected data dashed lines are the Cauchy model red lines are PSI data and green lines are DEL data.

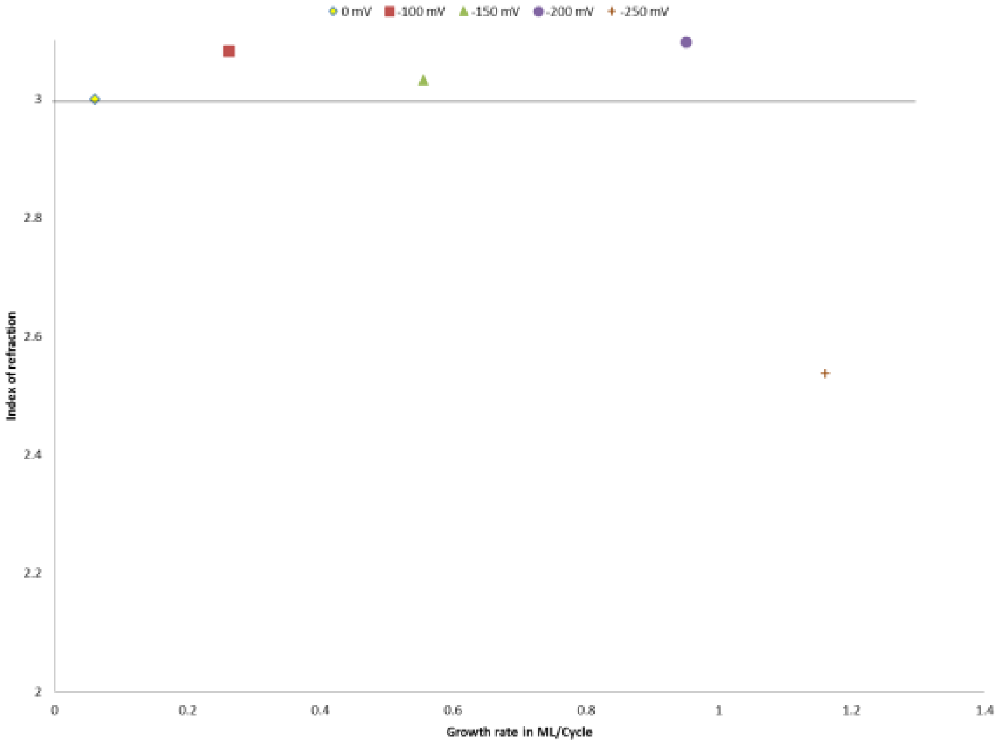

**Figure 2.5:** The effect of growth rate on the quality of E-ALD CdTe. Solid black line indicates the literature value of the index of refraction of CdTe.

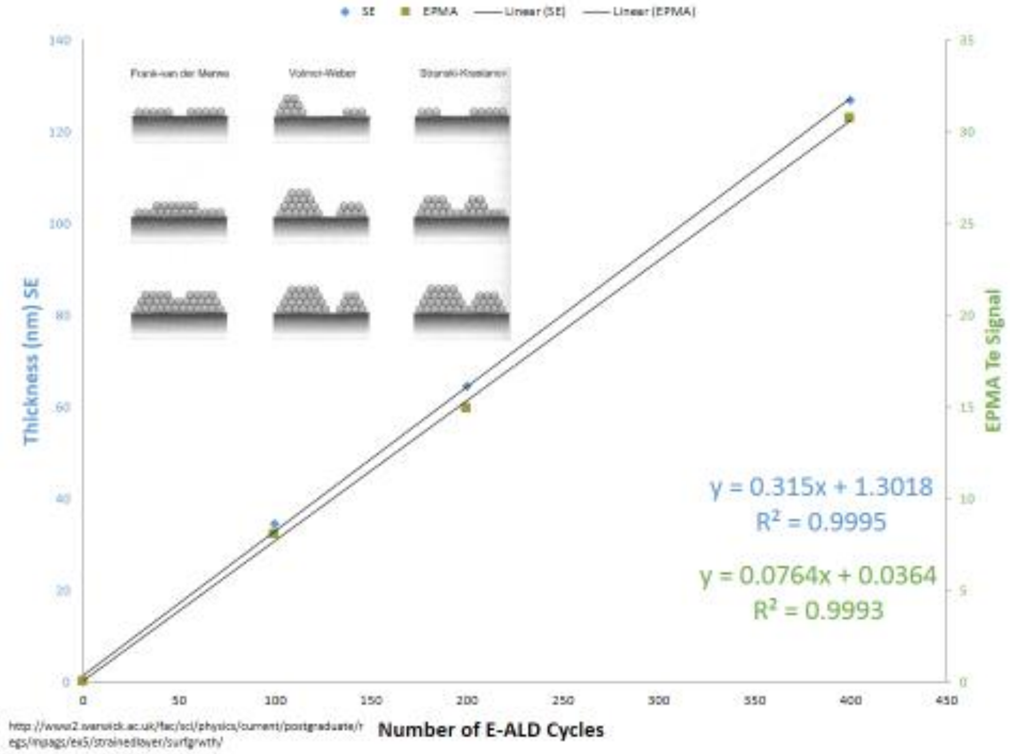

http://www2.warwick.ac.uk/fac/sci/physics/current/postgraduate/regs/mpags/ex5/strainedlayer/surfgrwth/

**Figure 2.6:** Frank van der Meer growth of E-ALD CdTe.

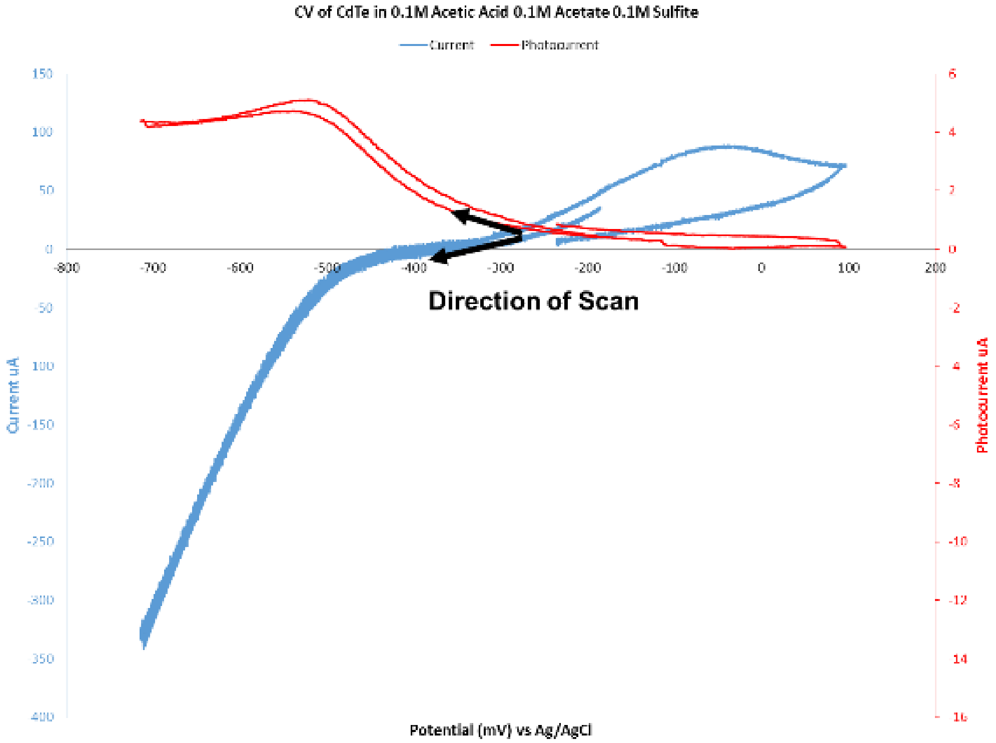

**Figure 2.7:** Photoelectrochemical studies of E-ALD CdTe in 0.1M acetic acid + 0.1 M acetate and 0.1M Sulfite scan rate 10 mV/sec illuminated with 532 nm light.

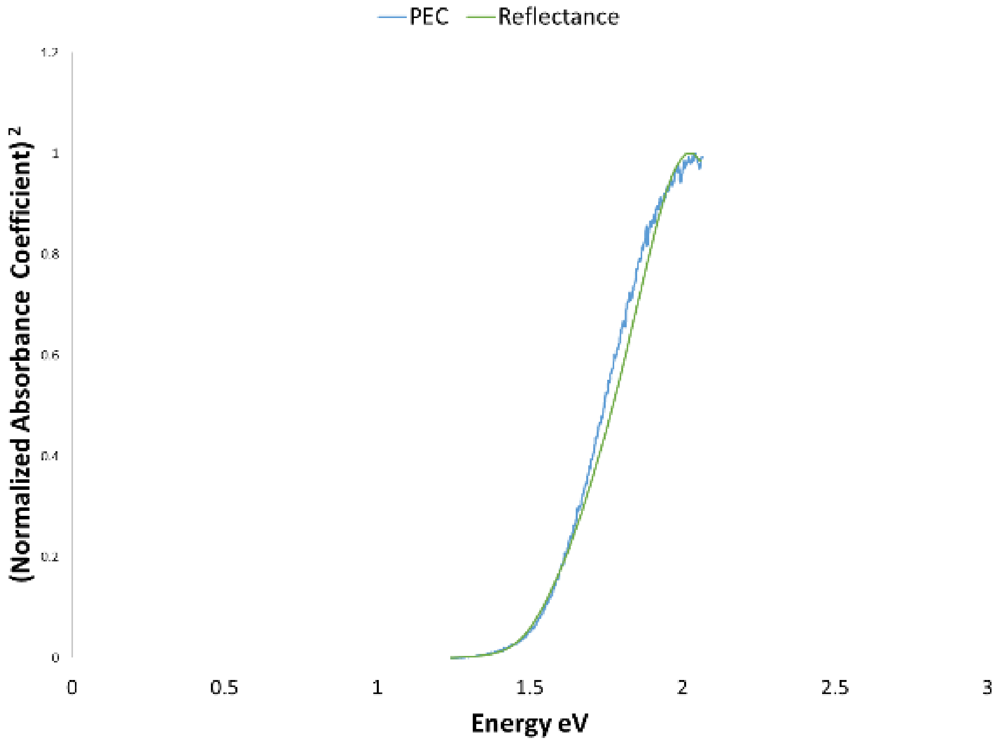

**Figure 2.8:** Bandgap estimation of E-ALD CdTe as estimated by photoelectrochemistry and reflectance.

# CHAPTER 3

# A COMPAIRISON OF CDS GROWN BY THRE DIFFERENT LOW COST METHODS FOR USE IN PHOTOVOLTAICS[2]

---

[2] B. Perdue, V. Stickney, M. Stickney, J. L. Stickney , To be submitted to *Journal of the Electrochemical Society (2014)*

## Abstract

The characterization of CdS by three different condensed phase deposition techniques are reported. CdS was synthesized by electrochemical atomic layer deposition (E-ALD) successive ionic layer absorption and reaction (SILAR) and chemical bath deposition (CBD). E-ALD is the condensed phase equivalent of atomic layer deposition (ALD). In ALD the deposition of a compound is achieved by means of sequential surface limited reactions in which the components are deposited one atomic layer at a time. In E-ALD the individual atomic layers are formed using underpotential deposition (UPD), an electrochemical surface limited reaction. In the SLIAR deposition process ions of one element are introduced to a substrate and adsorb onto the surface of that substrate, the excess ions are rinsed away. Then ions of the next element are introduced, these ions react with the adsorbed layer precipitating the desired compound, finally the remaining ions are rinsed away. The CBD of CdS is based on the thermal decomposition of thiourea to free $S^{2-}$ and the subsequent reaction with $Cd^{2+}$ ions. Thin films of CdS were fabricated with each condensed phase deposition technique and analyzed with various thin film characterization techniques including electron probe microanalysis (EPMA) X-ray diffraction (XRD) spectroscopic ellipsometry (SE) and photoelectrochemistry (PEC). Results show that the average Cd/S ratio, determined using EPMA, was 1.07, 1.10, and 1.05 for CBD, SILAR and ALD respectively. XRD indicates that SILAR and E-ALD produce crystalline deposits while CBD does not. SE shows that E-ALD and SILAR grow at similar rates and produce deposits with the proper optical constants, CBD deposits were too rough to produce accurate SE data. Photoelectrochemical results show that the photoresponse for E-ALD grown CdS was the highest while CBD was the least photoactive and all deposits produce n-type CdS with a bandgap of 2.4 eV.

## Introduction

CdS is a very important II-IV compound in the field of photovoltaics (PV). It has a bandgap of 2.4 eV which makes it a suitable compound to be used as a window layer[1-4]. In fact many thin film CdTe, CIGS, CIS, CZTS based PV used CdS as its window layer. As such it is important to find reliable methods to deposit high quality films of this material.

Many different deposition strategies can be used when depositing CdS[1,3] because it is a very stable compound. Two of the more popular methods include spray pyrolysis[5-8] and sputtering[9,10] owing to the fact that they can homogeneously cover larger areas using low cost precursors. These techniques have many advantages yet suffer from a few critical disadvantages. The first is that there is a high probability of the resulting deposit having pinholes[11]. The second is that these techniques are "line of sight" deposition and cannot conformally deposit onto nanostructures. The final drawback is that these techniques require a post deposition anneal step to produce PV grade material[1-4]. This is problematic because it increases the cost and energy required to fabricate the device

Condensed phase deposition processes are attractive because they are typically low cost and have the added benefit of conformal growth which limits the formation of pinholes. Three such deposition techniques are CBD, SILAR or more recently known as ionic layer deposition (ILD) and finally electrochemical atomic layer deposition (E-ALD). Each of these techniques have shown the potential to grow high quality CdS deposits without the need for a post deposition anneal.

The CBD of CdS was first demonstrated by Pavaskar in 1977[12]. Since its initial discovery it has been adapted to many different compounds as well as different deposition conditions[13]. The growth conditions of CBD CdS has been extensively characterized by Lincot et al[14,15]. The general mechanism of the deposition process is the thermal decomposition of thiourea to the sulfide ion which then reacts with a surface adsorbed complexed cadmium ion which then precipitates as CdS onto the surface. Lincot demonstrated that cadmium salts with different ligands can be used to control growth rate as well as quality of the deposit. CBD was used to deposit CdS for use in PV by Chu et al. which led to a high efficiency CdTe solar cell[16,17] demonstrating the technique's merit in the field.

SILAR was demonstrated in 1985 by Nicolau et al[18]. Akin to CBD, SILAR has also been adapted to a variety of compounds using various deposition conditions[19-26]. The SILAR process involves the sequential treatment of a surface to various solutions. In this study the substrate is introduced to a solution containing $Cd^{2+}$which spontaneously adsorb to the surface. The excess $Cd^{2+}$ ions are then removed with another solution. After the excess ions have been removed the substrate is introduced to the next solution containing the $S^{2-}$ ions. The $S^{2-}$ ions react with the adsorbed $Cd^{2+}$ ions to form a layer of CdS on the surface. The excess $S^{2-}$ ions are then removed with another solution and the process is repeated. Due to the layer by layer Frank–van der Merwe style growth SILAR gives superior control over the thickness of the deposit.

E-ALD pioneered by our group is the condensed phase equivalent to atomic layer epitaxy (ALE) introduced by Suntola[27-29]. ALE was developed in order to improve deposit morphology, crystallinity and stoichiometry and prevention of three dimensional growth. Analogous to ALE, E-ALD uses surfaces limited reactions to grow compounds one atomic layer at a time. Surface limited reactions are reactions that terminate after the substrate atoms have been covered by the depositing atoms. Electrochemical surfaces limited reactions are known as underpotential deposition (UPD). In UPD, and element will deposit onto another element prior to, its formal reduction potential. This occurs because it is more thermodynamically stable to deposit onto another element than it is to deposit onto itself. In a typical E-ALD cycle, a solution containing a reactant's electrochemical precursor is introduced to the substrate at a UPD potential. After the reaction is completed the solution is rinsed away using a blank solution, and a new solution containing a precursor for the next element is introduced at its UPD potential. After the reaction is complete, and the solution is rinsed from the cell, one cycle has been completed resulting in the formation of one compound bilayer. Just like SILAR the thickness of the deposited is determined by the number of E-ALD cycles grown. The E-ALD growth of CdS has been studied previously by this group[30-32] and extensively by Foresti et al.[33-40] so much is known by this system.

An article comparing the quality of CdS deposits made by SILAR and CBD has recently been published[41]. The goal of this work is to supplement the information presented in that work as well as investigate the optical behavior of CdS deposited by the three aforementioned deposition techniques. CdS deposits were made using the CBD formula devolved by Chu as it resulted in a high efficiency PV, SILAR and E-ALD CdS deposits were made with the E-ALD automated flow cell system. The deposits were compared using X-ray diffraction (XRD), electron probe microanalysis (EPMA), spectroscopic ellipsometry (SE), and photoelectrochemistry (PEC).

## Experimental

In these studies the films were grown using an automated flow cell system using a three electrode cell with a Ag/AgCl reference electrode controlled by a potentiostat. The basic setup for this procedure has the bottles containing the precursor solutions incased in a box so that the solution and the box can be purged of oxygen by nitrogen bubbling, with the $N_2$ box helping minimizing $O_2$ in the system. These bottles are hooked up to a valve block, with its outlet connected to the electrochemical flow cell. The outlet of the cell is attached to a peristaltic pump, which facilitates sucking solutions through the cell. The potentiostat, valves and the pump are controlled by a PC running SEQUENCER 4 software (Electrochemical ALD L.C., Athens GA). More details on flow cell can be found in following publications[42-45]. The electrodes used in these studies were polycrystalline Au on glass with a 50 nm Ti adhesion layer purchased from Evaporated Metal Films.

The solutions used for the E-ALD and SILAR experiments were the same. The cadmium solution used was a 0.5 mM $CdSO_4$ in 0.5M $NaClO_4$, pH 3 solution. The cadmium salt used was $3(CdSO_4)8H_2O$ 99.999% pure purchased from Alfa Æsar. The sulfide solution used was a 0.5mM $Na_2S$ in 0.5M $NaClO_4$, pH 10.3. The sulfur salt used was $Na_2S$ $9H_2O$ 99.99% purchased from Sigma Aldrich. Two blanks were prepared for this work both consisted of 0.5 M NaClO4 one of pH 3 for the cadmium blank and the other pH 10 for the sulfur blank. The purpose of the blank was to rinse out the electrochemical precursor while maintaining the proper pH. All solutions were prepared with 18MΩ water supplied from a Millipore water filtration system.

The deposition cycle used for the E-ALD and SILAR process was as follows. The Cd solution was pumped into the cell at a rate of 18 mL/min for 10 seconds at a potential of -500mV. This was followed by a quiescent deposition step that lasted 15 seconds to allow the system to come to equilibrium. The excess Cd ions were removed from the cell by pumping in the pH 3 blank solution for 20 seconds while maintaining the potential at -500mV. Next the sulfide solution was pumped into the cell at a rate of 18 mL/min for 10 seconds at a potential of -600mV. This was followed by a quiescent deposition step that lasted 15 seconds. The excess $S^{2-}$ ions were removed from the cell by pumping in the pH 10 blank solution for 20 seconds while maintaining the potential at -500mV.  The difference between the E-ALD cycle and the SILAR cycle was the lack of potential control, the SILAR deposition process was done at open circuit.

The chemical bath used to deposit CdS in these studies was adapted from the procedure Chu et al used[16,46].  This was done because this procedure led to a high efficiency PV as stated earlier.  This bath consisted of Cd(Acetate)$_2$ 99.999% pure purchased from Alfa Æsar, reagent grade ammonium acetate, reagent grade Ammonia, and 99.9% pure Thiosurea purchased from Sigma Aldrich.  The CdS CBD was carried out by adding 8mL of 0.033 M Cd(Acetate)$_2$, 5 mL of 1M ammonium acetate, and 15 mL of concentrated ammonia added dropwise to prevent Cd precipitation.  This mixture was diluted into 550 mL nanopure 18MΩ water and heated to 80°C. Once the temperature had reach equilibrium 8mL of 0.067M thiourea was added dropwise with a burette.  This mixture was then reacted for 40 min.

The stoichiometry of the deposits were probed with EPMA on a JEOL 8600 SUPERPROBE with a 10 KeV accelerating voltage, 15 nA beam current, and a 10 um beam diameter.  The large beam was used to average slight sample inhomogeneities.  Crystallinity of the deposits were examined on a PANanalytical X'PERT Pro with an open eulerian cradle utilizing a 1.54nm Cu K$\alpha_1$ source and a parallel plate collimator.  Optical properties of the deposits were analyzed with SE on a JA Woolam M-2000V.  Photoelectrochemial measurements were made using the electrolyte Foresti et al. used[36,37] which consisted of a 0.1M $Na_2S$ solution. 100 cycle SILAR and E-ALD deposits were made as well as CBD deposits and analyzed with the aforementioned techniques.  Results are summarized in Table 3.1.

## Results and Discussion

The electrochemical behavior of Cd is well understood.  Cd can UPD onto a Au electrode with coverages varying from 1/3 to 1 monolayer (ML) vs a Au(111) surface.  A monolayer is defined in this report relative to the number of surface atom in the substrate. Assuming the Au on glass substrates resemble a Au(111) surface, that would be about 1.35 X$10^{15}$ atom/$cm^2$ At slightly more negative potentials Cd ions can form a surface alloy with the the Au electrode before bulk Cd electrodeposition occurs. Due to Cd reactive behavior it is difficult to electrodeposit more noble elements onto it. The Cd atomic layer must be stabilized by compound formation for it to remain on the electrode. The electrochemistry of $S^{2-}$ is also known to this group. Thin layer electrode studies[32] show that sulfide ions will undergo oxidative UPD onto a Au surface at -600 mV. As the potential is scanned more positive sulfide will oxidize at around -200 mV. It is fortunate that atomic layers of both Cd and S are stable in the same potential ranges, which allows for flexibility in the potentials used in the E-ALD cycle.

The stoichiometry of the deposits were checked with EPMA. EPMA was used because it has better sensitivity and is more quantitative than energy dispersive X-ray spectroscopy (EDX). The average of 5 points were taken across the deposit. Results show an average Cd/S ratio of 1.07 1.1 1.05 for CBD, SILAR, and E-ALD respectively. The standard deviation expected for an $\eta$ of 5 under these conditions is about 0.1 which suggests that the deposited films made by the different chemistries are stoichiometric within the limitations of the instrument used. It is interesting to note that all of the deposits appear high in cadmium. This could be because of a presence of a cadmium gold surface alloy which is known to form. This surface alloy may not affect the stoichiometry of the deposit, but would be detected by EPMA which would result in an apparent excess of Cd. Based on the results gathered from EPMA, each of the deposition techniques can produce stoichiometric CdS deposits without the need of any post deposition treatments, thus demonstrating the inherent value in these deposition techniques.

The crystallinity of the deposition techniques were probed with glancing angle XRD. Results for these tests are shown in Figure 3.1. The XRD spectrum in Figure 3.1 indicates that unannealed E-ALD and SILAR CdS has a preferred orientation of (111) for a cubic system or (002) for a hexagonal system. Both of these reflections occur at 26.4°2θ so it is difficult to determine which crystal structure exists based on XRD alone. It is believed to be cubic because CdS undergoes recrystallization with a $CdCl_2$ treatment and annealing at 350°C which converts the cubic crystal into the hexagonal crystal[47-50]. The spectrum in Figure 3.1 show no difference in the quality of CdS prepared by E-ALD and SILAR. This would suggest that the two processes are more similar than previously thought. CBD does not show a very crystalline deposit. Most CBD deposits are subsequently annealed to achieve crystallinity[3,41,50-53]. CBD CdS deposits were annealed without a $CdCl_2$ treatment and crystallinity was achieved, however, the goal of this work was to show the quality of the deposits without any post deposition treatments. .

The optical properties of the CdS deposits were studied with SE. A typical spectrum is shown in Figure 3.2. Figure 3.2 shows the PSI and DEL measurements at 65, 70, 75 degrees. These angles were picked because the Brewster angle for Au at 632.8 nm is 72° so the measurements were taken below at and above the Brewster angle to obtain maximum information about the thin films. The wavelength of 632.8 nm was chosen because the tabulated optical constants[54,55] were calculated using a HeNe laser. The collected spectra was fitted with against the Cauchy equation which relates the thickness and optical constants of the material. The mean square error or MSE of the fit produced by E-ALD and SILAR was below 25 which is considered to be a good fit thus any values calculated from this model are reliable. This was not the case with the CBD deposit. The CBD deposit was very rough which made the data difficult to fit with the model used. A bad fit indicates that the values calculated from it would be unreliable. t.

Using the Cauchy model, the optical constants and thickness of E-ALD and SILAR deposits were evaluated. The calculated index of refection obtained from the model at 632.8 nm were 2.404 for the SILAR deposits and 2.356 for the ALD deposits. These values are essentially the same and agree with the recorded literature values of 2.4[51,54-56]. This is further evidence that the SILAR deposition process is very similar if not identical to the E-ALD process and has the ability to produce high quality deposits. The thickness of the deposits were also calculated from the model. The thickness calculated from the SILAR deposit as 20.2 nm and the thickness calculated for the E-ALD sample was 19.8 nm. Again there is no difference between the deposits produced by E-ALD and SILAR. The thickness of the CBD deposits were estimated by adding a roughness layer onto the Cauchy layer to improve the fit of the model. This improved the MSE however it still exceeded 100 which indicates a bad fit. With this amendment to the model the approximate thickness of deposits prepared in this manor was ~80 nm which is consistent with what Chu et al reported.

Combining spectroscopic ellipsometry and the data obtained from XRD the growth rate can be estimated. The XRD from Figure 3.1 indicated that the CdS has a strong preferred (111) orientation if cubic. The assumption that the CdS is cubic, not hexagonal, because it has not been annealed or $CdCl_2$ treated. As a result the CdS would fall in the space group of $F\bar{4}3m$ which has tetrahedrally bonded CdS. Another assumption is made that all growth is made in the (111) direction so the growth rate can be estimated by taking the thickness calculated from spectroscopic ellipsometry and dividing that number by the product of the number of cycles run and the thickness of a CdS compound bilayer.

Using geometry and the CdS cubic lattice constant, the thickness of a compound bilayer can be calculated. The distance from a Cd atom to the next Cd atom can be calculated with the Pythagorean Theorem. Using the CdS lattice constant of a=0.582 nm the Cd-Cd distance (x) can be calculated by $x = \sqrt{\frac{a^2}{2}}$ or 0.411 nm. Using this distance as the distance forming the edges of a regular tetrahedron the height of the tetrahedron given by geometry is calculated by $h = \sqrt{x^2 - \left(\frac{x}{\sqrt{3}}\right)^2} = \sqrt{\frac{2}{3}}x.$ When relating back to the lattice constant a we find that the height of a CdS compound bilayer in the (111) direction is equal to $h = \frac{a}{\sqrt{3}} = 0.336\,nm.$ By deviding the calcutlated thickness from spectroscopic ellipsometry by 0.336 multiplied the number of cycles run a growth rate can be estimated. The estimated growth rates for E-ALD and SILAR deposits are 0.6 ML/cycle. This is growth rate is consistent with other reports[21,31,34-36,41,57] implying sub compound bilayer growth per cycle.

Conductivity type band gap and external quantum efficiency (EQE) were measured using photoelectrochemistry. The photoelectrochemical behavior of thin films of CdS have been previously studied by Foresti et al[34,36-38]. Three things can be calculated by probing the films with photoelectrochemistry. The first is the conductivity type, the second is the EQE and the third is the bandgap. By forcing the semiconductor into depletion mode the type of the semiconductor can be determined. The assumption made is that when the semiconductor is depleted of its majority carrier any current produced will be due to exciton creation[58]. By poising the potential at a point where maximum photocurrent occurs, the EQE can be calculated. The EQE was calculated using the following formula $EQE = \frac{I_p}{I_d} * \frac{hc}{e\lambda} * SR(\lambda).$ Where $I_p$is the measured photocurrent, $I_d$is the current measured by calibrated Si detector, *h* is planks constant, *c* is the speed of light in vacuum, *e* is the fundamental charge of an electron, $\lambda$ is the wavelength, and $SR(\lambda)$ is the spectral response of the Si detector with the units of $\left(\frac{A}{W}\right)$. The bandgap is estimated by the method devolved by Davis and Mott[59] when assuming a direct bandgap the $(ABS*eV)^2$ is plotted vs eV and the x intercept is the estimated bandgap.

A typical Photoelectrochemical CV is shown in Figure 3.3. By scanning the potential positive an increase in photocurrent is observed, thus the majority carriers are electrons making the semiconductor n-type. Both E-ALD and SILAR grown CdS exhibit n-type behavior. CBD, however, was not photoresponsive enough to obtain consistent results. Thus the conductivity type of CBD CdS could not be determined by this method. Concluding these measurement the potential was poised at a point of maximum photocurrent to obtain bandgap and quantum efficiency data.

The external quantum efficiency results are plotted in Figure 3.4. These results indicate that A-LD is the most sensitive while CBD is the least. For actual values consult Table 3.1. For the first time a difference is shown between the behavior of E-ALD and SILAR. It is unknown at this time why there is such a difference when all other results indicate almost the exact behavior. Bandgaps were also calculated from these spectra and all methods produced CdS with a bandgap of ~2.4eV which is expected for CdS deposits.

## Conclusion

CdS deposits were fabricated and analyzed with different thin film characterization techniques. EPMA shows that the Cd/S ratio was 1.07, 1.10, and 1.05 for CBD, SILAR and ALD respectively. SILAR and E-ALD CdS grows crystalline while CBD does not. SE shows that E-ALD and SILAR grow at similar rates and produce deposits with the proper optical constants. Photoelectrochemical results show that the photoresponse for E-ALD grown CdS was the highest while CBD was the least photoactive and all deposits produce n-type CdS with a bandgap of 2.4 eV. E-ALD and SILAR produce CdS deposits of almost identical quality this is probably because the growing mechanisms are very similar.

# References

(1) Birkmire, R. W.; Eser, E. *Annual Review of Materials Science* **1997**, *27*, 625.

(2) Shah, A.; Torres, P.; Tscharner, R.; Wyrsch, N.; Keppner, H. *Science* **1999**, *285*, 692.

(3) Omura, K.; Hanahusa, A.; Arita, T.; Higuchi, H.; Aramoto, T.; Nishio, T.; Sibutani, S.; Kumazawa, S.; Murozono, M.; Yabuuchi, Y.; Takakura, H. *Renewable Energy* **1996**, *8*, 405.

(4) Chopra, K. L.; Paulson, P. D.; Dutta, V. *Progress in Photovoltaics* **2004**, *12*, 69.

(5) Ravichandran, K.; Muruganantham, G.; Sakthivel, B.; Philominathan, P. *Surface Engineering* **2010**, *26*, 590.

(6) Ravichandran, K.; Philominathan, P. *Applied Surface Science* **2009**, *255*, 5736.

(7) Rakhshani, A. E. *J. Appl. Phys.* **2001**, *90*, 4265.

(8) Patil, P. S. *Materials Chemistry and Physics* **1999**, *59*, 185.

(9) Compaan, A. D.; Gupta, A.; Lee, S.; Wang, S.; Drayton, J. *Solar Energy* **2004**, *77*, 815.

(10) Ellmer, K. *J. Phys. D-Appl. Phys.* **2000**, *33*, R17.

(11) Jones, E. W.; Barrioz, V.; Irvine, S. J. C.; Lamb, D. *Thin Solid Films* **2009**, *517*, 2226.

(12) Pavaskar, N. R.; Menezes, C. A.; Sinha, A. P. B. *Journal of the Electrochemical Society* **1977**, *124*, 743.

(13) Mane, R. S.; Lokhande, C. D. *Materials Chemistry and Physics* **2000**, *65*, 1.

(14) Lincot, D.; Borges, R. O. *Journal of the Electrochemical Society* **1992**, *139*, 1880.

(15) Ortegaborges, R.; Lincot, D. *Journal of the Electrochemical Society* **1993**, *140*, 3464.

(16) Chu, T. L.; Chu, S. S.; Ferekides, C.; Wu, C. Q.; Britt, J.; Wang, C. *J. Appl. Phys.* **1991**, *70*, 7608.

(17) Kim, H. C.; Fthenakis, V.; Choi, J. K.; Turney, D. E. *J. Ind. Ecol.* **2012**, *16*, S110.

(18) Nicolau, Y. F. *Applied Surface Science* **1985**, *22-3*, 1061.

(19) Nicolau, Y. F.; Menard, J. C. *Journal of Crystal Growth* **1988**, *92*, 128.

(20) Nicolau, Y. F.; Dupuy, M.; Brunel, M. *Journal of the Electrochemical Society* **1990**, *137*, 2915.

(21) Sankapal, B. R.; Mane, R. S.; Lokhande, C. D. *Materials Research Bulletin* **2000**, *35*, 177.

(22) Lokhande, C. D.; Sankapal, B. R.; Pathan, H. M.; Muller, M.; Giersig, M.; Tributsch, H. *Applied Surface Science* **2001**, *181*, 277.

(23) Sasagawa, M.; Nosaka, Y. *Journal of Electroanalytical Chemistry* **2002**, *536*, 141.

(24) Pathan, H. M.; Lokhande, C. D. *Bulletin of Materials Science* **2004**, *27*, 85.

(25) Sun, H.; Mu, J. *Journal of Dispersion Science and Technology* **2005**, *26*, 719.

(26) Ates, A.; Yildirim, M. A.; Kundakci, M.; Yildirim, M. *Chin. J. Phys.* **2007**, *45*, 135.

(27) Gregory, B. W.; Stickney, J. L. *Journal of Electroanalytical Chemistry* **1991**, *300*, 543.

(28) Gregory, B. W.; Suggs, D. W.; Stickney, J. L. *Journal of the Electrochemical Society* **1991**, *138*, 1279.

(29) Suntola, T. *Thin Solid Films* **1992**, *216*, 84.

(30) Colletti, L. P.; Teklay, D.; Stickney, J. L. *Journal of Electroanalytical Chemistry* **1994**, *369*, 145.

(31) Colletti, L. P.; Flowers, B. H.; Stickney, J. L. *Journal of the Electrochemical Society* **1998**, *145*, 1442.

(32) Lay, M. D.; Varazo, K.; Stickney, J. L. *Langmuir* **2003**, *19*, 8416.

(33) Foresti, M. L.; Pezzatini, G.; Cavallini, M.; Aloisi, G.; Innocenti, M.; Guidelli, R. *J. Phys. Chem. B* **1998**, *102*, 7413.

(34) Cecconi, T.; Atrei, A.; Bardi, U.; Forni, F.; Innocenti, M.; Loglio, F.; Foresti, M. L.; Rovida, G. *Journal of Electron Spectroscopy and Related Phenomena* **2001**, *114*, 563.

(35) Innocenti, M.; Pezzatini, G.; Forni, F.; Foresti, M. L. *Journal of the Electrochemical Society* **2001**, *148*, C357.

(36) Innocenti, M.; Cattarin, S.; Cavallini, M.; Loglio, F.; Foresti, M. L. *Journal of Electroanalytical Chemistry* **2002**, *532*, 219.

(37) Innocenti, M.; Cattarin, S.; Loglio, F.; Cecconi, T.; Seravalli, G.; Foresti, M. L. *Electrochimica Acta* **2004**, *49*, 1327.

(38) Loglio, F.; Innocenti, M.; Pezzatini, G.; Foresti, M. L. *Journal of Electroanalytical Chemistry* **2004**, *562*, 117.

(39) Cavallini, M.; Facchini, M.; Albonetti, C.; Biscarini, F.; Innocenti, M.; Loglio, F.; Salvietti, E.; Pezzatini, G.; Foresti, M. L. *Journal of Physical Chemistry C* **2007**, *111*, 1061.

(40) Salvietti, E.; Loglio, F.; Innocenti, M.; Cavallini, M.; Facchini, M.; Pezzatini, G.; Raiteri, R.; Foresti, M. L. *Electrochimica Acta* **2007**, *52*, 6034.

(41) Senthamilselvi, V.; Saravanakumar, K.; Begum, N. J.; Anandhi, R.; Ravichandran, A. T.; Sakthivel, B.; Ravichandran, K. *Journal of Materials Science-Materials in Electronics* **2012**, *23*, 302.

(42) Huang, B. M.; Colletti, L. P.; Gregory, B. W.; Anderson, J. L.; Stickney, J. L. *Journal of the Electrochemical Society* **1995**, *142*, 3007.

(43) Colletti, L. P.; Stickney, J. L. *Journal of the Electrochemical Society* **1998**, *145*, 3594.

(44) Flowers, B. H.; Wade, T. L.; Garvey, J. W.; Lay, M.; Happek, U.; Stickney, J. L. *Journal of Electroanalytical Chemistry* **2002**, *524-525*, 273.

(45) Lay, M. D.; Stickney, J. L. *Journal of the Electrochemical Society* **2004**, *151*, C431.

(46) Chu, T. L.; Chu, S. S.; Schultz, N.; Wang, C.; Wu, C. Q. *Journal of the Electrochemical Society* **1992**, *139*, 2443.

(47) Rose, D. H.; Hasoon, F. S.; Dhere, R. G.; Albin, D. S.; Ribelin, R. M.; Li, X. S.; Mahathongdy, Y.; Gessert, T. A.; Sheldon, P. *Progress in Photovoltaics* **1999**, *7*, 331.

(48) Dhere, R. G.; Al-Jassim, M. M.; Yan, Y.; Jones, K. M.; Moutinho, H. R.; Gessert, T. A.; Sheldon, P.; Kazmerski, L. L. *J. Vac. Sci. Technol. A-Vac. Surf. Films* **2000**, *18*, 1604.

(49) Paulson, P. D.; Dutta, V. *Thin Solid Films* **2000**, *370*, 299.

(50) Li, W. Y.; Cai, X.; Chen, Q. L.; Zhou, Z. B. *Materials Letters* **2005**, *59*, 1.

(51) Martinez, J. L.; Martinez, G.; Torres-Delgado, G.; Guzman, O.; Del Angel, P.; Zelaya-Angel, O.; Lozada-Morales, R. *Journal of Materials Science-Materials in Electronics* **1997**, *8*, 399.

(52) Martinez, M. A.; Guillen, C.; Herrero, J. *Applied Surface Science* **1998**, *136*, 8.

(53) Prabahar, S.; Dhanam, M. *Journal of Crystal Growth* **2005**, *285*, 41.

(54) D, P. E. *Handbook of Optical Constants of Solids*; Academic Press: Orlando, 1985.

(55) D, P. E. *Handbook of Optical Constants of Solids II*; Academic Press: Academic Press, 1991.

(56) Derin, H.; Kantarli, K. *Surface and Interface Analysis* **2009**, *41*, 61.

(57) Metin, H.; Erat, S.; Emen, F. M.; Kafadar, V.; Yazici, A. N.; Ari, M.; Kulcu, N. *Journal of Luminescence* **2010**, *130*, 1531.

(58) Bard, A. J. *Electrochemical methods : fundamentals and applications*; 2nd ed. ed.; New York: Wiley, 2001.

(59) Davis, E. A.; Mott, N. F. *Philosophical Magazine* **1970**, *22*, 903.

|  | EPMA Cd/S Ratio | Crystal Structure | Index of refraction η | Growth Rate ML/Cycle | Conductivity type | Max EQE | Band Gap EV |
|---|---|---|---|---|---|---|---|
| CBD | 1.07 | Cubic/Hexagonal | NA | NA | NA | 0.20% | 2.4 |
| SILAR | 1.1 | Cubic/Hexagonal | 2.404 | 0.6 | n | 7% | 2.4 |
| E-ALD | 1.05 | Cubic/Hexagonal | 2.356 | 0.6 | n | 21% | 2.4 |

**Table 3.1:** Summary of results of all characterization techniques with the different techniques.

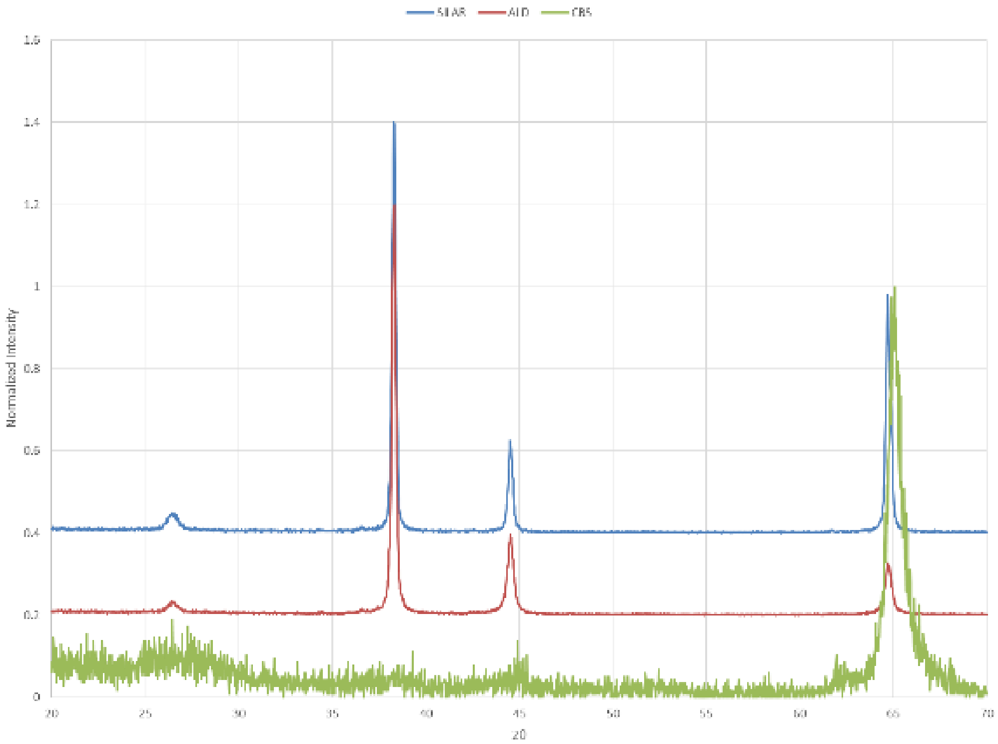

**Figure 3.1:** XRD of CdS grown by the three different deposition techniques.  The incident angle used was 0.5° using Cu $K_{\alpha 1}$ source.

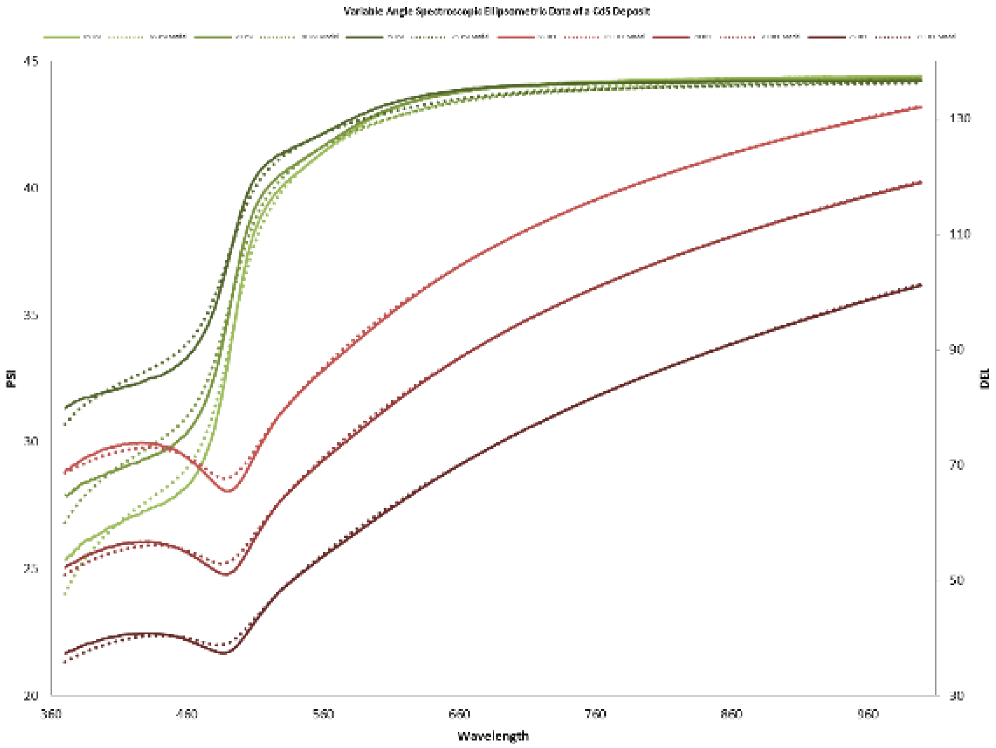

**Figure 3.2:** SE analysis of CdS sample. Green lines represent PSI data red lines represent DEL data. Solid lines represent collected data dashed lines are calculated from the Cauchy model.

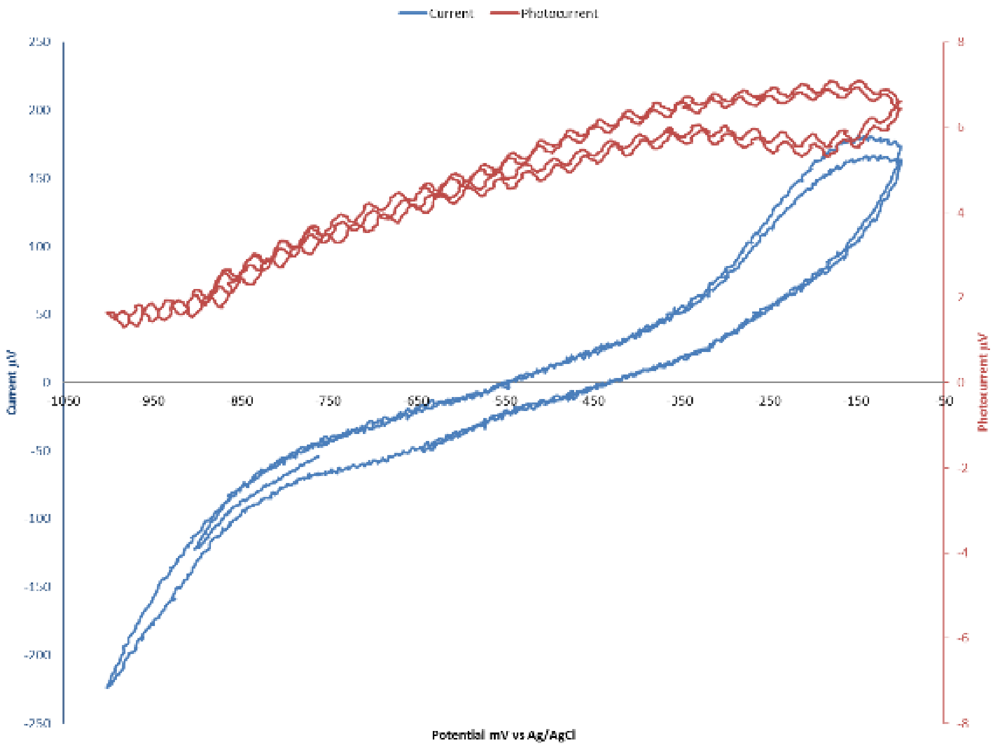

**Figure 3.3:** Photoelectrochemical scan of E-ALD grown CdS in 0.1M $Na_2S$ scan rate 10mV/sec illumined with 532 nm light.

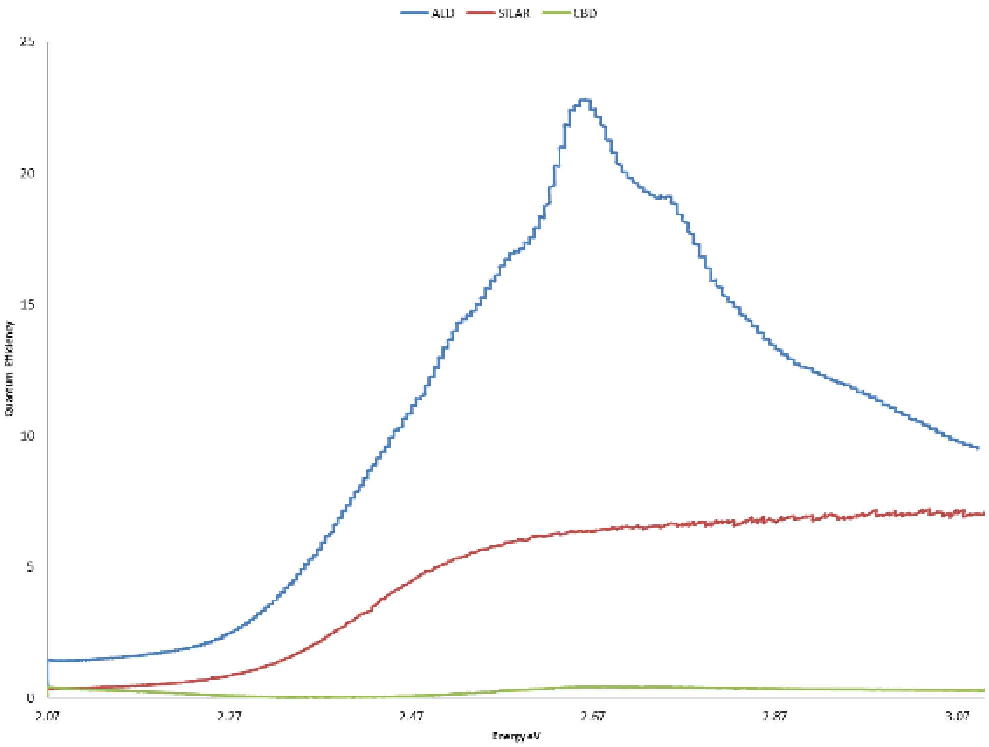

**Figure 3.4:** EQE results of CdS grown by the three different deposition techniques.

# CHAPTER 4

# PRELIMINARY STUDIES OF THE FORMATION OF A PHOTOVOLTAIC (PV) USING ELECTROCHEMICAL ATOMIC LAYER DEPOSITION (E-ALD)[3]

---

[3] B. Perdue, J. L. Stickney , To be submitted to *Journal of the Electrochemical Society (2014)*

## Abstract

Current progress in the formation of a CdTe/CdS photovoltaic by Electrochemical Atomic Layer Deposition (E-ALD) will be presented. Like atomic layer deposition (ALD) E-ALD achieves compound growth by alternating the deposition of atomic layers of each component element using surface limited reactions, however, unlike ALD, E-ALD does this in the condensed phase. The electrochemical surface limited reactions used for compound formation using E-ALD are known as underpotential deposition (UPD). In E-ALD, compounds are formed by the alternating the UPD of one element onto another element. This sequence can be repeated until the deposit has reached its desired thickness. E-ALD allows for the optimization of solution composition, pH, and deposition potential for each element used in the E-ALD cycle. In this study PV were fabricated in both the substrate and superstrate configurations. In this study devices fabricated in the superstrate configuration the indium (Sn) oxide/CdS/CdTe delaminated from the glass most likely due to excessive strain between the layers. PV fabricated in the substrate configuration with Au on glass serving as the back contact had 200 nm (~600cycles) of E-ALD grown CdTe, 80 nm of CBD grown CdS, and 100 nm magnetron sputtered ITO to serve as to front contact. Cells achieve a maximum current density of 0.65 mA/cm$^2$ comparable to modern devices with 1/10th the material; however appear to suffer from shunts. Work on these defects is underway.

## Introduction

The photovoltaic effect was discovered in 1839 by Edmond Becquerel. After the introduction of silicon as the prime semiconductor material in the late 1950s, silicon photovoltaic (PV) diodes became available. The oil crisis of 1973 led to the public awareness of the limitation of fossil fuels, and as a result many programs were commissioned to search for alternative energy sources, including PV solar energy[1,2].

The rise of oil prices caused the reevaluation of the issues dealing with energy supply and demand. In the 20th century, the population quadrupled, causing the demand for energy to increase 16 fold. The exponential increase in energy demand is exhausting nonrenewable fossil fuel supplies. About 13 terawatts (TW)/year of energy are currently needed to sustain the present lifestyle of 6.5 billion people in the world[3].

In order to meet the increasing demand for energy in the near future, we are forced to seek environmentally clean alternatives Renewable energy can be tapped from the available resources to help combat this problem. Solar energy striking the earth (120,000 TW) stands out as the only viable means of meeting our future energy demands[3]. Covering 0.1% of the earth's surface with solar cells at 10% efficiency would satisfy our current energy needs

PV materials are typically inorganic semiconductors, which form suitable junctions which exhibit a PV effect when exposed to light. If possible, the absorber material of an efficient single junction terrestrial thin film solar cell should be a direct bandgap semiconductor with a bandgap of about 1.5 eV (826 nm)[2,4-8], with a high solar optical absorption and quantum efficiency. In the simplest case, a pure elemental PV would be desirable because pure elements are easier to work with than compounds, for example Si PV. However there are no elemental semiconductors with a direct bandgap close to 1.5 eV. Silicon is an indirect band gap material with a bandgap of 1.1 eV. However, silicon is presently the most important PV material, despite its drawbacks.

A low cost method of manufacturing PV materials needs to be developed if it is to be a viable solution to the world's energy problems. A possible low cost manufacturing technique is electrochemical atomic layer deposition (E-ALD). E-ALD was pioneered by this group and is a form of condensed phase atomic layer deposition (ALD) or atomic layer epitaxy (ALE)[9,10]. This technique is being developed to improve electrodeposit morphology, crystallinity and stoichiometry and prevent 3D growth. As with ALD, E-ALD uses surfaces limited reactions to grow compounds one atomic layer at a time. A surface limited reaction is a reaction which self terminates when the surface atoms have been covered by the depositing atoms. Electrochemical surfaces limited reactions are known as underpotential deposition (UPD). In UPD, and one element can deposit onto a second at a potential prior to its formal reduction potential. This occurs because it is more thermodynamically stable to deposit onto another element than it is to deposit onto itself. In a typical E-ALD cycle, a solution containing a reactant's electrochemical precursor is introduced to the substrate at a UPD potential. After the reaction is completed the solution is rinsed away using a blank solution, and a new solution containing a precursor for the next element is introduced at its UPD potential. After the reaction is complete, and the solution is rinsed from the cell, one cycle has been completed resulting in the formation of one compound bilayer. The thickness of the deposited is determined by the number of E-ALD cycles performed. This layer by layer Frank-van der Merwe growth affords superior control over thickness, homogeneity, crystallinity, and the overall quality of the deposit. E-ALD has been used in the Stickney group to grow a variety of semiconductors which include the II-VI compounds CdS and CdTe[9-22]. This pair represents a popular setup for a thin film photovoltaic.

## Experimental

In these studies the films were grown using an automated flow cell system using a three electrode cell using a 3M Ag/AgCl reference electrode controlled by a potentiostat. The basic setup for this procedure has the bottles containing the precursor solutions incased in a box so that the solution and the box can be purged of oxygen by nitrogen bubbling, with the $N_2$ box helping minimizing $O_2$ in the system. These bottles are hooked up to a valve block, with its outlet connected to the electrochemical flow cell. The outlet of the cell is attached to a peristaltic pump, which facilitates sucking solutions through the cell. The potentiostat, valves and the pump are controlled by a PC running SEQUENCER 4 software (Electrochemical ALD L.C., Athens GA). More details on the flow cell can be found in previous publications[11,12,15,18,19]. The electrodes used in these studies were polycrystalline Au on glass, with a 50 nm Ti adhesion layer, purchased from Evaporated Metal Films.

Cd was electrodeposited from a solution containing 0.5 mM $CdSO_4$ in 0.5 M $NaClO_4$, pH 3. Te was electrodeposited from one of two solutions. The first being 0.1mM $TeO_2$ in 0.5 M $NaClO_4$, pH 3, or 0.1 mM $TeO_2$ in 0.5M $NaClO_4$ buffered with 50 mM sodium borate pH 9. Due to the limited solubility of $TeO_2$ in water, it needs to be first dissolved in concentrated $H_2SO_4$ or NaOH, before diluting to the final volume and pH. The blank consisted of 0.5 M $NaClO_4$, pH 3 and its purpose was to rinse out the cell of any precursors from previous solutions. All solutions were made with 18 MΩ water supplied from a Milipore water flirtation system. The electrochemical precursors were purchased from Alfa Æsar with a purity of 99.999%

Three different cycles were examined in this work: one using an acidic Te solution, one using an acidic Te solution together with a reductive Te stripping step, and one using a basic Te solution, no stripping step. For the E-ALD deposition of CdTe with acidic Te chemistry, the cycle can be broken down into 2 steps. The first step involved $Cd^{2+}$ ions being pumped into the cell at a 18 $\frac{mL}{min}$ for 5 seconds at a potential of -550mV. That was followed by holding the solution without flowing for 15 seconds of deposition, at the same potential, and allowing the system to come to equilibrium. The $Cd^{2+}$ ions were then rinsed from the cell with the blank solution for 15 seconds, concluding Cd deposition. For the Te step, a solution of $HTeO_2^+$ ions are pumped into the cell for 5 seconds at a potential of -200mV. This is followed by a quiescent deposition for 15 seconds, at the same potential. The $HTeO_2^+$ ions are then rinsed from the cell, using the blank solution, for 15 seconds, completing this E-ALD cycle for CdTe. Upon completion of an E-ALD cycle, approximately one compound bilayer of CdTe should have been electrodeposited. Some minor variations to this cycle are made, depending on the Te chemistry used. If a stripping steps is included at the end of the cycle, the Te deposition was shifted 100 mV more negative. The stripping step involves first rinsing with blank and then stepping the potential to -900mV for 15 seconds, where Te atoms in excess of an atomic layer are reduced to a soluble telluride species, which diffuse away. This is followed by rinsing again with blank for 15 seconds at the same potential to remove the telluride products. When using the basic Te chemistry the only difference is that the Te deposition potentials changes to -800 mV

The CdS layer was deposited by means of E-ALD, successive ionic layer absorption and reaction (SILAR), and chemical bath deposition (CBD). The solutions used for the E-ALD and SILAR experiments were the same. The cadmium solution used was a 0.5 mM $CdSO_4$ in 0.5M $NaClO_4$, pH 3 solution. The cadmium salt used was $3(CdSO_4)8H_2O$ 99.999% pure purchased from Alfa Æsar. The sulfur solution used was a 0.5mM $Na_2S$ in 0.5M $NaClO_4$, pH 10.3. The sulfur salt used was $Na_2S$ $9H_2O$ 99.99% purchased from Sigma Aldrich. Two blanks were prepared for this work both consisted of 0.5 M NaClO4 one of pH 3 for the cadmium blank and the other was a pH 10 for the sulfur blank.

The deposition cycle used for the E-ALD and SILAR process was as follows. The Cd solution was pumped into the cell at a rate of 18 $\frac{mL}{min}$for 10 seconds at a potential of -500mV. This was followed by a quiescent deposition step that lasted 15 seconds. The excess $Cd^{2+}$ ions were rinsed from the cell by pumping in the pH 3 blank solution for 20 seconds while maintaining the same potential. Next the sulfide solution was pumped into the cell at a rate of 18 $\frac{mL}{min}$ for 10 seconds at a potential of -600mV. This was followed by a quiescent deposition step that lasted 15 seconds at the same potential. The excess $S^{2-}$ ions were removed from the cell by pumping in the pH 10 blank solution for 20 seconds while maintaining the potential at -500mV. The difference between the E-ALD cycle and the SILAR cycle was the lack of potential control, the SILAR deposition process was done at open circuit.

The chemical bath used to deposit CdS in these studies was adapted from the procedure Chu et al used[23,24]. This was done because this procedure led to a high efficiency PV as stated earlier. This bath consisted of $Cd(Acetate)_2$ 99.999% pure purchased from Alfa Æsar, reagent grade ammonium acetate, reagent grade Ammonia, and 99.9% pure Thiosurea purchased from Sigma Aldrich. The CdS CBD was carried out by adding 8mL of 0.033 M $Cd(Acetate)_2$, 5 mL of 1M ammonium acetate, and 15 mL of concentrated ammonia added drop wise to prevent Cd precipitation. This mixture was diluted into 550 mL nanopure 18MΩ water and heated to 80°C. Once the temperature had reach equilibrium 8mL of 0.067M thiourea was added drop wise with a burette. This mixture was then reacted for 40 min.

Two types of ITO was used in this study. The first was 50 nm ITO on borosilicate glass purchased from DELTA. The second type of ITO was deposited with a KJ Lesker PVD 75 magnetron sputter. The growth conditions used a mixed gas with Ar as the primary sources with $Ar/O_2$ (90/10) slaved at 5% of the total supplied pressure which was 10 mtorr. The deposition power was 100 watts and the deposition lasted for an hour. This process resulted in an ITO layer of 100 nm confirmed with spectroscopic ellipsometry. The ITO films were then annealed at

300°C in a nitrogen atmosphere to increase conductance. After the annealing step the resistance was 10Ω over a cm.

## Results and Discussion

### Superstrate Configuration

The superstrate configuration implies that growth will occur from the front contact and will end with the back contact. Since most PV devices are made with high temperature high vacuum deposition processes it is a popular configuration to fabricate PV. The process can start on a borosilicate glass slide coated with a transparent conducting oxide (TCO) such as indium tin oxide (ITO) or fluorine doped tin oxide (FTO). This substrate also is safe to anneal at high temperatures with little migration occurring between layers.

TCOs presents a unique problem for electrodeposition. TCOs conduct macroscopically, however, conduction at the surface is a different issue. The majority of the surface will be an oxide which will not conduct. Only small isolated areas on the surface may conduct which may be the start of nucleation sites which may Ostwald ripen into films. The adhesion of such a film may not be very good and if subject to too much stress may delaminate. Another issue of TCOs serving as electrodes is their electrochemical stability. If the potential used is too negative the electrode may reduce from the oxide to the metallic state and in the process running the contact. If the potential for deposition is poised too positive the dopant may be oxidized out ruining the conductivity of the film.

With this in mind SILAR and CBD CdS were grown onto ITO substrates as they are not electrochemical processes and can be done without damaging the substrate. A representative absorbance spectrum of CdS on ITO is shown in Figure 4.1. This spectrum displays two important spectral features. The first is the sharp absorption starting at about 530 nm. This absorption is due to the deposited CdS layer. The second spectral feature occurring at 380 nm could be one of two things. The first is dynamic scattering off of small particles. The second is that it is absorption by the ITO layer. However since the spectrophotometer was referenced with an ITO substrate it is more likely that the feature is due to scattering off of small particles. There is little difference between SILAR and CDS deposits, the major is that CBD deposits exhibit more particle scattering. This is consistent with observations made with an optical microscope. CBD deposits are visibly rough with a 20x objective while SILAR deposits appear rough with the 100x objective. In order to decrease roughness post deposition annealing treatments were examined.

Both annealing and $CdCl_2$ treatments were investigated. When samples were annealed at 400°C for 30 min in a nitrogen atmosphere. The samples were analyzed again with absorbance. To the eye the color of the deposits changed from yellow to a darker yellow/ burnt orange color. This was confirmed with absorbance shown in Figure 4.2. Spectrum shows a red shift. The behavior is expected and documented in literature[25-30]. This phenomenon is expected because the smaller crystallites Ostwald ripen into larger crystallites when annealed which lowers the energy of the photon absorbed thus shifting the absorption edge. Larger crystallites are beneficial for PV because the produce less grain boundaries where charge carriers can become trapped causing decreased performance in the cell.

The $CdCl_2$ treatment is popular because it removes pinholes and promotes CdS grain growth[25,28,31-34]. CdS on ITO samples were dipped into a saturated $CdCl_2$ solution in methanol for one minute and subsequently anneal at 400°C for 30 min in a nitrogen atmosphere. $CdCl_2$ treated substrates show a similar absorbance transition as well as the expected hexagonal recrystallization in XRD. These avenues were explored in hopes to fabricate a working PV however the goal of this work is to fabricate a PV using deposition techniques such that no post deposition anneal processes would be needed.

With the TCO and CdS window layer finished the CdTe absorber layer had to be deposited to complete the PV. Typical CdTe based PV use around 2-3μm of CdTe[2]. The vast majority of this material is wasted because exciton created outside the depletion zone are expected to recombine before separating, thus not contributing to photocurrent. This sparked the genesis of what is known as the ultra-thin absorber based PV[35-39]. Ultra-thin absorber based PV utilize around 200-500 nm of material in hopes that the depletion zone spans the entire absorber layer. This is beneficial for the E-ALD process because its growth rate is slow when compared to other methods of deposition. It would take approximately 5 days of continuous growth to achieve 2μm, so for E-ALD 200-500 nm is more manageable.

E-ALD CdTe was grown onto the glass/TCO/CdS substrates. In total there were 6 different types, as deposited annealed, $CdCl_2$ treated with CBD and SILAR CdS, Despite the differences in treatments all devices showed the same result, delamination of the film. This was demonstrated in three ways: reduction of deposition current, visible holes in the deposit and absence of signal in EMPA. This is shown in Figure 4.3. Figure 4.3 a) shows the optical microscope image shows that in the deposition area the film delaminated leaving behind small islands of deposit. The EPMA elemental mapping shows the same result. Figure 4.3 c) shows small islands of deposit with nothing but glass in between. It is believed that the cause of this is stress and poor film adhesion. It is well known that the lattice mismatch between CdTe and CdS is about 10%. This puts a lot of stress on the crystal which could cause a buckling of the film if it is not properly bound to the substrate. Absorbance measurements also indicate that the structure was under so much stress that the ITO layer was removed from the glass as well. E-

ALD grown CdTe is very crystalline as deposited, ost cases this is an advantage, however, in this case it was a disadvantage because it caused too much stress. The stress of crystal growth caused a delamination of the CdS and the underlying ITO. From this we concluded that fabricating a PV with E-ALD grown materials may not be suited for the superstrate configuration.

Substrate Configuration

In the substrate configuration growth starts from the back contact then finishes with the front contact. This configuration is less popular because it is difficult to deposit good quality TCO without the use of a post deposition anneal step. This post deposition anneal step could allow for inter diffusion between layers which would have an adverse effect on the quality of the PV. Despite these drawbacks the substrate configuration is best suited for electrodeposition because you can start with a conductive substrate rather than an oxide. Electrodeposition allows for strong film adherence to the substrate because it is covalently bound to it. So in the substrate configuration film delamination should not be a problem.

The proposed substrate fabrication method is shown in Figure 4.4. Assuming the completion of an E-ALD cycle results in the deposition of 0.4 nm, 600 cycles will give a CdTe thickness of about 240 nm consistent with an ultra-thin absorber. Nail polish was used as a mask to prevent shorts. In this study CBD CdS was used because photoactivity in the window layer is parasitic to the performance to the photovoltaic[40]. So the least photoactive lowest quality of CdS was chosen for fabrication. The ITO deposition process required the deposits to be transferred to a clean room. It is possible that the power used for ITO deposition was too intense and some ITO would be imbedded into the CdS window layer.

The PV devices was tested after the ITO deposition process. Results are shown in Figure 4.5. Results show that the PV devices have a response to light. The current density is two orders of magnitude too low when compared to modern PV cells.  This is to be expected because the conductance of the ITO film without a post deposition anneal step is very poor.  It is possible that the PV is experiencing too much impedance to function properly.  In hopes to improve the performance of the PV the sample was annealed at 300°C for 10 min in a nitrogen atmosphere.

After the annealing step the performance of the PV increased.  The IV curves are shown in Figure 4.6.  The anneal step increased the produced a 100 fold increase in current.  The current produced by the PV is on the order of magnitude of modern CdTe PV with 1/10 the material. However despite the increase in current the open circuit voltage is severely lacking.  The lack of voltage is a strong indication that our PV is suffering from shorts.  This means that the chemistry works yet the fabrication process needs improvement to eliminate the shunts

## Conclusion

PV were fabricated in the substrate and superstrate configurations using E-ALD grown materials.  When devices were fabricated in the superstrate configuration, devices were delaminated from the glass most likely do to strain across the layers no matter the type of ITO or CdS used. PV fabricated in the substrate achieve a maximum current density of 0.65 mA/cm2 when exposed to light; however appear to suffer from shunts which lowered the open circuit voltage.   Work on these defects is underway.  Despite these shortcoming a PV was produced with a high current density with a 1/10 of the material used in current PV devices.

# References

(1) Shah, A.; Torres, P.; Tscharner, R.; Wyrsch, N.; Keppner, H. *Science* **1999**, *285*, 692.

(2) Birkmire, R. W.; Eser, E. *Annual Review of Materials Science* **1997**, *27*, 625.

(3) Kamat, P. V. *Journal of Physical Chemistry C* **2007**, *111*, 2834.

(4) Bosio, A.; Romeo, N.; Mazzamuto, S.; Canevari, V. *Progress in Crystal Growth and Characterization of Materials* **2006**, *52*, 247.

(5) Omura, K.; Hanahusa, A.; Arita, T.; Higuchi, H.; Aramoto, T.; Nishio, T.; Sibutani, S.; Kumazawa, S.; Murozono, M.; Yabuuchi, Y.; Takakura, H. *Renewable Energy* **1996**, *8*, 405.

(6) Kazmerski, L. L. *Journal of Electron Spectroscopy and Related Phenomena* **2006**, *150*, 105.

(7) Chu, T. L.; Chu, S. S. *Solid-State Electronics* **1995**, *38*, 533.

(8) Chopra, K. L.; Paulson, P. D.; Dutta, V. *Progress in Photovoltaics* **2004**, *12*, 69.

(9) Gregory, B. W.; Stickney, J. L. *Journal of Electroanalytical Chemistry* **1991**, *300*, 543.

(10) Gregory, B. W.; Suggs, D. W.; Stickney, J. L. *Journal of the Electrochemical Society* **1991**, *138*, 1279.

(11) Flowers, B. H.; Wade, T. L.; Garvey, J. W.; Lay, M.; Happek, U.; Stickney, J. L. *Journal of Electroanalytical Chemistry* **2002**, *524-525*, 273.

(12) Lay, M. D.; Stickney, J. L. *Journal of the Electrochemical Society* **2004**, *151*, C431.

(13) Villegas, I.; Stickney, J. L. *Journal of the Electrochemical Society* **1991**, *138*, 1310.

(14) Varazo, K.; Lay, M. D.; Sorenson, T. A.; Stickney, J. L. *Journal of Electroanalytical Chemistry* **2002**, *522*, 104.

(15) Colletti, L. P.; Flowers, B. H.; Stickney, J. L. *Journal of the Electrochemical Society* **1998**, *145*, 1442.

(16) Lay, M. D.; Sorenson, T. A.; Stickney, J. L. *J. Phys. Chem. B* **2003**, *107*, 10598.

(17) Venkatasamy, V.; Jayaraju, N.; Cox, S. M.; Thambidurai, C.; Happek, U.; Stickney, J. L. *J. Appl. Electrochem.* **2006**, *36*, 1223.

(18) Colletti, L. P.; Stickney, J. L. *Journal of the Electrochemical Society* **1998**, *145*, 3594.

(19) Huang, B. M.; Colletti, L. P.; Gregory, B. W.; Anderson, J. L.; Stickney, J. L. *Journal of the Electrochemical Society* **1995**, *142*, 3007.

(20) Suggs, D. W.; Stickney, J. L. *Surface Science* **1993**, *290*, 375.

(21) Colletti, L. P.; Teklay, D.; Stickney, J. L. *Journal of Electroanalytical Chemistry* **1994**, *369*, 145.

(22) Gregory, B. W.; Norton, M. L.; Stickney, J. L. *Journal of Electroanalytical Chemistry* **1990**, *293*, 85.

(23) Chu, T. L.; Chu, S. S.; Ferekides, C.; Wu, C. Q.; Britt, J.; Wang, C. *J. Appl. Phys.* **1991**, *70*, 7608.

(24) Chu, T. L.; Chu, S. S.; Schultz, N.; Wang, C.; Wu, C. Q. *Journal of the Electrochemical Society* **1992**, *139*, 2443.

(25) Kampmann, A.; Lincot, D. *Journal of Electroanalytical Chemistry* **1996**, *418*, 73.

(26) Metin, H.; Erat, S.; Durmus, S.; Ari, M. *Applied Surface Science* **2010**, *256*, 5076.

(27) Metin, H.; Erat, S.; Emen, F. M.; Kafadar, V.; Yazici, A. N.; Ari, M.; Kulcu, N. *Journal of Luminescence* **2010**, *130*, 1531.

(28) Ringel, S. A.; Smith, A. W.; Macdougal, M. H.; Rohatgi, A. *J. Appl. Phys.* **1991**, *70*, 881.

(29) Sahay, P. P.; Nath, R. K.; Tewari, S. *Crystal Research and Technology* **2007**, *42*, 275.

(30) Sankapal, B. R.; Mane, R. S.; Lokhande, C. D. *Materials Research Bulletin* **2000**, *35*, 177.

(31) Dhere, R. G.; Al-Jassim, M. M.; Yan, Y.; Jones, K. M.; Moutinho, H. R.; Gessert, T. A.; Sheldon, P.; Kazmerski, L. L. *J. Vac. Sci. Technol. A-Vac. Surf. Films* **2000**, *18*, 1604.

(32) Li, W. Y.; Cai, X.; Chen, Q. L.; Zhou, Z. B. *Materials Letters* **2005**, *59*, 1.

(33) Paulson, P. D.; Dutta, V. *Thin Solid Films* **2000**, *370*, 299.

(34) Rose, D. H.; Hasoon, F. S.; Dhere, R. G.; Albin, D. S.; Ribelin, R. M.; Li, X. S.; Mahathongdy, Y.; Gessert, T. A.; Sheldon, P. *Progress in Photovoltaics* **1999**, *7*, 331.

(35) Gupta, A.; Parikh, V.; Compaan, A. D. *Solar Energy Materials and Solar Cells* **2006**, *90*, 2263.

(36) Jones, E. W.; Barrioz, V.; Irvine, S. J. C.; Lamb, D. *Thin Solid Films* **2009**, *517*, 2226.

(37) Krishnakumar, V.; Barati, A.; Schimper, H. J.; Klein, A.; Jaegermann, W. *Thin Solid Films* **2013**, *535*, 233.

(38) Marsillac, S.; Parikh, V. Y.; Compaan, A. D. *Solar Energy Materials and Solar Cells* **2007**, *91*, 1398.

(39) Matin, M. A.; Amin, N.; Zaharim, A.; Sopian, K. *Ultra Thin High Efficiency CdS/CdTe Thin Film Solar Cells from Numerical Analysis*, 2009.

(40) Cunningham, D.; Rubcich, M.; Skinner, D. *Progress in Photovoltaics* **2002**, *10*, 159.

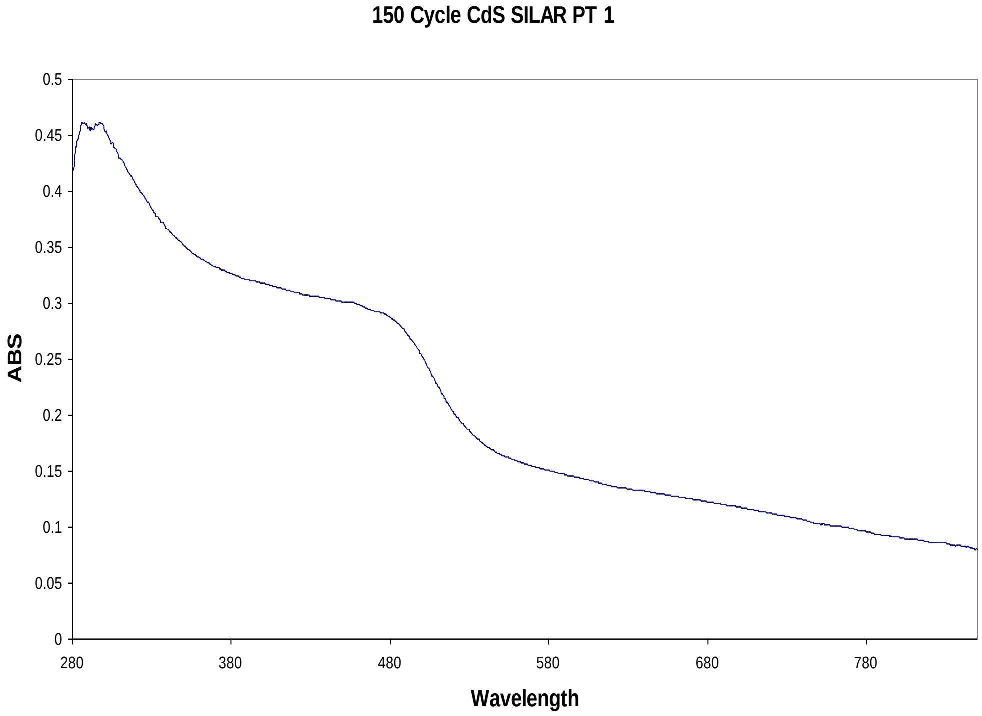

**Figure 4.1:** Absorbace spectrum of CdS onto ITO. Spectrum was blanked on the same piece of ITO

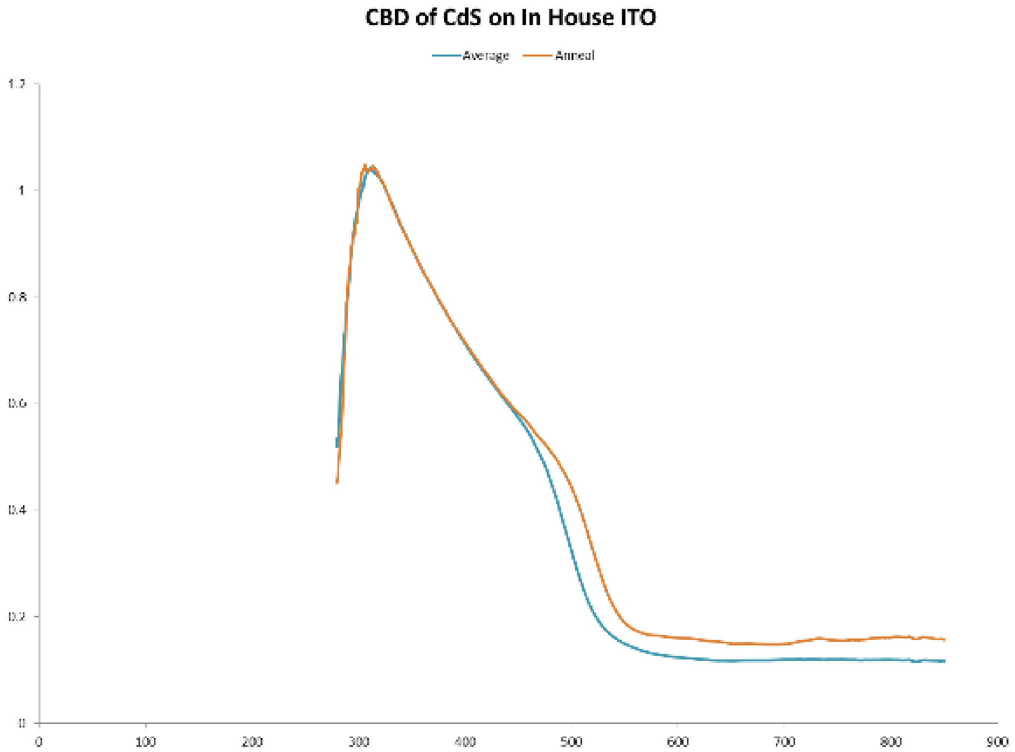

**Figure 4.2:** Effect of annealing on CdS deposited on ITO. The blue scan was as deposited the orange scan was after annealing treatment. Spectrum was blanked on the same piece of ITO

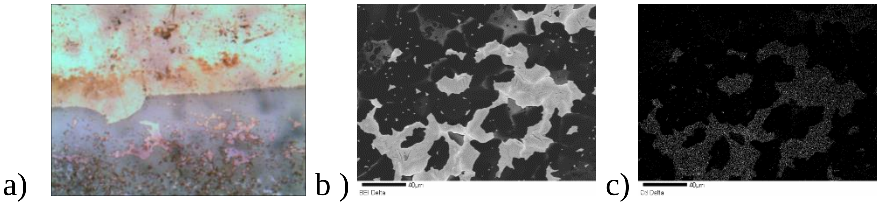

**Figure 4.3:** a) An optical microscope of a Glass/ITO/CdS/CdTe deposit magnified 1000x. The pale blue area is where the deposit broke apart and flaked off. b) Backscattered electron image of Glass/ITO/CdS/CdTe. c) Cd Elemental map of Glass/ITO/CdS/CdTe showing that the deposit has broken apart

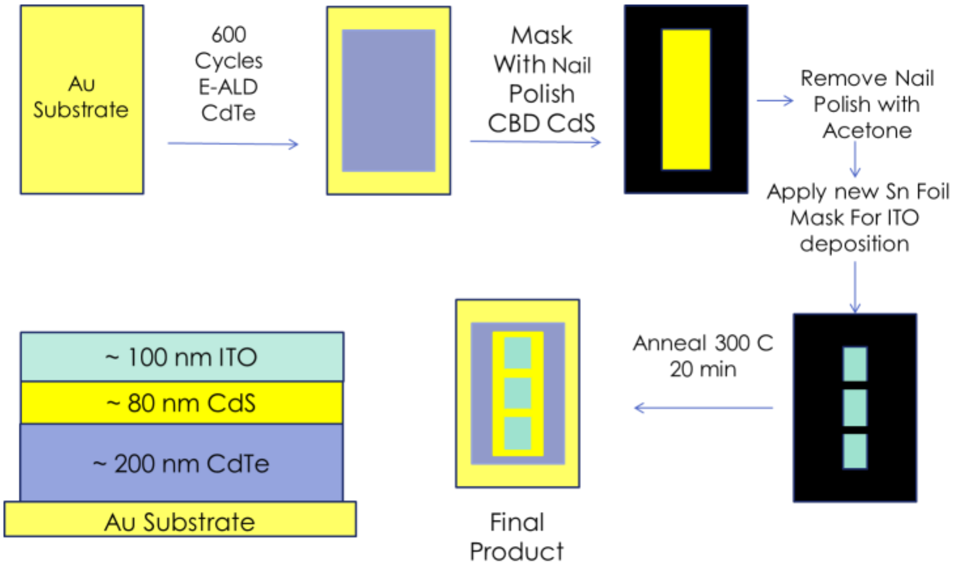

**Figure 4.4:** Proposed substrate configuration fabrication flowchart

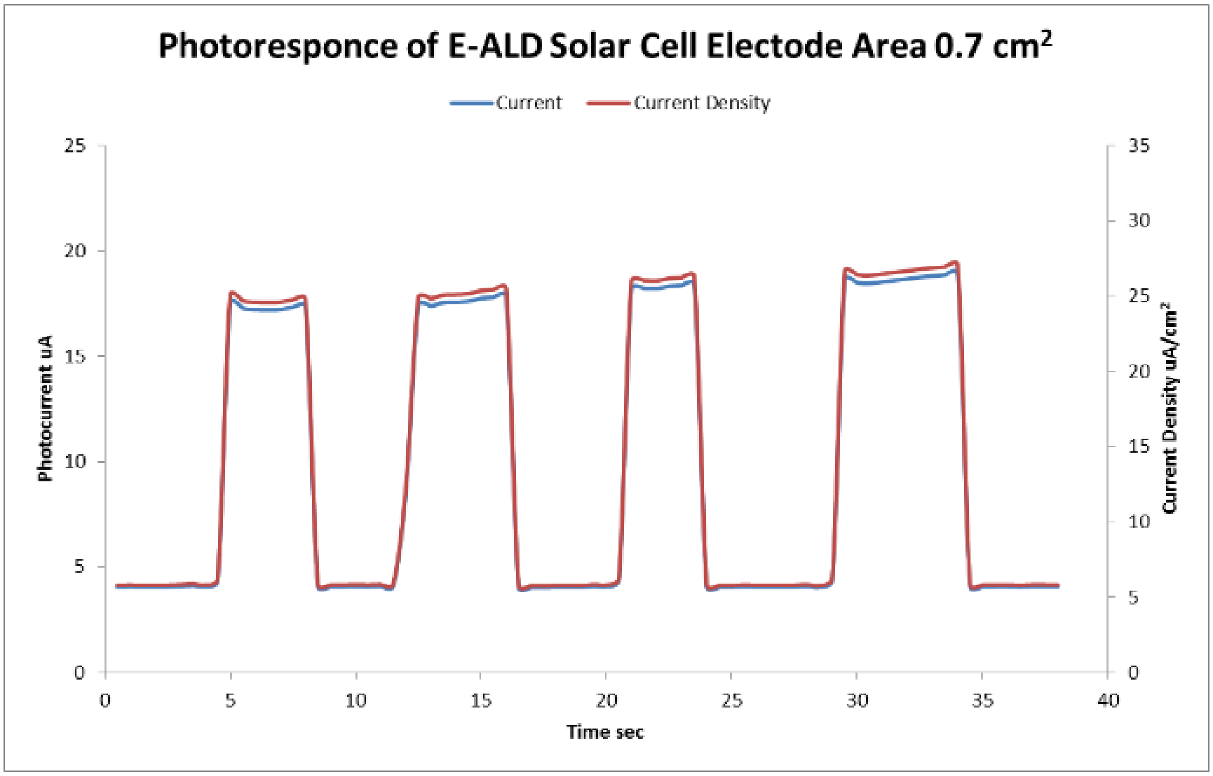

**Figure 4.5:** Response to as deposited E-ALD PV to light. Structure was illuminated with AM 1.5 light and the current was measured as a function of time

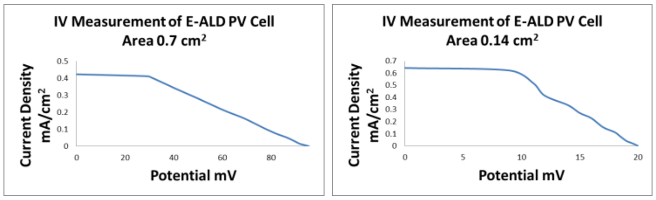

**Figure 4.6**: I-V measurements of two different E-ALD PV illuminated with AM 1.5 light.

# CHAPTER 5

# ELECTROCHEMICAL ATOMIC LAYER DEPOSITION (E-ALD) OF CDTE ONTO DIFFERENT ELEMENTS

---

[4] B. Perdue, J. L. Stickney , To be submitted to *Journal of the Electrochemical Society (2014)*

## Abstract

The growth of CdTe by E-ALD by different chemistries onto different metal and semiconductor substrates is discussed. Like atomic layer deposition (ALD) E-ALD achieves compound growth by alternating the deposition of atomic layers of each component element using surface limited reactions, however, unlike ALD, E-ALD does this in the condensed phase. The electrochemical surface limited reactions used for compound formation using E-ALD are known as underpotential deposition (UPD). In E-ALD, compounds are formed by the alternating the UPD of one element onto another element. This sequence can be repeated until the deposit has reached its desired thickness. E-ALD allows for the optimization of solution composition, pH, and deposition potential for each element used in the E-ALD cycle. The scope of this work was to investigate the influence substrate chemistry has on the deposition process. The substrates used in this study were Au, Ni, Cu, Ag, Ge, and Mo. Deposits of 100 E-ALD cycles were examined with various thin film characterization techniques including electron probe microanalysis (EPMA) X-ray diffraction (XRD) and spectroscopic ellipsometry (SE). Results show that when the substrate can oxidatively dissolve into ions, the resulting deposit is of lesser quality, whereas deposits grown on passivated substrates are of very high quality. The loss of quality is believed to be caused by the ions from the substrate codepositing as a chalcogenide compound impurity.

## Introduction

Cadmium Telluride CdTe is a versatile II-IV compound which has uses in many different optoelectronic fields[1]. One of the applications where CdTe excels is as a terrestrial solar absorber. CdTe is a direct gap semiconductor with a sharp optical absorption edge and large absorption coefficient at above bandgap wavelengths[2]. As a result about 1 μm of CdTe is sufficient to absorb 99% of the impinging radiation with photon energy higher than the bandgap energy[2,3]. The bandgap of CdTe is 1.5eV which is ideally for a single junction photovoltaic for terrestrial absorption, allowing 95% conversion of the theoretical maximum[4,5]. CdTe is not without issues. Cd is toxic and both Cd and Te are not earth abundant, so it is imperative that the amount used in photovoltaics (PV) be minimized.

Electrodeposition is technique which allows for uniform conformal deposits. Electrodeposition holds promise as a low cost, flexible room temperature technique for the production compound semiconductors. This technique has been applied to many II-IV compounds as well as CIS and CIGS[1,6]. A process was developed by Kroger[7] and Panicker[8] in which near stoichiometric CdTe was reductively deposited from on bath containing precursors for both Cd and Te. This process showed such promise that is was eventually commercialized by BP[9]. Unfortunately deposits fabricated by this method require annealing to produce PV grade material due to its poor crystallinity and to cover it from n-type, as deposited, to p-type as used in PV.

Electrochemical atomic layer deposition (E-ALD) was pioneered by this group and is a form of condensed phase atomic layer deposition (ALD) or atomic layer epitaxy (ALE)[10,11]. This technique is being developed to improve electrodeposit morphology, crystallinity and stoichiometry and prevent 3D growth. As with ALD, E-ALD uses surfaces limited reactions to grow compounds one atomic layer at a time. A surface limited reaction is a reaction in which the deposition self terminates when the surface atoms have been covered by the depositing atoms resulting in an atomic layer. Electrochemical surfaces limited reactions are known as underpotential deposition (UPD). In UPD, and one element can deposit onto a second at a potential prior to its formal reduction potential. This occurs because it is more thermodynamically stable to deposit onto another element than it is to deposit onto itself. In a typical E-ALD cycle, a solution containing a reactant's electrochemical precursor is introduced to the substrate at a UPD potential. After the reaction is completed the solution is rinsed away using a blank solution, and a new solution containing a precursor for the next element is introduced at its UPD potential. After the reaction is complete, and the solution is rinsed from the cell, one cycle has been completed resulting in the formation of one compound bilayer. The thickness of the deposited is determined by the number of E-ALD cycles performed. This layer by layer Frank-van der Merwe growth affords superior control over thickness, homogeneity, crystallinity, and the overall quality of the deposit. E-ALD deposition of CdTe has been studied by this group[11-20] and Foresti[21] so much is known about this system.

The goal of this work is to investigate the influence the electrode material has on the E-ALD process. A total of five different types of substrates were used ranging from valve metals to semiconductors. The quality of the deposits were tested with EPMA, XRD, and SE.

## Experimental

In these studies the films were grown using an automated flow cell system using a three electrode cell with a Ag/AgCl reference electrode controlled by a potentiostat. The basic setup for this procedure has the bottles containing the precursor solutions incased in a box so that the solution and the box can be purged of oxygen by nitrogen bubbling, with the $N_2$ box helping minimizing $O_2$ in the system. These bottles are hooked up to a valve block, with its outlet connected to the electrochemical flow cell. The outlet of the cell is attached to a peristaltic pump, which facilitates sucking solutions through the cell. The potentiostat, valves and the pump are controlled by a PC running SEQUENCER 4 software (Electrochemical ALD L.C., Athens GA). More details on the flow cell can be found in previous publications[12-15,17]. The electrodes used in these studies were polycrystalline Au on glass, with a 50 nm Ti adhesion layer, purchased from Evaporated Metal Films.

Cd was electrodeposited from a solution containing 0.5 mM $CdSO_4$ in 0.5 M $NaClO_4$, pH 3. Te was electrodeposited from one of two solutions. The first being 0.1mM $TeO_2$ in 0.5 M $NaClO_4$, pH 3, or 0.1 mM $TeO_2$ in 0.5M $NaClO_4$ buffered with 50 mM sodium borate pH 9. Due to the limited solubility of $TeO_2$ in water, it needs to be first dissolved in concentrated $H_2SO_4$ or NaOH, before diluting to the final volume and pH. The blank consisted of 0.5 M $NaClO_4$, pH 3 and its purpose was to rinse out the cell of any precursors from previous solutions. All solutions were made with 18 M□ water supplied from a Milipore water flirtation system. The electrochemical precursors were purchased from Alfa Æsar with a purity of 99.999%

Three different cycles were examined in this work: one using an acidic Te solution, one using an acidic Te solution together with a reductive Te stripping step, and one using a basic Te solution, no stripping step. A visual representation of a typical E-ALD cycle can be found in Figure 5.1. For the E-ALD deposition of CdTe with acidic Te chemistry, the cycle can be broken down into 2 steps. The first step involved $Cd^{2+}$ ions being pumped into the cell at 18 $\frac{mL}{min}$ for 5 seconds at a potential of -550mV vs. Ag/AgCl. That was followed by holding the solution without flowing for 15 seconds of deposition, at the same potential, and allowing the system to come to equilibrium. The $Cd^{2+}$ ions were then rinsed from the cell with the blank solution for 15 seconds, concluding Cd deposition. For the Te step, a solution of $HTeO_2^+$ ions are pumped into the cell for 5 seconds at a potential of -200mV vs. Ag/AgCl. This is followed by a quiescent deposition for 15 seconds, at the same potential. The $HTeO_2^+$ ions are then rinsed from the cell, using the blank solution, for 15 seconds, completing this E-ALD cycle for CdTe. Upon completion of an E-ALD cycle, approximately one compound bilayer of CdTe should have been electrodeposited. Some minor variations to this cycle are made, depending on the Te chemistry used. If a stripping steps is included at the end of the cycle, the Te deposition was shifted 100 mV more negative. The stripping step involves first rinsing with blank and then stepping the potential to -900mV for 15 seconds, where Te atoms in excess of an atomic layer are reduced to a soluble telluride species, which diffuse away. This is followed by rinsing again with blank for 15 seconds at the same potential to remove the telluride products. When using the basic Te chemistry the only difference is that the Te deposition potentials changes to -800 mV.

100 E-ALD cycle deposits were performed using the three different deposition chemistries, and the resulting deposits were analyzed using a variety of thin film characterization techniques. The stoichiometry of the deposits were investigated using electron probe microanalysis (EPMA) on a JEOL 8600 SUPERPROBE with a 10 KeV accelerating voltage 15 nA beam current and a 10 um beam diameter. Using the large beam helped to average slight sample inhomogeneities. Deposit crystallinity was examined on a PANanalytical X'PERT Pro with an open eulerian cradle utilizing a 1.54 nm Cu K□$_1$ source and a parallel plate collimator. Optical properties of the deposits were analyzed using a spectroscopic ellipsometer (SE), JA Woolam M-2000V.

## Results and Discussion

The E-ALD process allows for the optimization of the solutions for each of the electroactive species. The concentration, pH, buffering, and potential can be adjusted accordingly for each solution. This is one of E-ALD's great advantages, however, the reactivity of the electrode comes into play at some point. The Nernest equation dictates that the concentration of ions at the surface of the electrode cannot be zero. These substrate ions have the potential to react with each of the electroactive species causing a potential impurity. This is true to a certain extent, once the electrode is covered by the deposited compound this should no longer be a problem. The goal of this work was to investigate this. A summary of results can be found in Table 5.1.

In Table 5.1 the first column refers to the growth rate in monolayers/cycle and the second is the index of refraction at 632 nm. Both of these values were calculated from the data collected from SE. Ellipsometry measurements used three and in some cases four angles which were made above, at, and below the Brewster angle for the underlying substrate. This was done so the maximum and most relevant information could be obtained about the sample. The data was then fitted to the Cauchy equation which relates the thickness as well as optical constants of the material. The growth rate was estimated by using the crystallographic data from XRD and the thickness calculated from the Cauchy equation. The data from the XRD indicated that CdTe grew with a strong preferred (111) orientation. Thus the assumption was made that all thickness was due to growth in the (111) direction. Using geometry it is found that the distance between (111) planes is $\frac{a}{\sqrt{3}}$ where a is the lattice constant of CdTe. The growth rate is estimated by dividing the thickness calculated from spectroscopic ellipsometry by the product of the number of cycles run by $\frac{a}{\sqrt{3}}$ or 0.347 nm.

The final two columns are the Cd/Te ratio calculated from EPMA and the cryptographic information obtained from XRD. The variability of the instrument for the conditions used is translates to a variation of about ±0.1 in the Cd/Te ratio. The XRD information says that despite the initial electrode chemistry the resulting CdTe deposit displays the expected cubic character.

### Au

Au is an ideal electrode for growing films. It is noble and forms a passivating surface oxide layer rather than dissolving into ions. It is so chemically stable that it can be easily cleaned of any surface carbon contamination. The E-ALD growth of CdTe has been extensively studied so much is known about its chemistry. The deposits on Au will serve as a control, where the substrate chemistry is not considered. Results from Table 5.1 show crystalline stoichiometric CdTe despite the deposition chemistry used. The resulting deposits also exhibit the proper optical constants and similar growth rates. High quality deposits can be produced when using these conditions, however, this may be only when substrate chemistry is not taken into account.

### Ni

Ni is a fairly reactive metal. A bulk Ni electrode will oxidatively dissolve when the potential is poised positive of -400 mV vs Ag/AgCl. This is the first instance where the substrate chemistry could affect the resulting CdTe deposit. In the case of the CdTe acidic deposition cycle, the Te deposition potential is -200mV, this would strip the underlying Ni substrate to produce $Ni^{2+}$ ions. These $Ni^{2+}$ ions could subsequently redeposit as NiTe. This process could only occur until the CdTe deposit cover the Ni substrate preventing the oxidative dissolution of the Ni electrode. Results from Table 5.1 show that the deposits produced by this method exhibit a large excess of Te, however, remain crystalline and have close to the proper optical constant. The discrepancy between Ni and Au could be attributed to the stripped Ni ions codepositing with Te ions forming NiTe increasing the relative amount of Te to Cd in the first cycles until the CdTe deposit passivates the underlying Ni.

To circumvent the NiTe codeposition issue, a more negative Te deposition can be used. This was done by using Te stripping chemistry. For Te stripping chemistry a larger overpotential is used to deposit Te then the excess Te is reductively stripped electrochemically by means of a two electron process according to the following reaction $Te + 2e^- \rightarrow Te^{2-}$. The $Te^{2-}$ ions are water soluble and can diffuse away leaving behind a Te layer that is stabilized by compound formation.

This strategy ensures that the Ni will never oxidatively strip which may eliminate the possibility of NiTe codeposition. Deposits made from stripping chemistry still exhibit a slight Te excess as evidenced from Table 5.1. This may suggest that Te has higher affinity for Ni than Au. The same chemistry on a Au electrode did not produce an excess of Te as it did not Ni. The stripping chemistry would need to be optimized for a Ni surface because the stripping chemistry used for Au is not as effective on Ni.

There is one other method to deposit Te at a more negative potential without the use of a stripping step is the use a basic Te solution. Te reduces from $HTeO2^+$ according to the following reaction, $3H^+ + HTeO_2^+ + 4e^- \rightarrow Te + 2H_2O$ making the proton concentration or pH part of the Nernst equation. By raising the pH the deposition potential of Te shifts more negative which ensures that there will be less $Ni^{2+}$ present. Results show that the highest quality CdTe deposits on Ni are made with a basic Te solution. There is a slight excess of Te suggesting that very little NiTe was formed, or that the growth conditions were correct.

Cu

Copper is a coinage metal meaning it is fairly noble. Copper does not oxidatively strip until ~0 mV vs Ag/AgCl as a result it should not have any issues growing CdTe because the most positive potential used in any cycle -200 mV. According the Nernst equation, there will still be a small amount of copper ions present which could react with Te ions to form $Cu_2Te$. Cu forms stable compounds with all of the chalcogenide species, so Te would be no exception.

As a first attempt to grow CdTe on a Cu substrate, the acidic conditions were used and the results from this are shown in Table 5.1. When using an acidic Te solution resulting deposits have very little Cd in them. The resulting deposit behaves more like $Cu_2Te$ than it does CdTe. In this case it would seem that the formation of $Cu_2Te$ is more favorable than CdTe, if this is the case then $Cu_2Te$ would short circuit CdTe formation. The XRD shows a broad peak centered around 24° 2θ. This could be due to mixed phases of $Cu_2Te$ and CdTe whose (111) diffractions occur at 25.2° and 23.7° 2θ respectively. The possible presence of $Cu^{2+}$ ions seemed to have short circuited the E-ALD process in this case.

The acidic chemistry did not work for the Cu substrate it is hypothesized that $Cu^{2+}$ ions interfered with the process. To limit the amount of Cu ions present a more negative deposition potential would be required so basic chemistry was attempted. The basic chemistry dramatically improved the quality of the deposit based on the results shown in Table 5.1. The stoichiometry improved drastically from 0.15 to 0.83, however, there still is a significant Te excess in the deposit. Weather this is due to $Cu_2Te$ or just excess Te deposition it is difficult to determine. The XRD spectrum also shows more CdTe behavior with the major peak occurring around 23.7°. The index of refraction shifted closer to the reported literature value, yet still is slightly different. Again the excess Te being in the form of $Cu_2Te$ or elemental Te could be the cause of this.

Ag

Silver like gold and copper is a fairly stable nonreactive metal. Like copper silver readily forms compounds with the chalcogenides, however, due to silver's more stable nature fewer ions should be present at negative potentials which should prevent undesired compound formation. It was expected to have similar chemical behavior.

The first experiments done on silver electrodes used the basic chemistry. The resulting deposits were very rough and black in color as opposed to smooth and having a purple color. When the deposited is examined with an optical microscope, the deposit has very large bumps as shown in Figure 5.2. When this sample was sent to EPMA it was shown that the deposit were stoichiometric, however the sample was too rough to be grown by a layer by layer process.

These bumps were also examined with EPMA elemental mapping shown in Figure 5.3. This was done to determine whether or not the bumps were AgTe or CdTe. EPMA elemental mapping shows that the bumps are most likely CdTe, as the elemental mapping implies that the bumps are CdTe however it is also possible that they are AgTe coated with CdTe.

Since the basic Te chemistry did not work acidic chemistry was attempted. The potentials used in the acidic deposition are negative enough so that the substrate should not have an effect on the deposition. The acidic chemistry resulted in the same rough deposit. The charge for deposition increased as cycle number increased, consistent with electrochemical roughening. When deposits were examined with EPMA results show that the deposit has practically no Cd. This could be due to the fact that the Cd monolayer is not stable on the Ag surface. When the potential was stepped to -200 for Te deposition a large amount of oxidation was observed. This oxidation could have only been the deposited Cd layer. This was confirmed by examining the current time traces as shown in Figure 5.3.

The E-ALD deposition of CdTe onto Ag seemed to be the most difficult due to the influence of the Ag substrate. If E-ALD CdTe is to be grown onto a Ag surface there would need to be changes to the chemistry. The decreased Cd stability on the Ag surface forces a change in the Te deposition potential meaning the Te deposition potential must be shifted more negative so stripping chemistry must be used. Shifting the Te deposition potential will keep the Cd monolayer stabilized on the surface, however, there still the possibility of AgTe contamination. To avoid this $Cl^-$ was added to the deposition solution. It is well known that $Cl^-$ can stabilize Ag monolayers and by adding it to the deposition solutions should prevent any $Ag^+$ dissolution. If any $Ag^+$ ions are formed should precipitate out at AgCl which if in contact with the electrode would re reduce to Ag metal. The addition of $Cl^-$ should improve the quality of the deposit.

The changes to the chemistry improved the quality of the deposit. The deposits now had color to them as opposed to the black rough bumps, color is evidence of compound formation. The characterization of these deposits are shown in Table 5.1. The ratio calculated from EPMA shows an excess of Te. It is believed that the excess Te is in the form of elemental Te because there are visible chunks when viewed by an optical microscope. The addition of $Cl^-$ improved the deposit morphology, removing the black bumps for compound formation with small elemental Te rocks. Despite these rocks the XRD shows evidence of crystalline CdTe. No Te peaks were observed in the XRD spectrum however they may not be visible due to the limitations of the instrument. SE shows an optical constant essentially that of CdTe, the discrepancy may be explained by the excess of Te present in the deposit. The growth rate of over 1 ML per cycle indicates that the cycle chemistry still needs optimization.

### Ge

Germanium is an important semiconductor for a variety of reasons. It has a low bandgap and can be used in a multijunction photovoltaic. Thus the E-ALD deposition of CdTe onto this semiconductor is very important. Unlike metals, Ge is a semiconductor coated with an oxide surface so a pretreatment is needed before it can be electrodeposited on. The Ge wafer was first etched in HF to remove the surface oxide. The wafer the then ozone cleaned to remove organics and to make a thin surface oxide. This was then placed in the electrochemical cell. Before the E-ALD deposition the surface oxide was reduced at a negative potential. Ge is very reactive so positive potentials could not be used, thus basic Te was used to grow E-ALD CdTe.

The results of the E-ALD CdTe on a Ge wafer are shown in Table 5.1. The data shows a very high quality deposit close to the quality achieved on a Au substrate. Perhaps this is because like Au Ge does not produce any ions to interfere with the deposition process. EPMA shows the deposition of a stoichiometric compound. The reported ratio is within the uncertainty of the machine, however on the low end so it may be possible that there is a very small excess of Te, however, the resulting deposit is essentially stoichiometric. XRD shows a crystalline compound with a peak at 23.7° consistent with CdTe. The peak in the XRD spectrum is very small because it is dwarfed by the single crystal Ge peak. Finally the SE shows an index of refraction consistent with CdTe. The only drawback of growing on Ge is that the growth rate is slow.

### Mo

There has been some preliminary work on the E-ALD deposition onto a Mo substrate. Mo is important because it is a popular back contact metal for PV. Mo is a very reactive valve metal so it has a thick oxide layer that must be removed before it can be electrodeposited on. To do this the Mo electrode was reduced at -1.2V vs Ag/AgCl for five minutes then basic Te chemistry was used because the acidic chemistry would have re oxidized the surface.

The resulting process did not yield a continuous film rather small islands of deposit. The islands though small were CdTe which showed it characteristic blue color. XRD shows a very small peak consistent with CdTe. SE shows an optical constant consistent with CdTe and a slow growth rate akin to Ge. Though the deposit had limited coverage it was good quality.

## Conclusion

The scope of this work was to investigate the influence substrate chemistry plays on the deposition process. The substrates used in this study were Au, Ni, Cu, Ag, Ge, and Mo. 100 cycle deposits of E-ALD CdTe were grown onto each substrate and analyzed with EPMA, XRD and SE.  Results indicate that substrates that can oxidatively dissolve and produce ions (Ni Cu Ag) hinder the E-ALD deposition process and decrease the quality of the film grown.  It is proposed that competing compound formation reactions can occur when ions produced by the oxidative dissolution of the substrate are present with the E-ALD solution.  These reactions could potentially short circuit the E-ALD process in the early cycles.  Substrates that did not produce ions (Au Ge Mo) did not seem to affect the process and grew CdTe films of good quality, however, a surface pretreatment was required in some cases for successful electrodeposition.

# References

(1) Pauporte, T.; Lincot, D. *Electrochimica Acta* **2000**, *45*, 3345.

(2) Chu, T. L.; Chu, S. S. *Solid-State Electronics* **1995**, *38*, 533.

(3) Bosio, A.; Romeo, N.; Mazzamuto, S.; Canevari, V. *Progress in Crystal Growth and Characterization of Materials* **2006**, *52*, 247.

(4) Henry, C. H. *J. Appl. Phys.* **1980**, *51*, 4494.

(5) Shockley, W.; Queisser, H. J. *J. Appl. Phys.* **1961**, *32*, 510.

(6) Lincot, D. *Thin Solid Films* **2005**, *487*, 40.

(7) Kroger, F. A. *Journal of the Electrochemical Society* **1978**, *125*, 2028.

(8) Panicker, M. P. R.; Knaster, M.; Kroger, F. A. *Journal of the Electrochemical Society* **1978**, *125*, 566.

(9) Cunningham, D.; Rubcich, M.; Skinner, D. *Progress in Photovoltaics* **2002**, *10*, 159.

(10) Gregory, B. W.; Stickney, J. L. *Journal of Electroanalytical Chemistry* **1991**, *300*, 543.

(11) Gregory, B. W.; Suggs, D. W.; Stickney, J. L. *Journal of the Electrochemical Society* **1991**, *138*, 1279.

(12) Colletti, L. P.; Flowers, B. H.; Stickney, J. L. *Journal of the Electrochemical Society* **1998**, *145*, 1442.

(13) Colletti, L. P.; Stickney, J. L. *Journal of the Electrochemical Society* **1998**, *145*, 3594.

(14) Flowers, B. H.; Wade, T. L.; Garvey, J. W.; Lay, M.; Happek, U.; Stickney, J. L. *Journal of Electroanalytical Chemistry* **2002**, *524-525*, 273.

(15) Huang, B. M.; Colletti, L. P.; Gregory, B. W.; Anderson, J. L.; Stickney, J. L. *Journal of the Electrochemical Society* **1995**, *142*, 3007.

(16) Lay, M. D.; Sorenson, T. A.; Stickney, J. L. *J. Phys. Chem. B* **2003**, *107*, 10598.

(17) Lay, M. D.; Stickney, J. L. *Journal of the Electrochemical Society* **2004**, *151*, C431.

(18) Varazo, K.; Lay, M. D.; Sorenson, T. A.; Stickney, J. L. *Journal of Electroanalytical Chemistry* **2002**, *522*, 104.

(19) Venkatasamy, V.; Jayaraju, N.; Cox, S. M.; Thambidurai, C.; Happek, U.; Stickney, J. L. *J. Appl. Electrochem.* **2006**, *36*, 1223.

(20) Villegas, I.; Stickney, J. L. *Journal of the Electrochemical Society* **1991**, *138*, 1310.

(21) Forni, F.; Innocenti, M.; Pezzatini, G.; Foresti, M. L. *Electrochimica Acta* **2000**, *45*, 3225.

|  | Ml/Cycle | n | EPMA | XRD |
|---|---|---|---|---|
| Au | 0.6 | 3 | 1.02 | Cubic |
| Au Basic | 0.6 | 3 | 0.98 | Cubic |
| Au Strip | 0.6 | 2.9 | 0.9 | Cubic |
| Acid Te on Ni | 0.89 | 3.1 | 0.66 | Cubic |
| Acid Te strip on Ni | 1 | 2.8 | 0.88 | Cubic |
| Basic Te on Ni | 0.63 | 3.1 | 0.95 | Cubic |
| Acid Te on Cu | 1.1 | 2.5 | 0.15 | Cubic |
| Basic Te on Cu | 0.71 | 2.88 | 0.83 | Cubic |
| Acid Te on Ag with Cl -400 dep -750 strip | 1.3 | 2.8 | 0.82 | Cubic |
| Basic Te on Ge | 0.43 | 2.94 | 0.98 | Cubic |

**Table 5.1:** Summery of XRD EPMA and SE results for each substrate

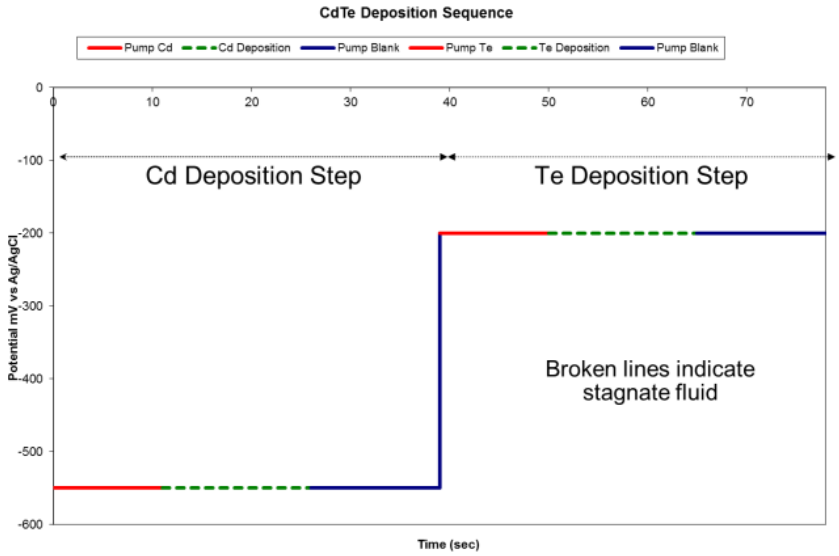

**Figure 5.1**: CdTe deposition sequence diagram. The above is the sequenced used with acidic Te deposition chemistry

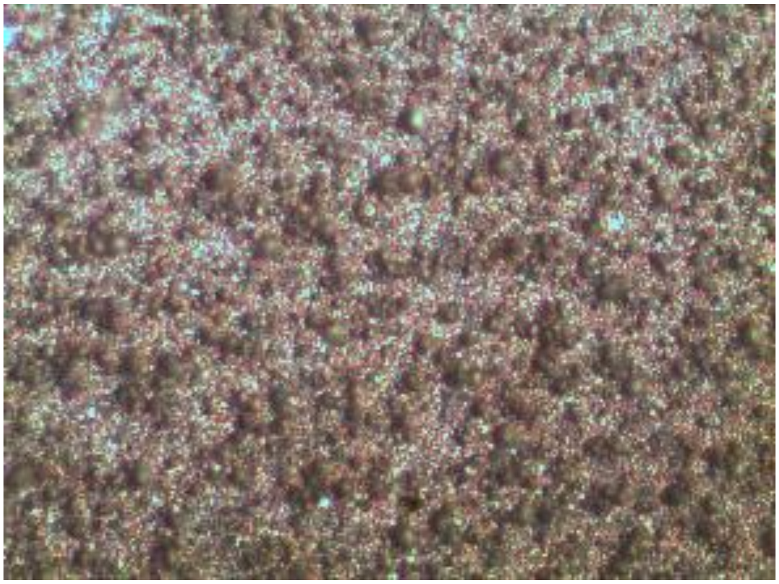

**Figure 5.2:** Optical microscope image of CdTe on Ag magnified 1000X

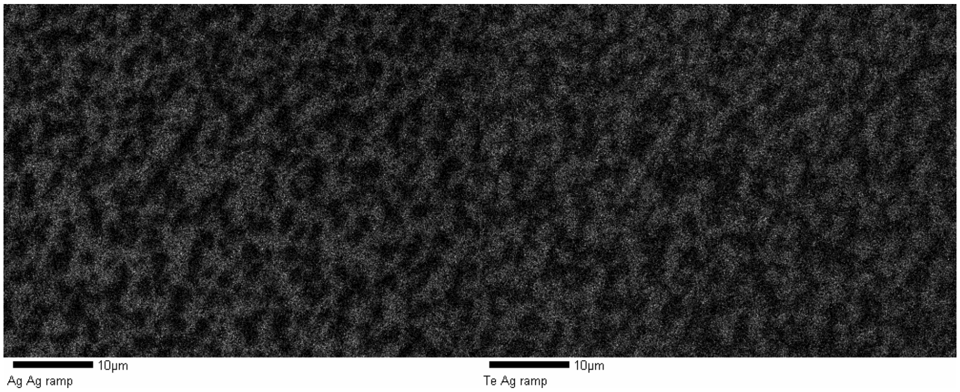

**Figure 5.3:** EPMA elemental mapping of CdTe on Ag. Left image is Ag signal right image is Te signal

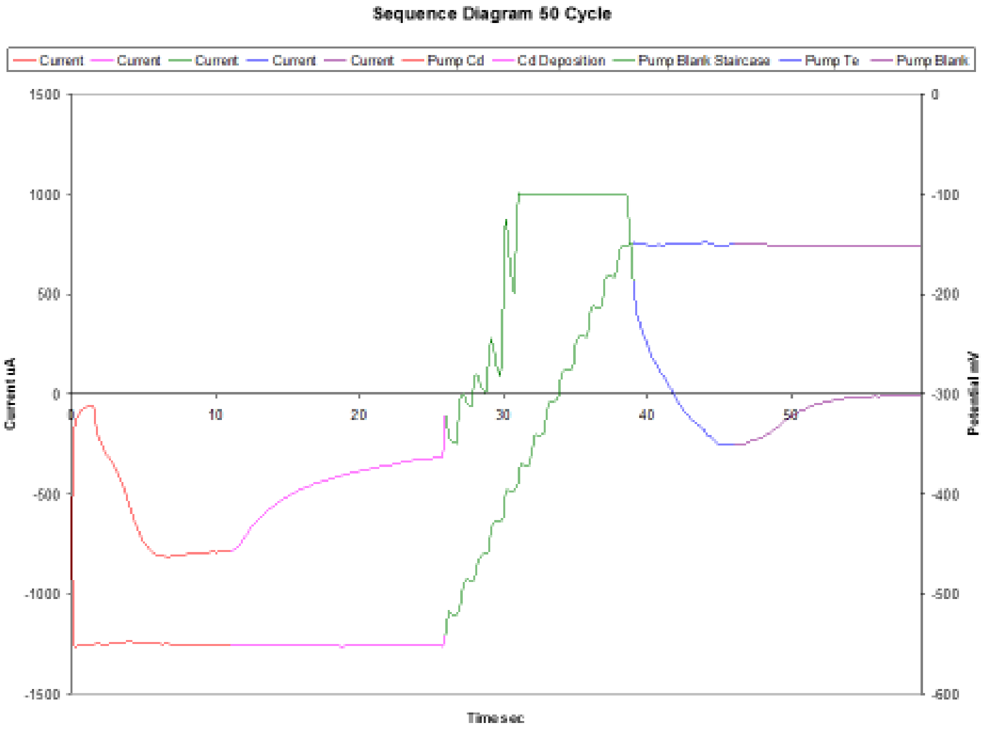

**Figure 5.4:** Current time trace of an E-ALD cycle, electrode area 1.82,

# CHAPTER 6

# CDTE NANOWIRE FABRICATED WITH ELECTROCHEMICAL ATOMIC LAYER DEPOSITION (E-ALD) AND LITHOGRAPHY PATTERNED NANOWIRE ELECTRODEPOSITION (LPNE)[5]

---

[5] B. Perdue, J. L. Stickney , To be submitted to *Journal of the Electrochemical Society (2014)*

## Abstract

The formation of CdTe nanowires by LPNE and E-ALD is discussed. LPNE is a 7 step process that allows for the low cost fabrication of nanowires and structures which involves electrodeposition of the desired material onto a sacrificial metal trench electrode. Like atomic layer deposition (ALD), E-ALD involves the growth of compounds one atomic layer at a time using surface limited reactions. However, in E-ALD the reactions are carried out in the condensed phase (aqueous solutions) rather than the gas phase. Electrochemical surface limited reactions are generally referred to as under potential deposition (UPD). In E-ALD, compounds are formed by alternating the UPD of one element onto another element. The optimization of the E-ALD process on a Ni electrode was performed before attempting the LPNE process. Different growing chemistries were attempted, an acidic Te solution, a basic Te solution, and with and without a Te reductive stripping step, and examined to see what chemistries were compatible with a Ni electrode. These deposits were examined with electron probe microanalysis (EPMA) spectroscopic ellipsometry (SE) and X-ray diffraction (XRD). EPMA results show variations in the stoichiometry with a Cd/Te ratio of 0.7, 0.8 0.9 for acidic, stripping and basic chemistries, this is most likely due to the influence of the Ni electrode, XRD shows all deposits produce crystalline CdTe with a strong preferred (111) orientation. SE results show differences in growth rates and quality for each deposition chemistry with the basic chemistry producing the best results. After the optimization, E-ALD CdTe Nanowires were fabricated with the LPNE process and examined with atomic force microscopy (AFM) and scanning electron microscopy (SEM). AFM and SEM results for E-ALD CdTe LPNE nanowires indicate that the nanowires produced are on average 200 nm in width which is inconsistent with an E-ALD process. The most probable cause for this discrepancy is diffusion of the electroactive species into and out of the

trench. It was demonstrated however that E-ALD CdTe can successfully be grown onto LPNE grown nanowires.

## Introduction

Nanowires have many versatile properties that can be applied to many fields including chemical sensing, signal processing and nanoelectroics. There are two main strategies in the synthesis of nanowires. The first utilizes physical constraints to control the growth of the nanowire. These methods are referred to as the "Top Down" approach and include techniques like lithography and anodized alumina templates. The other method uses chemical specificity to control the growth of the nanowire. These methods are referred to as the "Bottom Up" approach and includes techniques like the Vapor-Liquid-Solid or the spontaneous self-assembly of nanoparticles. These methods of nanowire synthesis are explained in various reviews[1,2].

Recently a new method of nanowire synthesis was introduced that combines both top down and bottom up aspects to synthesize the nanowires. This technique is called lithographically patterned nanowire electrodeposition (LPNE) and was developed by Penner et.al[3-5]. LPNE uses lithography combined with the versatility of electrodeposition to create different types of nanowires on insulating surfaces. This is done via the electrodeposition of the desired material onto a sacrificial Ni nanotrench electrode who's geometry is defined by photolithography[3]. LPNE has been used to fabricate a variety of different nanowires including noble metals[3-19], semiconductors[20-24], and even oxides[25-27].

The electrodeposition of semiconducting nanowires is of particular interest to this group. A semiconducting compound of interest is CdTe. The electrodeposition of compound semiconductors from a single bath was first described by Kroger[28]. This idea was then applied to CdTe by Panicker and Kroger[29] and this has served as the basis for the electrochemical codeposition of most semiconductors[30]. Deposits made in this fashion are essentially stoichiometric and crystalline[31-35]. The flexibility of this technique has allowed for the electrochemical formation of CdTe nanowires from anodized alumina templates [36-38] as well as LPNE nanowires[39].

Electrochemical atomic layer deposition (E-ALD) pioneered by our group is the condensed phase equivalent to atomic layer deposition (ALD) and atomic layer epitaxy (ALE)[40,41]. This technique is being developed to improve electrodeposit morphology, crystallinity and stoichiometry and prevent 3D growth. As with ALD, E-ALD uses surface limited reactions to grow compounds one atomic layer at a time. A surface limited reaction is a reaction in which deposition is terminated after the surface atoms have been covered by the depositing atoms, resulting in the deposition of an atomic layer. Electrochemical surfaces limited reactions are known as underpotential deposition (UPD). In UPD, one element can deposit onto a second at a potential prior to its formal reduction potential. This occurs because it is more thermodynamically stable to deposit onto another element than it is to deposit onto itself. In a typical E-ALD cycle, a solution containing a reactant’s electrochemical precursor is introduced to the substrate at a UPD potential. After the reaction is completed the solution is rinsed away using a blank solution, and a new solution containing a precursor for the next element is introduced at its UPD potential. After the reaction is complete, and the solution is rinsed from the cell, one cycle has been completed resulting in the formation of one compound bilayer. The thickness of the deposited is determined by the number of E-ALD cycles performed. This layer by layer Frank-van der Merwe growth affords superior control over thickness, homogeneity, crystallinity, and the overall quality of the deposit. E-ALD deposition of CdTe has been studied by this group[40-52] and Foresti[53] so much is known about this system.

The advantage of using E-ALD as opposed to Kroger deposition in the LPNE process is that the wire thickness of E-ALD grown wire is that the wire width will be based on the number of E-ALD cycles grown as opposed to time spent depositing which may be controlled by diffusion. It is the goal of this work is to first optimize E-ALD conditions for the electrodeposition of CdTe onto a Ni electrode. After conditions have been optimized a series of wires will be grown. The wires will be characterized with AFM, SEM, EPMA elemental mapping and other thin film techniques.

## Experimental

In these studies the films were grown using an automated flow cell system using a three electrode cell with a Ag/AgCl reference electrode controlled by a potentiostat. The basic setup for this procedure has the bottles containing the precursor solutions incased in a box so that the solution and the box can be purged of oxygen by nitrogen bubbling, with the $N_2$ box helping minimizing $O_2$ in the system. These bottles are hooked up to a valve block, with its outlet connected to the electrochemical flow cell. The outlet of the cell is attached to a peristaltic pump, which facilitates sucking solutions through the cell. The potentiostat, valves and the pump are controlled by a PC running SEQUENCER 4 software (Electrochemical ALD L.C., Athens GA). More details on the flow cell can be found in previous publications[42,43,46,49,50]. The electrodes used in these studies were polycrystalline Au on glass, with a 50 nm Ti adhesion layer, purchased from Evaporated Metal Films.

Cd was electrodeposited from a solution containing 0.5 mM $CdSO_4$ in 0.5 M $NaClO_4$, pH 3. Te was electrodeposited from one of two solutions. The first being 0.1mM $TeO_2$ in 0.5 M $NaClO_4$, pH 3, or 0.1 mM $TeO_2$ in 0.5M $NaClO_4$ buffered with 50 mM sodium borate pH 9. Due to the limited solubility of $TeO_2$ in water, it needs to be first dissolved in concentrated $H_2SO_4$ or

NaOH, before diluting to the final volume and pH. The blank consisted of 0.5 M $NaClO_4$, pH 3 and its purpose was to rinse out the cell of any precursors from previous solutions. All solutions were made with 18 MΩ water supplied from a Milipore water flirtation system. The electrochemical precursors were purchased from Alfa Æsar with a purity of 99.999%

Three different cycles were examined in this work: one using an acidic Te solution, one using an acidic Te solution together with a reductive Te stripping step, and one using a basic Te solution, no stripping step. A visual representation of a typical E-ALD cycle can be found in Figure 6.1. For the E-ALD deposition of CdTe with acidic Te chemistry, the cycle can be broken down into 2 steps. The first step involved $Cd^{2+}$ ions being pumped into the cell at a 18 $\frac{mL}{min}$ for 5 seconds at a potential of -550mV vs. Ag/AgCl. That was followed by holding the solution without flowing for 15 seconds of deposition, at the same potential, and allowing the system to come to equilibrium. The $Cd^{2+}$ ions were then rinsed from the cell with the blank solution for 15 seconds, concluding Cd deposition. For the Te step, a solution of $HTeO_2^+$ ions are pumped into the cell for 5 seconds at a potential of -200mV vs. Ag/AgCl. This is followed by a quiescent deposition for 15 seconds, at the same potential. The $HTeO_2^+$ ions are then rinsed from the cell, using the blank solution, for 15 seconds, completing this E-ALD cycle for CdTe. Upon completion of an E-ALD cycle, approximately one compound bilayer of CdTe should have been electrodeposited. Some minor variations to this cycle are made, depending on the Te chemistry used. If a stripping steps is included at the end of the cycle, the Te deposition was shifted 100 mV more negative. The stripping step involves first rinsing with blank and then stepping the potential to -900mV for 15 seconds, where Te atoms in excess of an atomic layer are reduced to a soluble telluride species, which diffuse away. This is followed by rinsing again with blank for 15 seconds at the same potential to remove the telluride products. When using the basic Te chemistry the only difference is that the Te deposition potentials changes to -800 mV.

When preforming the Ni optimization of E-ALD CdTe 100 E-ALD cycle deposits were analyzed using a variety of thin film characterization techniques. The stoichiometry of the deposits were investigated using EPMA on a JEOL 8600 SUPERPROBE with a 10 KeV accelerating voltage 15 nA beam current and a 10 um beam diameter. Using the large beam helped to average slight sample inhomogeneities. Deposit crystallinity was examined on a PANanalytical X'PERT Pro with an open eulerian cradle utilizing a 1.54 nm Cu $K\alpha_1$ source and a parallel plate collimator. Optical properties of the deposits were analyzed using a spectroscopic ellipsometer (SE), JA Woolam M-2000V. AFM measurements were made on a Bruker Innova.

## Results and Discussion

The UPD behavior of Cd and Te has been studied by our group [40-52]. Cd UPD can occurs reductively from $Cd^{2+}$ ions, resulting in a coverage of between 0.3 and 1 monolayers (ML). A monolayer is defined in this report relative to the number of surface atom in the substrate. Assuming the Au on glass substrates resemble a Au(111) surface, that would be about $1.35 X10^{15}$ atom/cm$^2$. Due to reactive nature of Cd it is unstable at more positive potentials which presents a challenge when trying to deposit more noble elements onto it. Formation of Te monolayers onto Cd can be done in a few different ways. The first method is to exploit electrochemical irreversibility of Te. Te has very slow deposition kinetics as such all features observed in cyclic voltammetry are seen at overpotentials. When constructing an E-ALD cycle the proper overpotetial and deposition time must be chosen to obtain the desired atomic layer. This Te overpotential must also be at a potential which the Cd atomic layer will be stable and not oxidatively dissolve. Another strategy for depositing a Te monolayer is to deposit bulk Te then reductively strip the bulk Te to $Te^{2-}$ which is a water soluble species leaving behind a Te monolayer that has been stabilized by compound formation. This method is desirable because a Te deposition potential can be chosen such that the Cd monolayer is stable and the bulk Te can be removed afterwards. The drawback to this methodology is that it results in increased cycle times due to the fact that 2 extra steps in the cycle must be added. The final method is to change the Te solution chemistry. The $E^{o\prime}$for Te deposition shifts more negative as the pH increases[47].

Ni is a fairly reactive metal. Its electrochemical behavior as a substrate is also unknown to our group. As a first attempt the conditions for the E-ALD deposition of CdTe onto Au were used on a Ni electrode. Chronoamperometry of cycle 50 out of 100 is shown in Figure 6.2. This demonstrates the reactive nature of Ni. Large oxidative current occurs when the Te solution is pumped in at -200 mV. This oxidative current does not appear when a Au substrate is used which indicates that the Ni substrate could be oxidatively dissolving. This is confirmed by inspection of the deposit under an optical microscope, sections of the substrate have been removed and the underlying glass can be seen. Oxidative Ni stripping is a major problem for two reasons the first being that the nature of the electrode is dynamic, and second the $Ni^{2+}$ ions could react with Te and form NiTe impurities in the film. In order to avoid these issues optimization of E-ALD CdTe growth on Ni needed to be carried out.

Different CdTe deposition chemistries were developed and tested to produce quality deposits without damaging the electrode. The first was a deposition cycle which involved the reductive stripping of Te. In the CdTe stripping chemistry, Te is deposited at an overpotential during its deposition step this results bulk amount of Te. In the subsequent step the potential is step to a potential where elemental Te can be reduced to $Te^{2-}$, a water soluble species which then diffuses away. This stripping potential is picked such that only the Te stabilized by CdTe formation remains while the excess bulk is dissolved away. This chemistry is favorable because the potentials used are such that the Ni electrode will be stable, as well as controlling the amount of deposition per cycle. The other chemistry optimized is Te deposition from a basic Te solution. As mentioned earlier the increasing of the pH shifts the $E_o'$of Te deposition to more negative potentials. This is favorable again because at these negative potentials the Ni electrode will be stable and not oxidatively dissolve. These chemistries were used to grow thin films of CdTe onto Ni substrates then analyzed with XRD EPMA and SE.

The stoichiometry of the deposits was examined with EPMA. Results of the three deposition chemistries are shown in Table 6.1. The stoichiometry was measured in 5 spots in various positions across the deposits. This was done to probe the uniformity of the deposit. Results show that the deposition chemistry used yields different stoichiometry. The Cd/Te ratios for each of the deposits are 0.66, 0.84 and 0.96 for the acidic Te chemistry, stripping chemistry, and basic Te chemistry. All deposits show an excess of Te in the deposit, with the basic chemistry producing the best deposit. If there are Ni ions present from oxidative Ni stripping, then there is the possibility that NiTe would form in the presence of $HTeO_4^+$ ions. If NiTe was codeposited, it would decrease the Cd/Te ratio because there would be excess Te present in the form of NiTe. This could account for the discrepancies seen in the Cd/Te ratio obtained from EPMA.

Crystallinity of the deposits were examined with grazing incidence XRD. A typical XRD of a CdTe deposit is shown in Figure 6.3. This spectrum shows four peaks at 2θ of 23.7° 39.3°, 44.5° and 51.9°. The peaks at 23.7° and 39.3° can be assigned to CdTe (111) and (311) according to card number 12-0770 for cubic $F\bar{4}3m$ CdTe. The remaining peaks at 2θ of 44.5°

and 51.9° are assigned to the low index planes of the Ni substrate according to card number 97-0712. This indicates that E-ALD CdTe has a strong preferred (111) orientation without annealing consistent with the reports in the literature[30,33,34,40-52]. Despite the discrepancies shown in the stoichiometry, all deposition chemistries show a CdTe (111) reflection with no evidence of NiTe. This could mean that either no NiTe exists or that it does exist but not in large enough domains to produce a Bragg reflection.

Next the films were evaluated with SE. The data was collected below, at, and above the Brewster angle for Ni at 682.8 nm in order to obtain the maximum amount of information about the film. The data was then fitted with the Cauchy equation which relates thickness and optical constants, two very valuable pieces of information. The index of refraction at 632.8 nm and the thickness were calculated from the model. In these studies the mean square error (MSE) of the fit were below 50 which is an indication of a good fit implying that the values calculated from the model are reliable.

A typical SE spectrum is shown in Figure 6.4 and a summary of ellipsometric data can be found in Table 6.2. When examining the calculated thickness of each deposition chemistry, the growth rate of the deposit can be estimated. Based on the XRD data in Figure 6.3 the assumption will be made that all vertical growth of the sample will be in the (111) direction. Using geometry and the CdTe lattice constant, the distance between compound bilayers (distance between atomic planes) can be calculated. It is found that the distance between compound bilayers is $\frac{a}{\sqrt{3}}$ where $a$ is the CdTe lattice constant 0.648 nm. The growth rate of the deposits can be estimated by taking the thickness calculated from SE then dividing by the product of 0.374 and the number of cycles run to give an estimated ML/cycle growth rate. This data is represented in Figure 6.5. Figure 6.5 shows that the Te stripping potential must be negative of -

700mV to obtain the desired sub monolayer growth per cycle.  All chemistries produce the desired result based on the estimated growth rate and calculated optical constant.

After the optimization for the growth of E-ALD CdTe on Ni the chemistry was attempted with the LPNE process.  LPNE substrates were etched in 0.8M $HNO_3$ for 10 minutes to form the trenches.  The substrates were then rinsed with copious amounts of water to prevent further etching.  Substrates were then placed in the E-ALD electrochemical cell and CdTe was grown onto the Ni nanotrench electrodes.  Currents produced by this process were too small to be measured by the E-ALD potentiostat.  So to confirm that nanowires had been grown the photoresist was removed with acetone and then the samples were taken to EPMA to do elemental mapping.

Results for EPMA elemental mapping are show in Figure 6.6.  EPMA shows the presence of a CdTe deposit on the outer edge of the Ni wire.  However the approximate size of the CdTe deposit is ~500nm which is an order of magnitude thicker than it should be based on the number of E-ALD cycles grown.  The separation between the Ni wire and the CdTe deposit cannot be explained.  Despite this it shows that the two techniques can be combined to synthesize wires. The next step was to make a series of deposits with varying cycle number to see if the wires increase in size with cycle number.  Chemistries used were Te Stripping chemistry and the conditions used for Au.

The next set of experiments involved the actual fabrications of CdTe nanowires with the LPNE method.  Nanowires were grown in a similar fashion as above then the excess Ni was removed with a final nitric acid etch to produce free standing E-ALD CdTe nanowires.  The resulting nanowires are shown in Figure 6.7.  The wire produced by growing 200 E-ALD cycles is approximately twice as large as the 100 E-ALD cycle deposit, which is to be expected for a layer by layer process. However the wires is an order of magnitude thicker than they should be based on the E-ALD process. Figure 6.7 sugest that something may be occuring durring the etching step to cause the non ideal wire sizes. In order to produce better quality wires this process should be better understood.

The etching process was investigated with AFM. The LPNE process was examined at each step with AFM to see abnormal etching causes the E-ALD wires to be larger than they should be. It was belived that parabolic etching of the Ni durring the nitric acid step causes the E-ALD grown CdTe wires to be too large. AFM eximination of the Ni electrode afer the nitric acid etch is shown in Figure 6.8. The AFM images shows a very sharp etch profile as well as some risidual Ni that was not etched. The AFM images does not show evidice of irregular etching, it shows a very clean sharp profile which is consistant with literature reports[4]. CdTe LPNE wires were examined with AFM as well these reuslts are shown in Figure 6.9. Figure 6.9 shows that the CdTe LPNE wires are consistant with the SEM images, which indicates that these wires are too wide to be grown by an ALD process. Despite the descrepency in width the wires are the proper hight, the same hight of the Ni electode which sugessts that the growth is occuring in the proper place. A possible answer for this discrepency is diffusion. The E-ALD flow cell rinces laminarlly across the photoresist, this emplies that the electroactive species must diffuse into the depth of the trench. If electroactive species are not sufficently rinsed away then when the potential is stepped to a more negative value, then ions that have not diffused away could be electrodeposited. This excess deposition could account for the wires being thicker than they should be.

The final stage of this project was to see if we could use E-ALD to grown onto LPNE nanowires. This posed a few unique problems. LPNE Au wire are very fragile. The parastaltic pump set at maximum speed would rip the wires apart. The E-ALD cycle needed to be alter to account for a reduced flowrate. The pump speed was reduced to 5 $\frac{mL}{min}$ to avoide the delamination of the LPNE Au nanowires. Similarly with the LPNE process the currents produced from the growth of CdTe onto these wires is too small to measure with the E-ALD potentiostat so success of the expierement needed to be confirmed post deposition.

Figure 6.10 shows the EPMA elemental mapping of the LPNE produced nanowires and the E-ALD CdTe deposit. EPMA elemental mapping shows the conformal coating of the Au LPNE nanowires with CdTe (Red from CdTe + Blue Au =purple overlap). This image also shows that not all Au nanowires have electrical conductivity. The right most Au wire must be broken somewhere and as a result did not get electrodeposited on. The CdTe deposit seem to conformally coat the wire without changing the morphology of the wire.

## Conclusion

The optimization of the E-ALD process on a Ni electrode was performed on Ni electrodes. Three different growing chemistries were examined, acidic Te, acidic Te with stripping and basic Te, and examined to see what chemistries were compatible with a Ni electrode. These deposits were examined with EPMA, SE and XRD. EPMA results show variations in the stoichiometry with a Cd/Te ratio of 0.7, 0.8 0.9 for acidic, stripping and basic chemistries, this is most likely due to the influence of the Ni electrode, XRD shows all deposits produce crystalline CdTe with a strong preferred (111) orientation. SE results show differences in growth rates and quality for each deposition chemistry with the basic chemistry producing the best results. AFM and SEM results for E-ALD CdTe LPNE nanowires indicate that the nanowires produced are on average 200 nm in width which is inconsistent with an E-ALD process. The most probable cause for this discrepancy is diffusion of the electroactive species into and out of the trench. It was demonstrated however that E-ALD CdTe can successfully be grown onto LPNE grown nanowires.

# References

(1) Lu, W.; Lieber, C. M. *Nat. Mater.* **2007**, *6*, 841.

(2) Law, M.; Goldberger, J.; Yang, P. D. *Annual Review of Materials Research* **2004**, *34*, 83.

(3) Menke, E. J.; Thompson, M. A.; Xiang, C.; Yang, L. C.; Penner, R. M. *Nat Mater* **2006**, *5*, 914.

(4) Xiang, C.; Thompson, M. A.; Yang, F.; Menke, E. J.; Yang, L.-M. C.; Penner, R. M. *Phys. Status Solidi C* **2008**, *5*, 3503.

(5) Xiang, C.; Kung, S.-C.; Taggart, D. K.; Yang, F.; Thompson, M. A.; Guell, A. G.; Yang, Y.; Penner, R. M. *ACS Nano* **2008**, *2*, 1939.

(6) Kim, H.; Xiang, C.; Guell, A. G.; Penner, R. M.; Potma, E. O. *J. Phys. Chem. C* **2008**, *112*, 12721.

(7) Halpern, A. R.; Nishi, N.; Wen, J.; Yang, F.; Xiang, C.; Penner, R. M.; Corn, R. M. *Anal. Chem. (Washington, DC, U. S.)* **2009**, *81*, 5585.

(8) Xiang, C.; Kim, J. Y.; Penner, R. M. *Nano Lett.* **2009**, *9*, 2133.

(9) Xiang, C.; Yang, Y.; Penner, R. M. *Chem. Commun. (Cambridge, U. K.)* **2009**, 859.

(10) Chen, Y.; Kung, S.-C.; Taggart, D. K.; Halpern, A. R.; Penner, R. M.; Corn, R. M. *Anal. Chem. (Washington, DC, U. S.)* **2010**, *82*, 3365.

(11) Colaianni, L.; Kung, S. C.; Taggart, D. K.; De, G. V.; Greaves, J.; Penner, R. M.; Cioffi, N. *Sens. Lett.* **2010**, *8*, 539.

(12) Kung, S. C.; Xing, W.; Donavan, K. C.; Yang, F.; Penner, R. M. *Electrochim. Acta* **2010**, *55*, 8074.

(13) Yang, F.; Kung, S.-C.; Cheng, M.; Hemminger, J. C.; Penner, R. M. *ACS Nano* **2010**, *4*, 5233.

(14) Yang, F.; Kung, S.-C.; Taggart, D. K.; Penner, R. M. *Sens. Lett.* **2010**, *8*, 534.

(15) Arter, J. A.; Taggart, D. K.; Diaz, J. E.; Penner, R. M.; Weiss, G. A.; American Chemical Society: 2011, p BIOT.

(16) Taggart, D. K.; Yang, Y.; Kung, S.-C.; McIntire, T. M.; Penner, R. M. *Nano Lett.* **2011**, *11*, 125.

(17) Yang, F.; Jung, D.; Penner, R. M. *Anal. Chem. (Washington, DC, U. S.)* **2011**, *83*, 9472.

(18) Arter, J. A.; Diaz, J. E.; Donavan, K. C.; Yuan, T.; Penner, R. M.; Weiss, G. A. *Anal. Chem. (Washington, DC, U. S.)* **2012**, *84*, 2776.

(19) Halpern, A. R.; Donavan, K. C.; Penner, R. M.; Corn, R. M. *Anal Chem* **2012**, *84*, 5053.

(20) Yang, Y.; Kung, S. C.; Taggart, D. K.; Xiang, C.; Yang, F.; Brown, M. A.; Guell, A. G.; Kruse, T. J.; Hemminger, J. C.; Penner, R. M. *Nano Lett.* **2008**, *8*, 2447.

(21) Yang, Y.; Taggart, D. K.; Brown, M. A.; Xiang, C.; Kung, S.-C.; Yang, F.; Hemminger, J. C.; Penner, R. M. *ACS Nano* **2009**, *3*, 4144.

(22) Kung, S.-C.; van, d. V. W. E.; Yang, F.; Donavan, K. C.; Penner, R. M. *Nano Lett.* **2010**, *10*, 1481.

(23) Yang, Y.; Taggart, D. K.; Cheng, M. H.; Hemminger, J. C.; Penner, R. M. *J. Phys. Chem. Lett.* **2010**, *1*, 3004.

(24) Ayvazian, T.; Xing, W.; Yan, W.; Penner, R. M. *ACS Appl Mater Interfaces* **2012**, *4*, 4445.

(25) Yan, W.; Ayvazian, T.; Kim, J.; Liu, Y.; Donavan, K. C.; Xing, W.; Yang, Y.; Hemminger, J. C.; Penner, R. M. *ACS Nano* **2011**, *5*, 8275.

(26) Yan, W.; Yang, Y.; Penner, R.; American Chemical Society: 2011, p INOR.

(27) Yan, W.; Kim, J. Y.; Xing, W.; Donavan, K. C.; Ayvazian, T.; Penner, R. M. *Chem. Mater*. **2012**, *24*, 2382.

(28) Kroger, F. A. *Journal of the Electrochemical Society* **1978**, *125*, 2028.

(29) Panicker, M. P. R.; Knaster, M.; Kroger, F. A. *Journal of the Electrochemical Society* **1978**, *125*, 566.

(30) Lincot, D. *Thin Solid Films* **2005**, *487*, 40.

(31) Pauporte, T.; Lincot, D. *Electrochimica Acta* **2000**, *45*, 3345.

(32) Kampmann, A.; Cowache, P.; Vedel, J.; Lincot, D. *Journal of Electroanalytical Chemistry* **1995**, *387*, 53.

(33) Lepiller, C.; Lincot, D. *Journal of the Electrochemical Society* **2004**, *151*, C348.

(34) Kampmann, A.; Lincot, D. *Journal of Electroanalytical Chemistry* **1996**, *418*, 73.

(35) Josell, D.; Beauchamp, C. R.; Jung, S.; Hamadani, B. H.; Motayed, A.; Richter, L. J.; Williams, M.; Bonevich, J. E.; Shapiro, A.; Zhitenev, N.; Moffat, T. P. *Journal of the Electrochemical Society* **2009**, *156*, H654.

(36) Ohgai, T.; Gravier, L.; Hoffer, X.; Ansermet, J. P. *J. Appl. Electrochem.* **2005**, *35*, 479.

(37) Zhao, A. W.; Meng, G. W.; Zhang, L. D.; Gao, T.; Sun, S. H.; Pang, Y. T. *Applied Physics a-Materials Science & Processing* **2003**, *76*, 537.

(38) Xu, D. S.; Chen, D. P.; Xu, Y. J.; Shi, X. S.; Guo, G. L.; Gui, L. L.; Tang, Y. Q. *Pure and Applied Chemistry* **2000**, *72*, 127.

(39) Kum, M. C.; Jung, H.; Chartuprayoon, N.; Chen, W.; Mulchandani, A.; Myung, N. V. *J. Phys. Chem. C* **2012**, *116*, 9202.

(40) Gregory, B. W.; Suggs, D. W.; Stickney, J. L. *Journal of the Electrochemical Society* **1991**, *138*, 1279.

(41) Gregory, B. W.; Stickney, J. L. *Journal of Electroanalytical Chemistry* **1991**, *300*, 543.

(42) Flowers, B. H.; Wade, T. L.; Garvey, J. W.; Lay, M.; Happek, U.; Stickney, J. L. *Journal of Electroanalytical Chemistry* **2002**, *524-525*, 273.

(43) Lay, M. D.; Stickney, J. L. *Journal of the Electrochemical Society* **2004**, *151*, C431.

(44) Villegas, I.; Stickney, J. L. *Journal of the Electrochemical Society* **1991**, *138*, 1310.

(45) Varazo, K.; Lay, M. D.; Sorenson, T. A.; Stickney, J. L. *Journal of Electroanalytical Chemistry* **2002**, *522*, 104.

(46) Colletti, L. P.; Flowers, B. H.; Stickney, J. L. *Journal of the Electrochemical Society* **1998**, *145*, 1442.

(47) Lay, M. D.; Sorenson, T. A.; Stickney, J. L. *J. Phys. Chem. B* **2003**, *107*, 10598.

(48) Venkatasamy, V.; Jayaraju, N.; Cox, S. M.; Thambidurai, C.; Happek, U.; Stickney, J. L. *J. Appl. Electrochem.* **2006**, *36*, 1223.

(49) Colletti, L. P.; Stickney, J. L. *Journal of the Electrochemical Society* **1998**, *145*, 3594.

(50) Huang, B. M.; Colletti, L. P.; Gregory, B. W.; Anderson, J. L.; Stickney, J. L. *Journal of the Electrochemical Society* **1995**, *142*, 3007.

(51) Suggs, D. W.; Stickney, J. L. *Surface Science* **1993**, *290*, 375.

(52) Gregory, B. W.; Norton, M. L.; Stickney, J. L. *Journal of Electroanalytical Chemistry* **1990**, *293*, 85.

(53) Forni, F.; Innocenti, M.; Pezzatini, G.; Foresti, M. L. *Electrochimica Acta* **2000**, *45*, 3225.

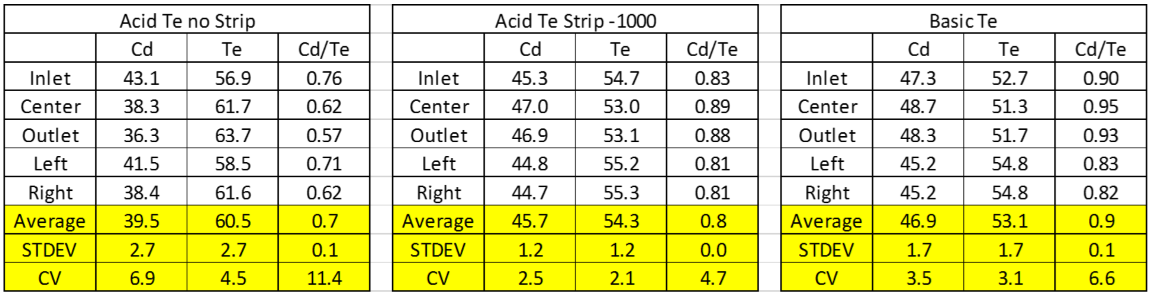

| Acid Te no Strip | | | |
|---|---|---|---|
| | Cd | Te | Cd/Te |
| Inlet | 43.1 | 56.9 | 0.76 |
| Center | 38.3 | 61.7 | 0.62 |
| Outlet | 36.3 | 63.7 | 0.57 |
| Left | 41.5 | 58.5 | 0.71 |
| Right | 38.4 | 61.6 | 0.62 |
| Average | 39.5 | 60.5 | 0.7 |
| STDEV | 2.7 | 2.7 | 0.1 |
| CV | 6.9 | 4.5 | 11.4 |

| Acid Te Strip -1000 | | | |
|---|---|---|---|
| | Cd | Te | Cd/Te |
| Inlet | 45.3 | 54.7 | 0.83 |
| Center | 47.0 | 53.0 | 0.89 |
| Outlet | 46.9 | 53.1 | 0.88 |
| Left | 44.8 | 55.2 | 0.81 |
| Right | 44.7 | 55.3 | 0.81 |
| Average | 45.7 | 54.3 | 0.8 |
| STDEV | 1.2 | 1.2 | 0.0 |
| CV | 2.5 | 2.1 | 4.7 |

| Basic Te | | | |
|---|---|---|---|
| | Cd | Te | Cd/Te |
| Inlet | 47.3 | 52.7 | 0.90 |
| Center | 48.7 | 51.3 | 0.95 |
| Outlet | 48.3 | 51.7 | 0.93 |
| Left | 45.2 | 54.8 | 0.83 |
| Right | 45.2 | 54.8 | 0.82 |
| Average | 46.9 | 53.1 | 0.9 |
| STDEV | 1.7 | 1.7 | 0.1 |
| CV | 3.5 | 3.1 | 6.6 |

**Table 6.1:** EPMA results of E-ALD CdTe deposition onto a Ni substrate, results reported in relative percentages.

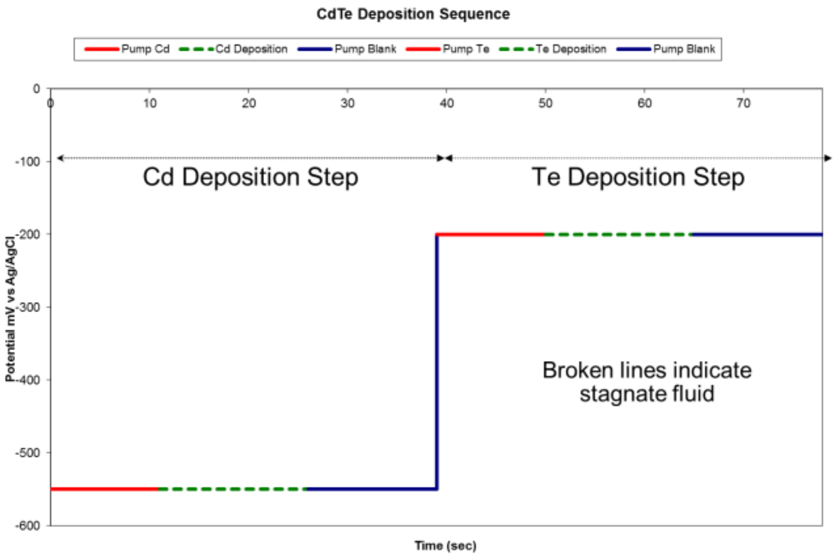

**Figure 6.1**: CdTe deposition sequence diagram. The above is the sequenced used with acidic Te deposition chemistry

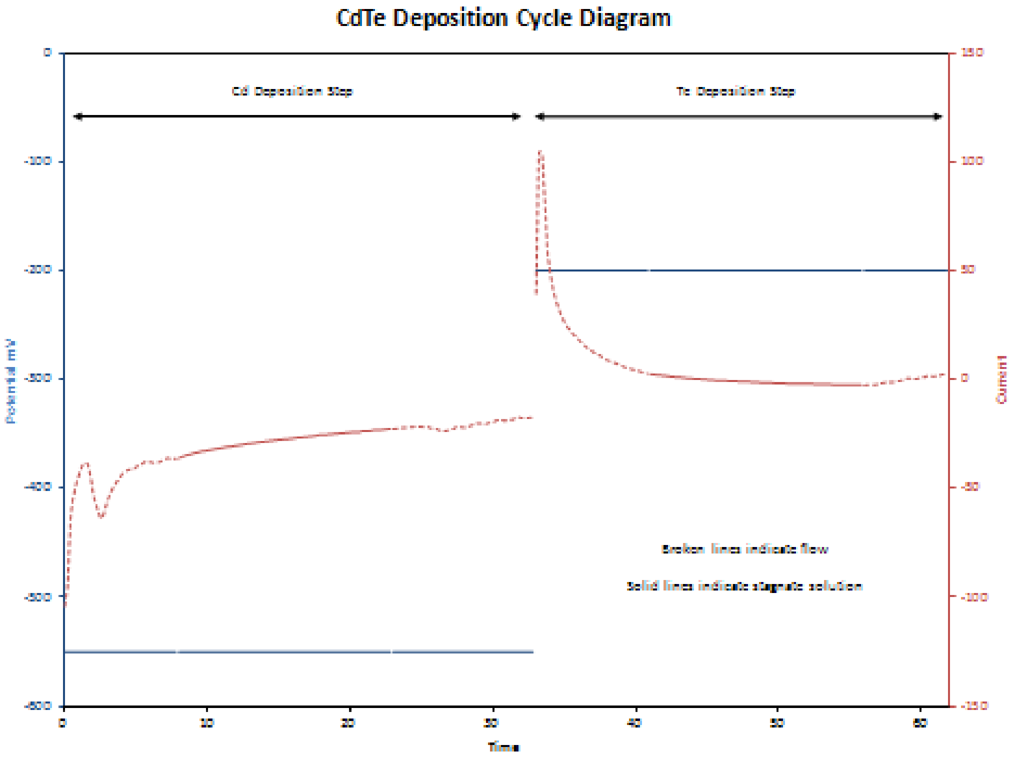

**Figure 6.2:** Current time trace of cycle 50 of E-ALD CdTe process.

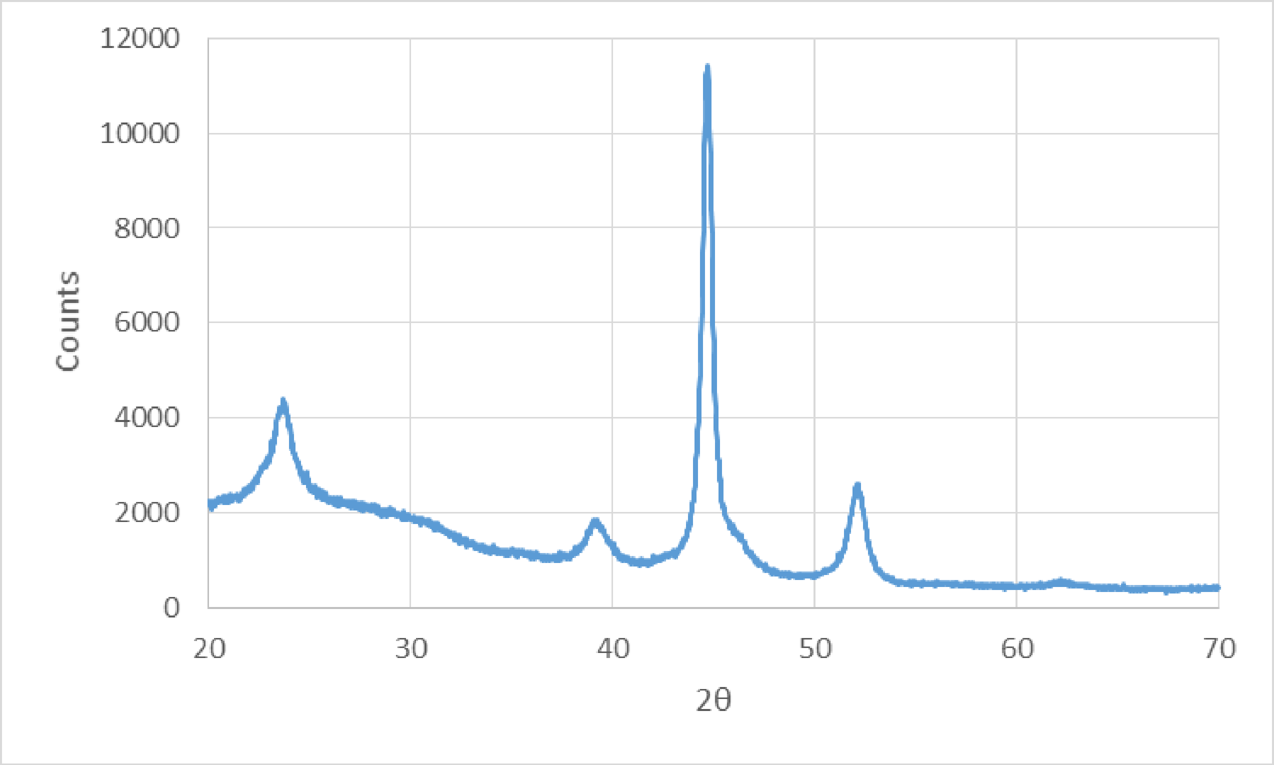

**Figure 6.3:** XRD of E-ALD CdTe on a Ni substrate. Incident angle used is 0.5° using a Cu $K_{\alpha 1}$ radiation

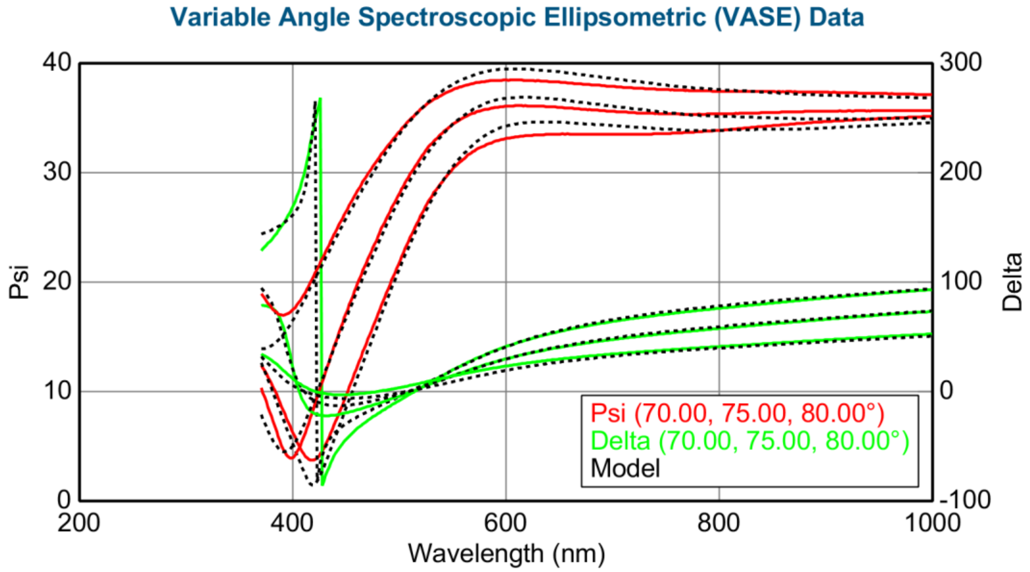

**Figure 6.4:** SE data of E-ALD grown CdTe on a Ni substrate.

|  | η | Thickmess | Growth Rate |
|---|---|---|---|
| Acid | 3.34 | 27.3 | 0.73 |
| Strip (-900) | 2.77 | 37.24 | 1.00 |
| Basic | 2.9 | 28.9 | 0.77 |

**Table 6.2:** Summary of SE data for each growing chemistry

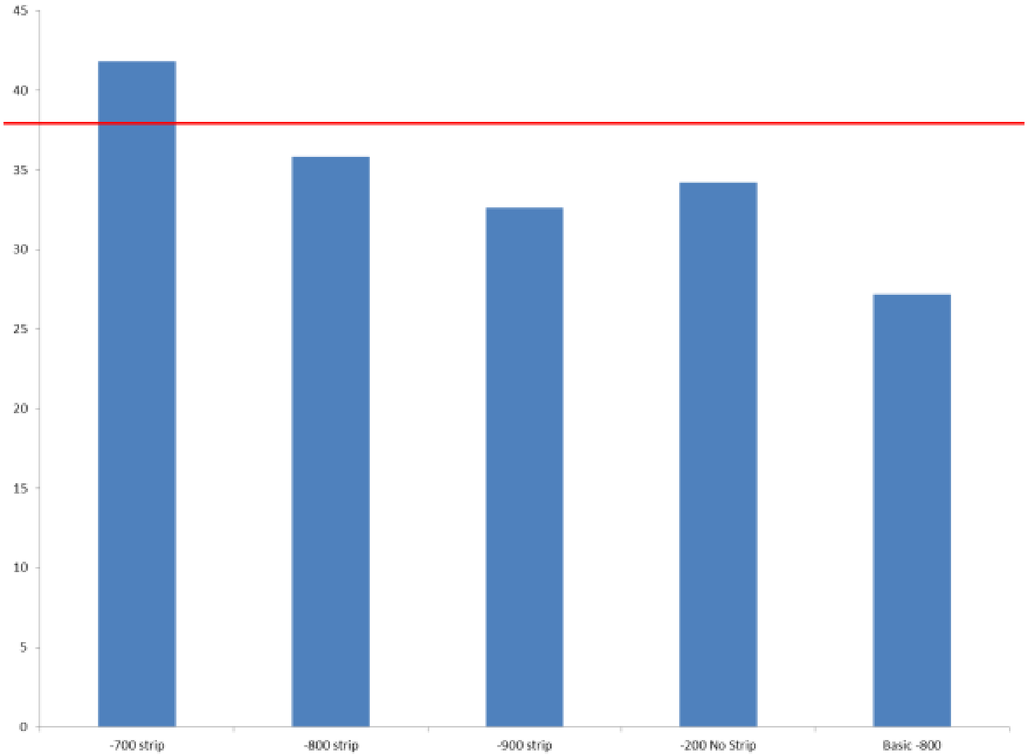

**Figure 6.5:** Average thickness resulting from each of the deposition Chemistries. The red line indicates the 1 ML/Cycle growth thickness.

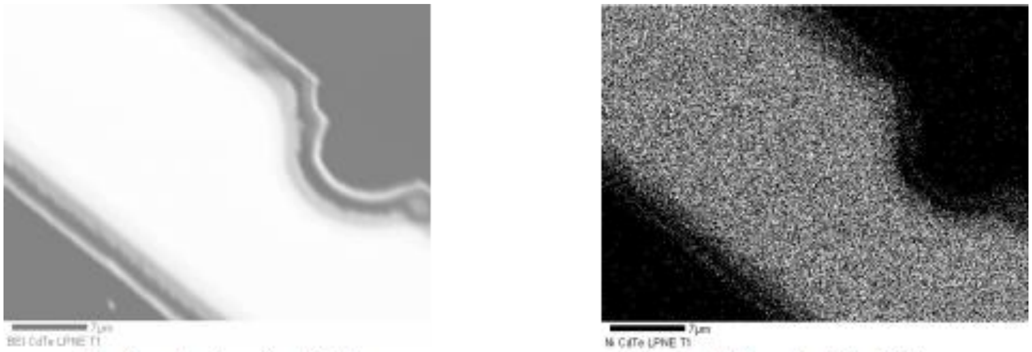

Electron back scatter SEM

Ni Xrays (white dots)

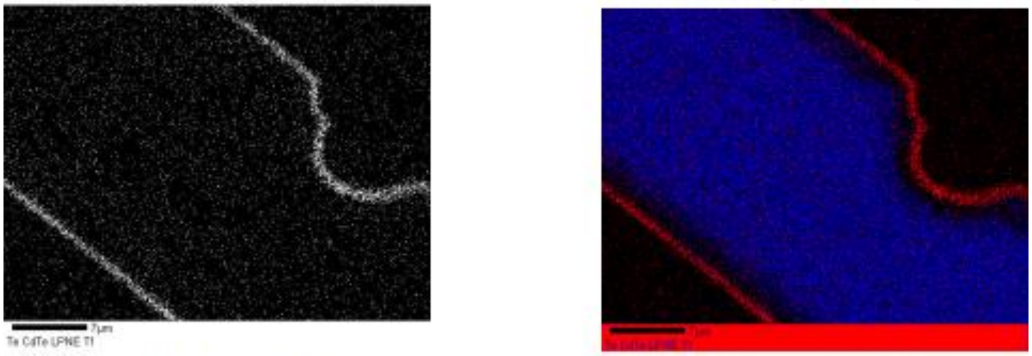

Te Xrays from CdTe (white dots)

Overlaid Image Ni is Blue Te is Red

**Figure 6.6:** EPMA elemental mapping of E-ALD CdTe onto the entrenched Ni electrode.

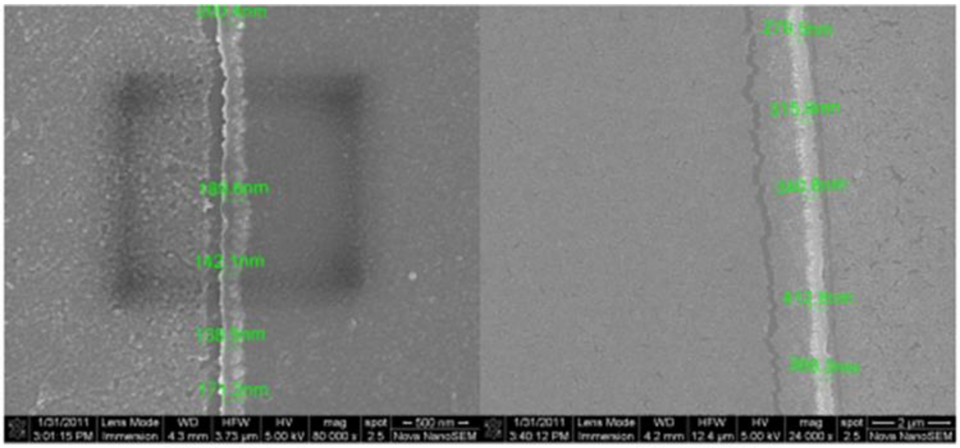

100 E-ALD Cycles

200 E-ALD Cycles

**Figure 6.7:** SEM of E-ALD CdTe grown LPNE nanowires

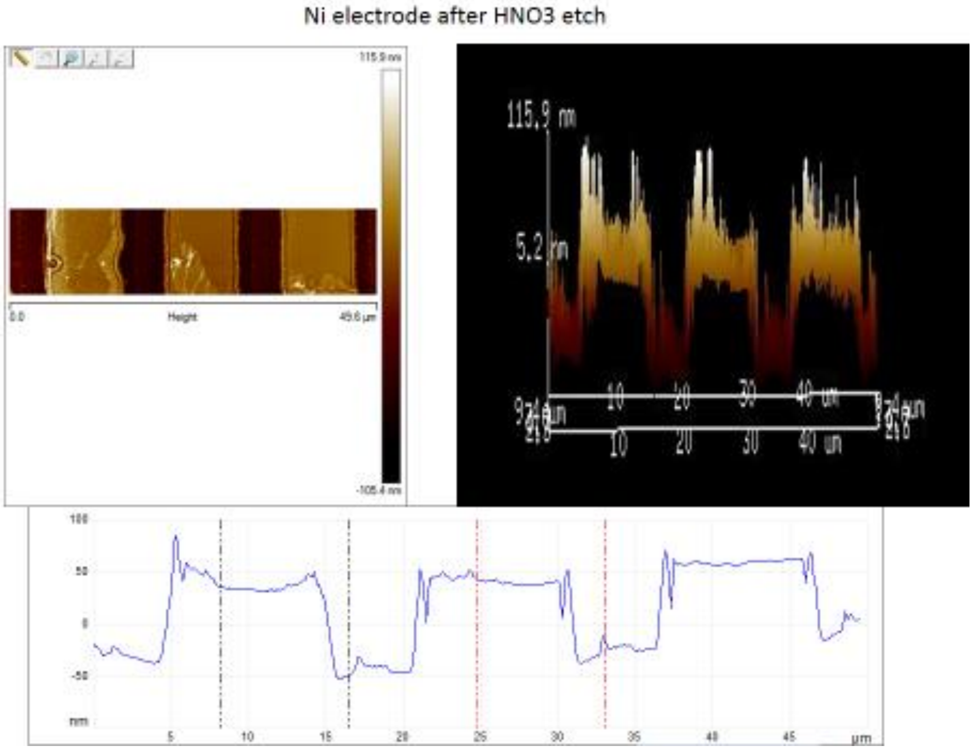
Ni electrode after HNO3 etch

**Figure 6.8:** AFM of Ni electrode after initial nitric acid etch.

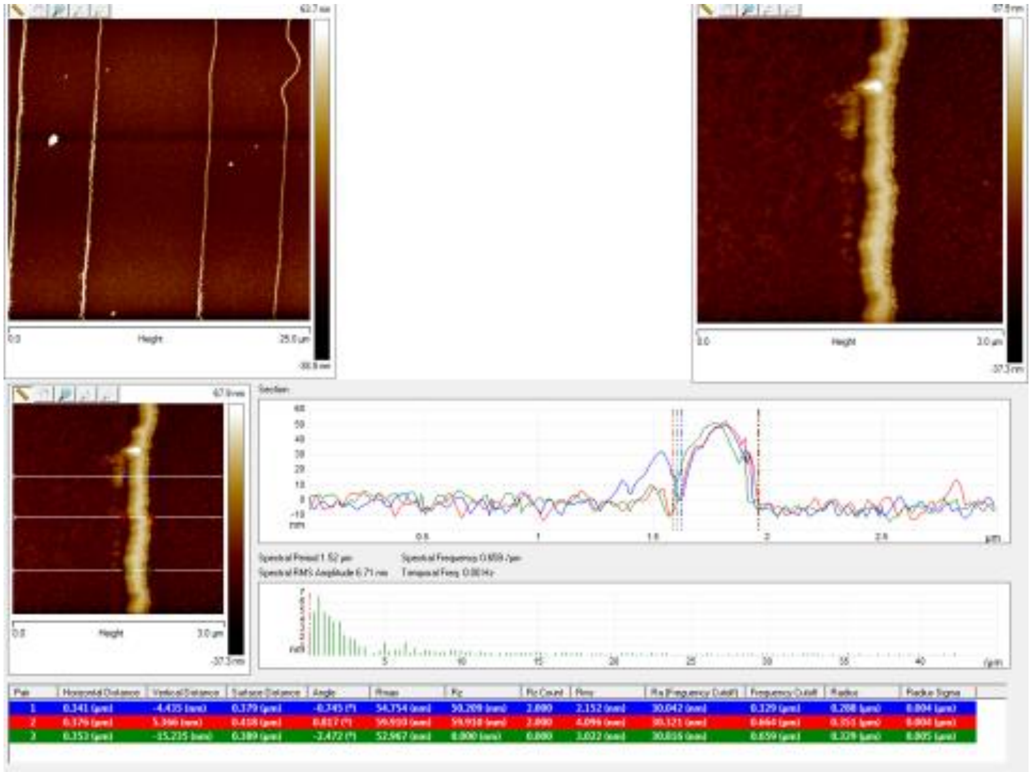

Spectral Period 1.52 µm
Spectral Frequency 0.659 /µm
Spectral RMS Amplitude 6.71 nm
Temporal Freq 0.00 Hz

| Pair | Horizontal Distance | Vertical Distance | Surface Distance | Angle | Rmax | Rz | Rz Count | Rms | Ra (Frequency Cutoff) | Frequency Cutoff | Radius | Radius Sigma |
|---|---|---|---|---|---|---|---|---|---|---|---|---|
| 1 | 0.341 (µm) | -4.435 (nm) | 0.379 (µm) | -0.745 (°) | 54.754 (nm) | 50.209 (nm) | 2.000 | 2.152 (nm) | 30.042 (nm) | 0.329 (µm) | 0.208 (µm) | 0.004 (µm) |
| 2 | 0.376 (µm) | 5.366 (nm) | 0.418 (µm) | 0.817 (°) | 59.910 (nm) | 59.910 (nm) | 2.000 | 4.096 (nm) | 30.121 (nm) | 0.664 (µm) | 0.351 (µm) | 0.004 (µm) |
| 3 | 0.353 (µm) | -15.235 (nm) | 0.389 (µm) | -2.472 (°) | 52.967 (nm) | 0.000 (nm) | 0.000 | 3.022 (nm) | 30.816 (nm) | 0.659 (µm) | 0.329 (µm) | 0.005 (µm) |

**Figure 6.9:** AFM of E-ALD grown CdTe LPNE nanowire

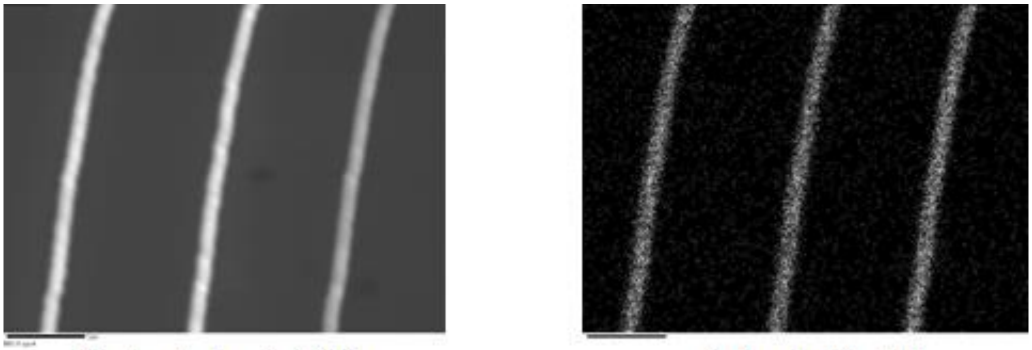

Electron back scatter SEM

Au Xrays (white dots)

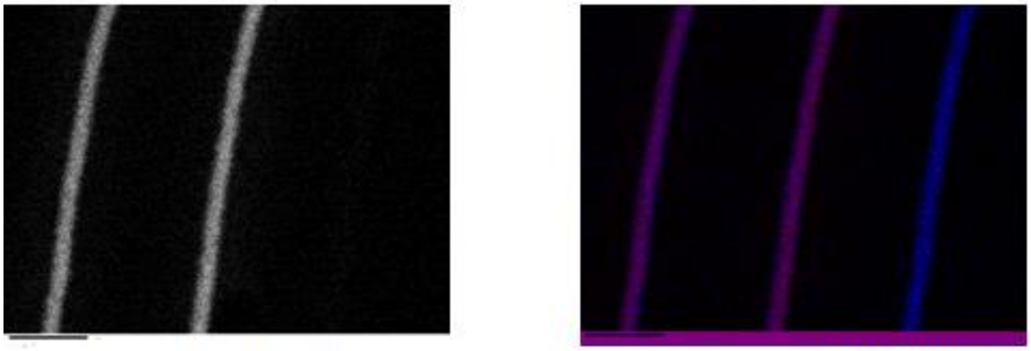

Te Xrays from CdTe (white dots)

Overlaied image Ni Blue Te Red Overlap purple

**Figure 6.10:** EPMA elemental mapping of E-ALD grown CdTe onto a LPNE grown Au nanowire

# CHAPTER 7

# POSSIBLE FORMATION OF TWO DIMENSIONAL GERMANIUM (GERMANENE) BY ELECTROCHEMICAL ATOMIC LAYER DEPOSITION (E-ALD)[6]

---

[6] B. Perdue, M. Ledina , X. Liang, O. Rivera, R. Dluhy, Y.-G. Kim, J. L. Stickney. To be submitted to *American Chemical Socity NANO (2014)*

## Abstract

In the present work we investigate the possible formation of germanene, the two-dimensional (2D) allotrope of germanium, deposited by E-ALD, the condensed phase variant of atomic layer deposition (ALD). In ALD the deposition of a compound is achieved by means of sequential surface limited reactions in which the components are deposited one atomic layer at a time. In E-ALD the individual atomic layers are formed using underpotential deposition (UPD), an electrochemical surface limited reaction. The deposits were probed for the existence of germanene with scanning tunneling microscopy (STM) and micro-Raman. *Ab initio* calculations of germanene predict a Ge-Ge bond distance of ~2.4 Å, a small bucking of the sheet with a magnitude of 0.7 Å as well as a "G like" Raman shift at 290 cm$^{-1}$. STM results show the formation of atomically flat terraces at negative potentials. The atomically resolved STM images suggest a Ge-Ge bond distance of ~2.2 Å. This small discrepancy could be explained by a smaller Ge-Ge bond distance, measurement error or the combination of the two. The micro-Raman results show a strong Raman shift at 290 cm$^{-1}$ at different points across the deposit. The STM images and the collected micro-Raman spectra are clearly suggesting the presence of an electrochemically grown germanene monolayer.

## Introduction

2D inorganic compounds have attracted much interest recently. Graphene's electronic properties has motivated researchers to look for similar or even better properties in other layered materials. These materials could be eventually integrated into the current nanoelectronic technology[1-4]. The idea of having a different group four element with a similar structure, is promising, but also very attractive because of its possible integration into devices[5-13]. One such material is germanene.

Electrodeposition holds promise as a low cost, flexible, room temperature technique for the production compound semiconductors. Similarly to atomic layer epitaxy[14](gas phase), electrochemical atomic layer deposition (E-ALD) achieves compound growth by alternating surface limited reactions. In a surface limited reaction, the deposition terminates when all of the surface atoms have been covered by the depositing atoms. E-ALD alternates the electrodeposition of the component elements one atomic layer at a time[15]. This layer by layer Frank-van der Merwe growth affords superior control over thickness, homogeneity, crystallinity, and the overall quality of the deposit.

Our group has studied the electrochemical behavior of germanium previously[16,17]. Results from these studies suggest that only surface limited amounts of deposition occur forming well-ordered structures on the surface. When the potential was poised negatively, large atomically flat terraces were observed. The growth of thicker layers of Ge was possible using a special E-ALD cycle. As stated previously, the rise of 2D materials has caused a reevaluation of our previous work, and has led us to different conclusions. This report will be on the reinterpretation of our previous studies of the electrochemical behavior of Ge when germanene is used as the model.

## Results and Discussion

### Ab Initio

There are many recent publications concerning *ab initio* calculations on germanene and its hydrogen terminated form germanane[7,13,18-30]. In these reports the consensus is that the most stable germanene structure is a “chair” like configuration which has a Ge-Ge bond distance of ~2.4Å and a buckle of ~0.7Å as depicted in Figure 7.1. *Ab initio* calculations also predict a graphene like or “g-like” Raman active mode occurring around 290 $cm^{-1}$ [13,28].

When imaging this structure with STM it is highly probable that the expected honeycomb structure will not be observed. It is very likely that only every other atom will be imaged because of the 0.7Å buckle. That is to say only the bright red atoms in Figure 7.2 will be imaged. The distance to every other atom (eg bright red to bright red) can be calculated using geometry. Two 30°60°90° triangles can be formed by connecting two bright red atoms with a line and bisecting the internal angle as shown. When doing this the Ge-Ge bond serves as the hypotenuse of the right triangle which then makes the opposing side $\frac{\sqrt{3}}{2}$ the Ge-Ge bond distance for one of the triangles. Thus the distance between every other atom is $\sqrt{3}$ multiplied by the Ge-Ge bond distance.

The other consequence of the buckled structure is the inaccuracy of the distances measured in STM. Germanene from the top down appears flat like grapheme, however in reality that is not the case. The distances measured in STM will be the projection of the Ge-Ge bond onto a plane perpendicular to the tip assuming the tip is orthogonal to the surface. This discrepancy can also be accounted for by geometry. A right triangle can be created by using the Ge-Ge bond as the hypotenuse and the buckling distance as the height. Using the Pythagorean Theorem the Ge-Ge bond projection is calculated to be 2.3 Å. This is the bond distance the STM should measure.

STM

The presence of germanene was investigated with STM. Figure 7.3 is an STM image of a gold bead electrode with a possible germanene monolayer. The layer was formed by poising the potential at -700 mV vs Ag/AgCl. The image shows a very large (300nm) atomically flat terrace and is consistent with the possible formation of an adsorbed germanene monolayer on the Au bead electrode. This adsorbed layer can be destroyed and reformed by scanning the potential negatively then positively as shown in Figure 9 of the following reference[16]. Height analysis of the STM image suggests that the steps between terraces are consistent with the height of an atomic step. This further supports they hypothesis that the Au electrode has an atomically thick adsorbed layer on it which we suspect is germanene.

When zooming in on the flat terrace at the same potential an atomically resolved Moiré pattern is observed demonstrated by Figure 7.4. This also supports the evidence of a germanene layer because Ge and Au atoms are difference sizes which is the cause of the Moiré pattern. The image is also consistent with the proposed buckled structure of germanene in that only every other atom is imaged. Calculating the bond distance and applying the $\sqrt{3}$ correction it is found that the Ge-Ge bond distance is ~2.1Å. This is 10% off from the predicted 2.3Å. Possible explanations for this discrepancy include a calibration error in the STM, STM tip drift, a shorter Ge-Ge bond distance or a higher buckling distance than predicted in the calculations, or a convolution of any of these factors. The atomically resolved Moiré pattern supports the claim that there is a germanene monolayer adsorbed onto the gold electrode.

### Raman

Micro-Raman was used as another method to investigate for the presence of germanene. Micro-Raman was taken at various points across the sample and the spectra are plotted in Figure 7.5. Spectra show a strong shift at 290 $cm^{-1}$ which is consistent with the *ab inito* predication of the germanene “g like” mode. The varying intensities implies that gremanene coverages vary and may exist as a minority species. To insure that we were not electrodepositing elemental germanium a Ge wafer spectra was compared to the possible germanene Raman spectrum and the results are shown in Figure 7.6. The observed germanium transvers optic (TO) is consistent with literature values[28]. There is an apparent difference (~ 5 $cm^{-1}$) between the Ge wafer and the spectra collected from our sample suggesting that what was electrodeposited is different than elemental Ge. The presented Raman data supports the hypothesis that germanene was electrodeposited onto the surface.

## Conclusion

The advent of two dimensional materials caused a reevaluation of our previous work on germanium electrodeposition. New hypotheses were formulated using germanene as the model. These hypotheses were tested with STM and micro-Raman. STM results show the formation of large atomically flat terraces. When zooming in on one of the terraces an atomically resolved a Moiré pattern is produced. The Moiré pattern is consistent with the chair configuration of germanene. The bond distances calculated from the Moiré pattern are consistent with the bond distances predicted from the Ab initio calculations. Finally the samples were probed with micro-Raman which show a strong Raman shift at 290 cm$^{-1}$ which is consistent with the *Ab Initio* calculations. The new interpretation of the data implies the presence of electrodeposited germanene.

# References

(1) Novoselov, K. S.; Geim, A. K.; Morozov, S. V.; Jiang, D.; Zhang, Y.; Dubonos, S. V.; Grigorieva, I. V.; Firsov, A. A. *Science* **2004**, *306*, 666.

(2) Castro Neto, A. H.; Guinea, F.; Peres, N. M. R.; Novoselov, K. S.; Geim, A. K. *Reviews of Modern Physics* **2009**, *81*, 109.

(3) Geim, A. K. *Science* **2009**, *324*, 1530.

(4) Geim, A. K.; Novoselov, K. S. *Nature Materials* **2007**, *6*, 183.

(5) Tabert, C. J.; Nicol, E. J. *Physical Review B* **2013**, *87*.

(6) Pang, Q.; Zhang, Y.; Zhang, J.-M.; Ji, V.; Xu, K.-W. *Nanoscale* **2011**, *3*, 4330.

(7) Houssa, M.; Scalise, E.; Sankaran, K.; Pourtois, G.; Afanas'ev, V. V.; Stesmans, A. *Applied Physics Letters* **2011**, *98*.

(8) Houssa, M.; Pourtois, G.; Afanas'ev, V. V.; Stesmans, A. *Applied Physics Letters* **2010**, *96*.

(9) Wang, Y.; Ding, Y. *Physica Status Solidi-Rapid Research Letters* **2013**, *7*, 410.

(10) Kaltsas, D.; Tsetseris, L. *Physical Chemistry Chemical Physics* **2013**, *15*, 9710.

(11) Wang, Y.; Ding, Y. *Solid State Communications* **2013**, *155*, 6.

(12) Tabert, C. J.; Nicol, E. J. *Physical Review Letters* **2013**, *110*.

(13) Scalise, E.; Houssa, M.; Pourtois, G.; van den Broek, B.; Afanas'ev, V.; Stesmans, A. *Nano Research* **2013**, *6*, 19.

(14) Suntola, T. *Thin Solid Films* **1992**, *216*, 84.

(15) Gregory, B. W.; Stickney, J. L. *Journal of Electroanalytical Chemistry* **1991**, *300*, 543.

(16) Liang, X. H.; Kim, Y. G.; Gebergziabiher, D. K.; Stickney, J. L. *Langmuir* **2010**, *26*, 2877.

(17) Liang, X. H.; Zhang, Q. H.; Lay, M. D.; Stickney, J. L. *Journal of the American Chemical Society* **2011**, *133*, 8199.

(18) Cahangirov, S.; Topsakal, M.; Ciraci, S. *Physical Review B* **2010**, *81*.

(19) Aufray, B.; Kara, A.; Vizzini, S.; Oughaddou, H.; Leandri, C.; Ealet, B.; Le Lay, G. *Applied Physics Letters* **2010**, *96*.

(20) Xu, M.; Liang, T.; Shi, M.; Chen, H. *Chemical Reviews* **2013**, *113*, 3766.

(21) Garcia, J. C.; de Lima, D. B.; Assali, L. V. C.; Justo, J. F. *Journal of Physical Chemistry C* **2011**, *115*, 13242.

(22) Wang, Y.; Zheng, J.; Ni, Z.; Fei, R.; Liu, Q.; Quhe, R.; Xu, C.; Zhou, J.; Gao, Z.; Lu, J. *Nano* **2012**, *7*.

(23) Voon, L. C. L. Y.; Sandberg, E.; Aga, R. S.; Farajian, A. A. *Applied Physics Letters* **2010**, *97*.

(24) Gao, J.; Zhao, J. *Scientific Reports* **2012**, *2*.

(25) Liu, C.-C.; Feng, W.; Yao, Y. *Physical Review Letters* **2011**, *107*.

(26) Kara, A.; Enriquez, H.; Seitsonen, A. P.; Voon, L.; Vizzini, S.; Aufray, B.; Oughaddou, H. *Surface Science Reports* **2012**, *67*, 1.

(27) Durgun, E.; Tongay, S.; Ciraci, S. *Physical Review B* **2005**, *72*.

(28) Bianco, E.; Butler, S.; Jiang, S.; Restrepo, O. D.; Windl, W.; Goldberger, J. E. *Acs Nano* **2013**, *7*, 4414.

(29) Ni, Z.; Liu, Q.; Tang, K.; Zheng, J.; Zhou, J.; Qin, R.; Gao, Z.; Yu, D.; Lu, J. *Nano Letters* **2012**, *12*, 113.

(30) Matthes, L.; Gori, P.; Pulci, O.; Bechstedt, F. *Physical Review B* **2013**,

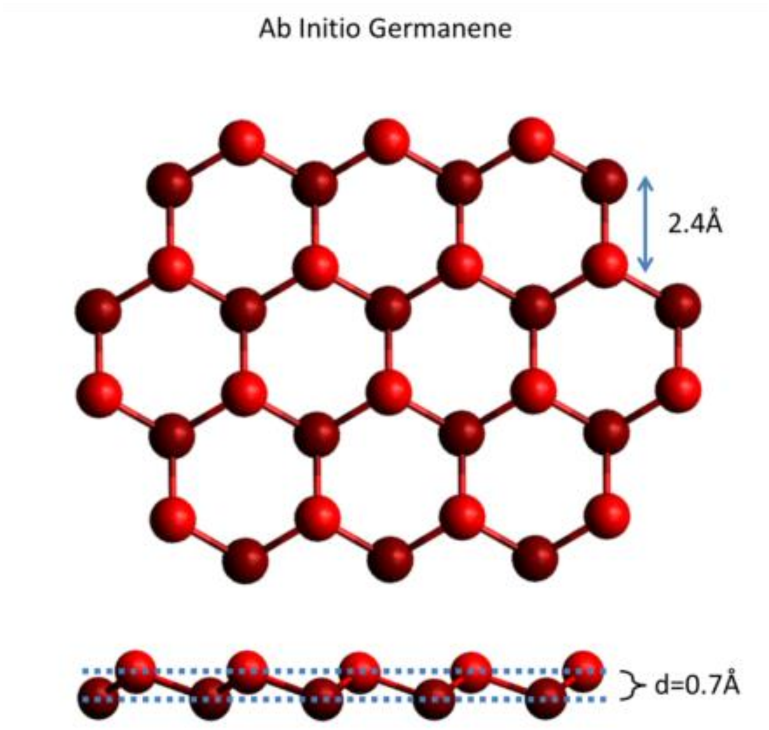

**Figure 7.1:** Predicted Ab Initio structure of germanene. Predicted structure has a Ge-Ge bond distance of ~2.4Å with a slight buckle of 0.7 Å. The different color atoms indicate that the atoms are at different heights.

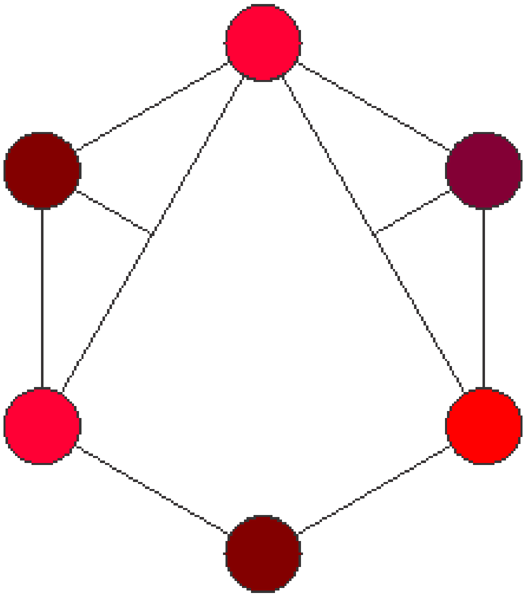

**Figure 7.2:** Hexagonal symmetry of germanene

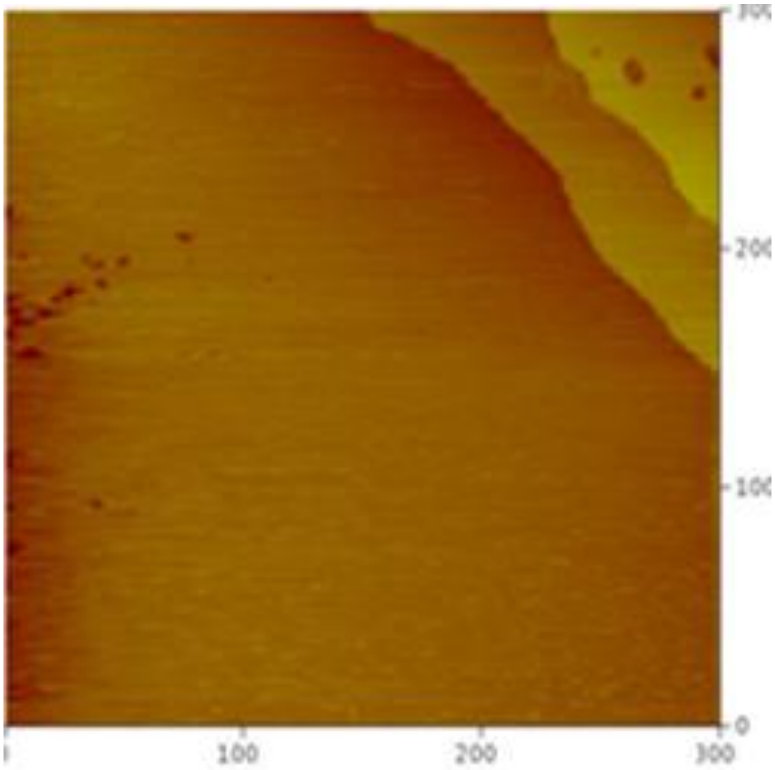

**Figure 7.3:** STM image of large (111) terrace on a Au bead electrode with a possible germanene layer adsorbed onto it.

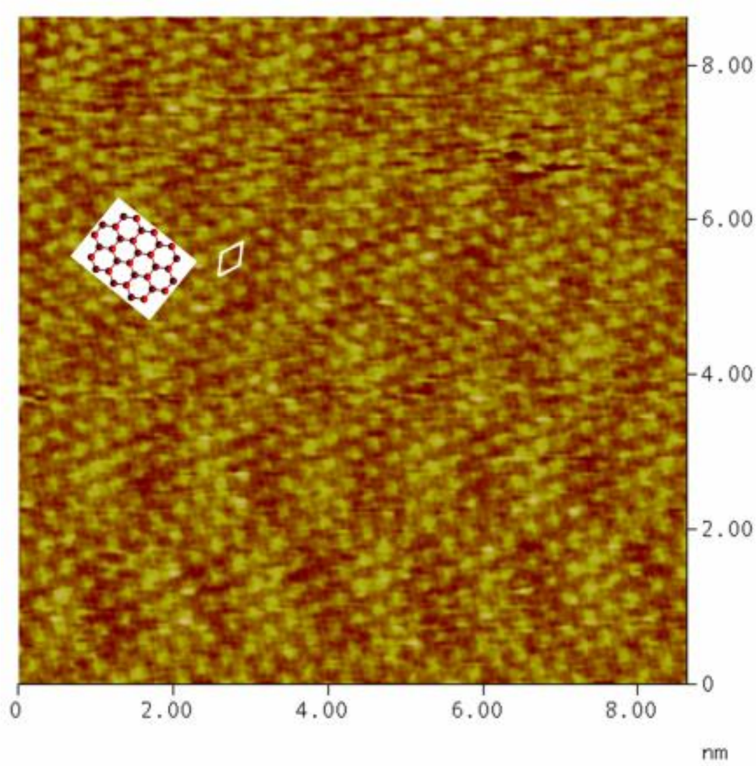

**Figure 7.4:** Moiré pattern of possible germanene monolayer

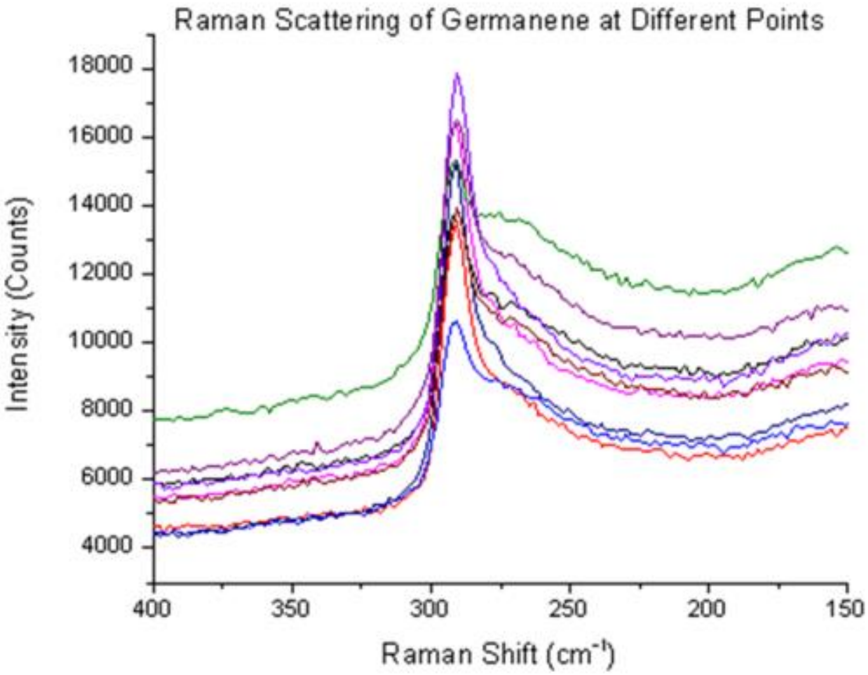

**Figure 7.5:** Micro-Raman of possible germanene monolayers at different spots across the deposit. Spectra were collected with a 514 nm laser and a 25x objective.

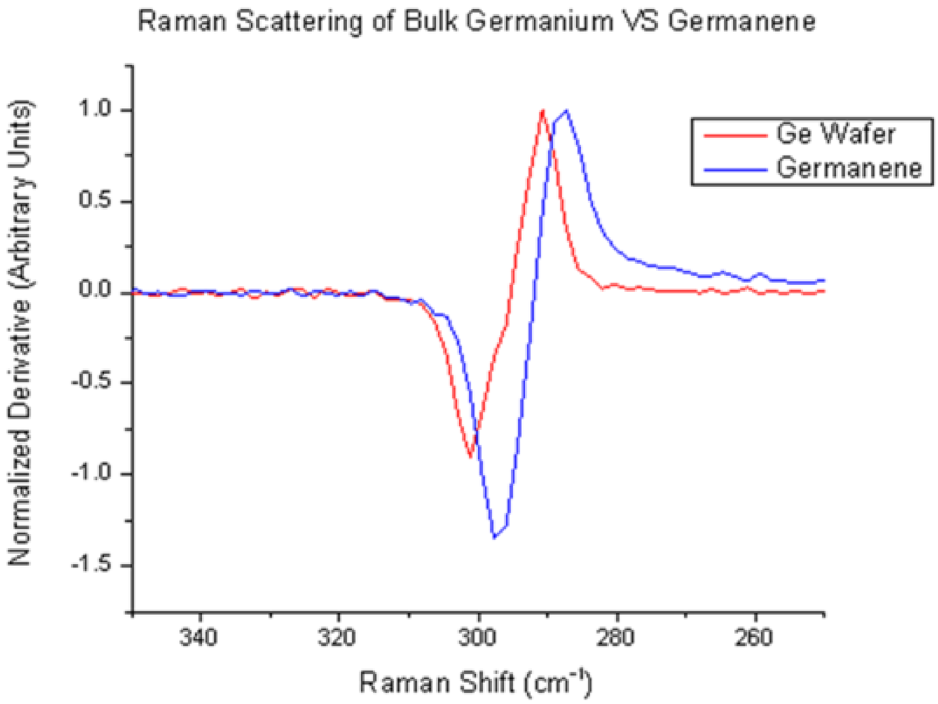

**Figure 7.6:** Spectral derivative of Germanium wafer and possible germanene monolayer

# CHAPTER 8

# IS PULSE DEPOSITION OF $CU_2SE$ POSSIBLE?

---

[1] B. Perdue, J. L. Stickney , To

be submitted to *Journal of the Electrochemical Society (2014)*

## Abstract

The formation of $Cu_2Se$ by electrochemical pulse deposition is presented. This proof of concept work shows that electrochemical pulsed deposition of $Cu_2Se$ using an automated flow cell is possible. Solution composition, pulse width, cathodic and anodic pulse potential, were examined when developing the $Cu_2Se$ pulsing chemistry. Films of $Cu_2Se$ were examined with electron probe microanalysis (EPMA), X-ray diffraction (XRD), and spectroscopic ellipsometry (SE) to ascertain film quality. Results from EPMA showed that $Cu_{2.1}Se$ is the predominate species formed despite the sequence used. XRD results indicated crystalline $Cu_2Se$ with a preferred (111) orientation. SE results revealed an index of refraction of 1.9 as well as an average growth rate of 0.2mL per pulse and a direct bandgap of 1.7eV. The process appears to grow linearly with pulse number.

## Introduction

Typically, photovoltaic (PV) materials are inorganic semiconductors, which form PN diode junctions with other materials and exhibit a PV effect when exposed to light. Ideally, the absorber material of an efficient terrestrial solar cell should be a direct bandgap semiconductor that maximizes the Schottky Queisser limit[1-8] with both high solar absorption and quantum efficiency. CdTe, copper indium selenide $CuInSe_2$ (CIS) copper indium gallium selenide $Cu(InGa)Se_2$ (CIGS) are just a few of these compounds. The aforementioned compounds are very good terrestrial solar absorbers, however, if solar is to become a solution to the world's energy crisis it is imperative the compounds that do not use critical raw elements be found.

To new compounds have recently caught the eye of the PV community and they are composed of earth abundant nontoxic elements, Copper zinc tin sulfide (CZTS) and copper zinc tin selenide (CZTSe) are to compound semiconductors which have a tunable direct bandgap with high solar absorption and quantum efficiency[9-13] thus they are ideally suited for terrestrial solar absorption. These compounds can be synthesized in many different ways including vacuum and nonvacuum codeposition techniques[13]. The codeposition of binary compounds is an effective way to make quaternary structures such as CZTS CZTSe. When considering the codeposition of binary compounds to form CZTSe, CuSe and $Cu_2Se$ are possible candidates for stable compounds that can be easily synthesized. $Cu_2Se$ can be fabricated using different deposition techniques for various applications[12,14-24]. One area of interest is the electrodeposition of $Cu_2Se$.

Electrodeposition holds promise as a low cost, flexible room temperature technique for the production compound semiconductors. This technique has been applied to many compounds as well as CIS and CIGS[25,26]. A process was developed by Kroger[27] in which a compound can be electrodeposited from a bath containing the component elements assuming there is a suitable driving force for compound formation. $Cu_2Se$ is one such compound that falls under this category.

The scope of this work is to the use the electrochemical atomic layer deposition (E-ALD) flow cell for a codeposition process. Electrochemical atomic layer deposition (E-ALD) was pioneered by this group and is a form of condensed phase atomic layer deposition (ALD) or atomic layer epitaxy (ALE)[28,29]. This technique is being developed to improve electrodeposited morphology, crystallinity and stoichiometry and prevent 3D growth. As with ALD, E-ALD uses surfaces limited reactions to grow compounds one atomic layer at a time. A surface limited reaction is a reaction in which the deposition is terminated after the surface atoms have been covered by the depositing atoms. Electrochemical surfaces limited reactions are known as underpotential deposition (UPD). In UPD, and one element can deposit onto a second at a potential prior to its formal reduction potential. This occurs because it is more thermodynamically stable to deposit onto another element than it is to deposit onto itself. In a typical E-ALD cycle, a solution containing a reactant's electrochemical precursor is introduced to the substrate at a UPD potential. After the reaction is completed the solution is rinsed away using a blank solution, and a new solution containing a precursor for the next element is introduced at its UPD potential. After the reaction is complete, and the solution is rinsed from the cell, one cycle has been completed resulting in the formation of one compound bilayer. The thickness of the deposited is determined by the number of E-ALD cycles performed. This layer by layer Frank-van der Merwe growth affords superior control over thickness, homogeneity, crystallinity, and the overall quality of the deposit. CuSe and $Cu_2Se$ have been previously grown by E-ALD[14,16] however the objective here is to grow CuSe or $Cu_2Se$ by sing a single bath using the flow cell. This work will serve as a proof of concept as there are many aspects to be investigated. Films will be analyzed with EPMA, XRD, and SE to determine the quality of the films grown..

## Experimental

In these studies the films were grown using an automated flow cell system using a three electrode cell with a 3M Ag/AgCl reference electrode controlled by a potentiostat. The basic setup for this procedure has the bottles containing the precursor solutions incased in a box so that the solution and the box can be purged of oxygen by nitrogen bubbling, with the $N_2$ box helping minimizing $O_2$ in the system. These bottles are hooked up to a valve block, with its outlet connected to the electrochemical flow cell. The outlet of the cell is attached to a peristaltic pump, which facilitates sucking solutions through the cell. The potentiostat, valves and the pump are controlled by a PC running SEQUENCER 4 software (Electrochemical ALD L.C., Athens GA). More details on the flow cell can be found in previous publications[30-34]. The electrodes used in these studies were polycrystalline Au on glass, with a 50 nm Ti adhesion layer, purchased from Evaporated Metal Films

Two solutions were used in these studies. The first was a 0.1mM $CuClO_4$ with 0.1mM $SeO_2$ in 0.5M $NaClO_4$, pH 3 solution and the second was a 1.5 mM $Cu(ClO4)_2$ with 1.5 mM $SeO_2$ in 0.5M $NaClO_4$, pH 3. The copper salt used was purchased from Sigma $Cu(ClO4)_2$ * $6H_2O$ with a purity of 98% and the $SeO_2$ was purchased from Alfa Æsar with a purity of 99.999%. All solutions were prepared in 18 MΩ water supplied from a Millipore water flirtation system.

The stoichiometry of the deposits were probed with EPMA on a JEOL 8600 SUPERPROBE with a 10 KeV accelerating voltage, 15 nA beam current, and a 10 um beam diameter. Using the large beam helped to average slight sample inhomogeneities. Crystallinity of the deposits were examined on a PANanalytical X'PERT Pro with an open eulerian cradle utilizing a 1.54nm Cu $K\alpha_1$ source and a parallel plate collimator. Optical properties of the deposits were analyzed with SE on a JA Woolam M-2000V.

## Results and discussion

A typical E-ALD cycle can last anywhere from 30 to 80 seconds depending on the pump being used and the size of the cell[14,16,29-32,35]. It is assumed that the completion of one E-ALD cycle results in the deposition of one compound bilayer which translates to a growth rate of around 0.4 nm/min. One of the fundamental flaws of E-ALD is that the growth rate is very slow when compared to different deposition techniques. Electrochemical codeposition developed by Kroger is considerably faster, however, the diffusion of ions becomes very important for prolonged depositions which may change the composition of the deposit over time.

In hopes of circumventing these two problems, pulsed deposition is to be used. Pulse electrodeposition has been used to electrodeposit chalcogenide based thermoelectrics with great success[36-39]. In the case of CuSe the aim is to exploit the irreversibility of Se as well as the reversibility of Cu to design a pulsing sequence where a fraction of a monolayer of Se is deposited and coated with bulk Cu in a cathodic pulse then removing the bulk Cu with an anodic pulse leaving CuSe behind.

To properly design a pulsing scheme the electrochemistry of the each component elements needed to be analyzed. Cyclic voltammetry for both Cu and Se are shown in Figures 8.1, and 8.2 respectively. The cyclic voltammogram for copper shows the characteristic features, Cu UPD onto Au and bulk Cu electrodeposition, however, due to the solution being very dilute it appears as if the Cu deposition is suffering from mass transfer issues because bulk deposition does not start until -150mV instead of the expected 0 MV. The Se voltammogram shows a UPD feature at 275 mV and the onset of bulk Se deposition occurring between 100mV and 0mV. These voltammograms give insight to where the bulk and UPD processes occur for both elements, however, they do not give any information as to how they will interact with each other.

To investigate the interaction between Cu and Se a clean Au electrode was immersed into a Se electrode where the potential was scanned from open circuit to 240 mV then back to 500mV. The scanning process resulted in the deposition of ~960 μC of charge. A gold (111) surface contains 1.3x1015 atoms/cm$^2$ based on the Au lattice constant of 0.408nm in an FCC crystal. Using Faradays law it can be calculated that there is 220μC/cm$^2$/1e$^-$ of charge for that Au surface, this will be the definition of a monolayer used in this discussion. The coverage of Se deposited from the scan is approximately 0.6ML vs. Au (111) assuming a four electron process and a cell area of 1.82cm$^2$. After the Se deposition the Se was rinsed out of the cell and the copper solution was introduced at 500mV.

The window opening of a Se coated Au electrode in a copper solution is shown in Figure 8.3. The cathodic UPD process of Cu onto Se forming CuSe is maximized at a potential of 50mV, the anodic stripping of this process occurs at 250 mV so the upper limit of the anodic pulse cannot exceed 250 mV. It seems as if the Se monolayer further stabilizes the bulk copper because its anodic stripping occurs at around 100mV while on a Au electrode it occurs at around 25 mV. It is possible that the Se layer floats on top of the Cu surface and bulk stripping has to diffuse through the Se layer which causes the bulk stripping to happen at an over potential.

The voltammetry in Figures 8.1-8.3 gave insight as to what potentials to use for anodic and cathodic pulsing, another variable to be investigated was pulse width. The potential was stepped to 0 mV, -100 mV, and -200 mV for 2, 1, 0.5, and 0.2 seconds to deposit Cu and Se. The resulting deposit was then oxidatively stripped in sulfuric acid and quantified, results for these studies are found in Figures 8.4 and 8.5.

The goal of the pulsing studies was to determine the conditions required to deposit less than a ML per pulse. Figure 8.4 shows the copper coverage under the different pulsing conditions. According to Figure 8.4 the amount of copper put down is always a surface limited amount. This is consistent with Figure 8.2, copper at this low of a concentration suffers from mass transfer limitations. According to Figure 8.3 the potential or time used in the pulse does not change the coverage of Cu. Figure 8.5 shows the results for the Se pulsing studies. There are several conditions for Se that will deposit the desired amount, however, the coverage also seems to increase linearly with potential which may indicate that Se is also diffusion limited.

Using the information gathered it was time to design a cycle to test the pulsing chemistry. Based on the pulsing studies a cathodic pulse to -100mV for 0.5 seconds then should produce the desired coverage and an anodic pulse to 100mV for two seconds should strip any bulk copper formed. This process was repeated five times then the pump was turned on for 5 seconds at 2mL/min to refresh the diffuse layer. This pulsing scheme was repeated for 1100 cycles when the deposit began to show color. EPMA shows that $Cu_2Se$ was formed with an average Cu/Se ratio of 2.2 indicating a slight excess of copper. The deposit formed was much too thin when considering that each pulse was supposed to deposit a 0.5mL of Se. Based on the pulsing studies and the cyclic voltammetry it was concluded that the solution concentration was too dilute

Increasing the concentration of the Cu and Se needed to be done if a faster growth rate was to be achieved. The pulse width limit of a 6009 DAQ and Sequencer 4 is 30ms, with this information the diffusion layer thickness was calculated. The diffusion constant for $Cu^{2+}$ is $7.14\text{x}10^{-6}$, using Fick's first law of linear diffusion in one dimension, the diffusion length for a $Cu^{2+}$ ion in 30 ms is 6.5μm. The volume of solution associated with this process would be the diffusion length multiplied by the area of the electrode ($1.82\text{cm}^2$) which is estimated to be 1.2μL. The desired coverage for a cathodic pulse is 0.5ML, if a (111) surface contains 2.3 $\text{nmol/cm}^2$ then 0.5ML covering $1.82\text{cm}^2$ would require 4.2nmol. Thus the approximate concentration needed to deposit 0.5ML in a 30ms pulse would be $\frac{4.2\ nmol}{1.2\ \mu L}$ or 1.7mM. As a test to see whether or not 0.1mM was diffusion limited the same process was repeated with the 1.5 mM concentration bath and a much thicker deposit was obtained. This deposit had black rocks which is evidence of Se overgrowth. The presence of elemental Se was confirmed with XRD.

It was apparent that the pulsing cycle needed to be redesigned due to the overgrowth of Se present with the new concentrations. So the cycle was redesigned to have a cathodic pulse for

30 ms and an anodic pulse for 0.5sec. This process was repeated 5 times then the pump was turned on for 3 seconds at 2mL/min, this was the new pulsing cycle. New potentials were chosen as well to prevent overgrowth. Cathodic pulses of -100mV and -50mV were used in junction with anodic pulses of 100mV and 50mV with the idea being to put less down and take less off. Combinations of these cathodic and anodic pulses were run 6600 times to try to find the optimal conditions and these results were analyzed with EPMA, XRD, SE and the optical microscope.

After examining all of the combinations of the pulsing experiments it was found that the best deposits were grown using -50 mV as the cathodic pulse and +50 as the anodic pulse. This was determined by the optical microscope. This chemistry gave a homogeneous deposit with no apparent Se overgrowth. When the deposits were examined with EPMA it appeared that the deposits were infinitely thick, so no information can be obtained about the relative thickness between the samples, however, the EPMA did confirm that $Cu_2Se$ was synthesized with a slight excess of Cu in all cases. An attempt was made to see if the samples grew linearly with pulse number. Three samples were grown using the same conditions however varying the number of pulses, the results are shown in Figure 8.6. Unfortunately the limit of the machine was reach by the second sample, 3300 pulses looks like 6600 pulses so the 6600 pulse data point was thrown out. It is possible that the machine could saturate out before 3300 pulse, however no data has been taken to support this yet. Despite this, the data in Figure 8.6 does appear to support the claim that the samples grow linearly with number of pulses.

It is possible that the slight copper excess could be due to an excess $Cu^{2+}$ at the surface of the electrode. A typical current time trace is shown in Figure 8.7. Figure 8.7 shows that for each pulse the resulting net charge results in the deposition of 0.02mL of $Cu_2Se$ assuming a $6e^-$

process for the following reaction $2Cu^{2+} + HSeO2^{+} + 3H^{+} + 6e^{-} \rightarrow Cu_2Se + 2H_2O$. For each anodic pulse oxidation current is observed, based on the cyclic voltammetry discussed earlier the only species that could strip at this potential is Cu. This oxidized copper may not have time to completely diffuse away creating a higher concentration of $Cu^{2+}$ at the electrode's surface which may result in excess Cu deposition which is consistent with the presented EPMA results.

The crystallinity of the deposits were examined with XRD. The best conditions (no Se rocks) gave the XRD spectrum shown in Figure 8.8. The XRD spectrum shown in Figure 8.8 shows 5 peaks. Three of which can be attributed to the low index planes of Au, (111) occurring at 38°, Au (200) occurring at 44° and Au (220) occurring at 65° according to card number 04-0784. The remaining peaks at 26, and 51 are assigned to $Cu_2Se$ according to card 79-1841. There may be a possible Cu2Se (220) peak at 43° superimposed with the Au peak at 45 because that peak has a larger FWHM than the rest of the peaks. When a sample with visible Se rocks is analyzed with XRD a new peak arises at 25° which can be assigned to Se (100) according to card number 83-2437. In all cases the pulse deposition grows a crystalline material.

Finally the films were examined with SE. Like EPMA Se could not gleam any information off of the thick samples because to the samples exceeded the optical penetration depth so to the light the samples were opaque, as a result only the 1100 pulse samples were examined. The samples were measured at angles of 65°,70°,75° which measure above, at and below the Brewster angle for Au at 632.8nm so the maximum information can be obtain by the sample. The collected spectrum was then fitted to the Cauchy equation which would allow the calculation of the optical constants as well as the thickness. Figure 8.9 shows a SE spectrum. The spectrum in Figure 8.9 demonstrates a good fit as the MSE is below 50, thus all quantities calculated from the model should be accurate. The index of refraction calculated from this model is 1.9, which seems consistent with $Cu_2Se$ however this deposit has a slight excess of copper which would change the optical constant slightly. The thickness calculated from the model suggests that the sample is ~75nm thick which would indicate a growth rate of 0.2 ML per pulse assuming the distance between $Cu_2Se$ layers in the (111) direction is 0.35nm. This is the growth rate that we were aiming for.

The bandgap of the $Cu_2Se$ films was also estimated from SE. SE data contains a reflectance spectrum which can be converted to an absorbance spectrum. The absorbance spectrum can be manipulated to estimate the bandgap via a method developed by Mott and Davis[40]. The estimation of the bandgap of $Cu_2Se$ is shown in Figure 8.10. $Cu_2Se$ should have a direct bandgap which implies that the absorbance coefficient should be squared. When preforming this Figure 8.10 suggests that the bandgap for Cu2Se is 1.7 which is consistent with literature values[14,15].

## Conclusion

The proof of concept work in the formation of $Cu_2Se$ by electrochemical pulse deposition is presented. Results show that $Cu_{2.1}Se$ is the predominate species formed despite the sequence used. The slight Cu excess is most likely due to the excess of $Cu^{2+}$ ions created at the surface of the electrode during the anodic pulse which do not have time to completely diffuse away. XRD results indicate crystalline $Cu_2Se$ with a preferred (111) orientation. Excess selenium observed with the optical microscope is confirmed with XRD as well. SE results show an index of refraction of 1.9 as well as an average growth rate of 0.2mL per pulse and a direct bandgap of 1.7eV. The process appears to grow linearly with pulse number.

# References

(1) Bosio, A.; Romeo, N.; Mazzamuto, S.; Canevari, V. *Progress in Crystal Growth and Characterization of Materials* **2006**, *52*, 247.

(2) Birkmire, R. W.; Eser, E. *Annual Review of Materials Science* **1997**, *27*, 625.

(3) Omura, K.; Hanahusa, A.; Arita, T.; Higuchi, H.; Aramoto, T.; Nishio, T.; Sibutani, S.; Kumazawa, S.; Murozono, M.; Yabuuchi, Y.; Takakura, H. *Renewable Energy* **1996**, *8*, 405.

(4) Kazmerski, L. L. *Journal of Electron Spectroscopy and Related Phenomena* **2006**, *150*, 105.

(5) Chu, T. L.; Chu, S. S. *Solid-State Electronics* **1995**, *38*, 533.

(6) Chopra, K. L.; Paulson, P. D.; Dutta, V. *Progress in Photovoltaics* **2004**, *12*, 69.

(7) Henry, C. H. *J. Appl. Phys.* **1980**, *51*, 4494.

(8) Shockley, W.; Queisser, H. J. *J. Appl. Phys.* **1961**, *32*, 510.

(9) Chen, S. Y.; Walsh, A.; Gong, X. G.; Wei, S. H. *Advanced Materials* **2013**, *25*, 1522.

(10) Bar, M.; Schubert, B. A.; Marsen, B.; Wilks, R. G.; Blum, M.; Krause, S.; Pookpanratana, S.; Zhang, Y.; Unold, T.; Yang, W.; Weinhardt, L.; Heske, C.; Schock, H. W. *Journal of Materials Research* **2012**, *27*, 1097.

(11) Suryawanshi, M. P.; Agawane, G. L.; Bhosale, S. M.; Shin, S. W.; Patil, P. S.; Kim, J. H.; Moholkar, A. V. *Materials Technology* **2013**, *28*, 98.

(12) Zhao, Y. X.; Burda, C. *Energy & Environmental Science* **2012**, *5*, 5564.

(13) Wang, H. X. *International Journal of Photoenergy* **2011**.

(14) Vaidyanathan, R.; Mathe, M. K.; Sprinkle, P.; Cox, S. M.; Happek, U.; Stickney, J. L. *Mater. Res. Soc. Symp. Proc.* **2003**, *744*, 289.

(15) Deng, Z.; Mansuripur, M.; Muscat, A. J. *Journal of Materials Chemistry* **2009**, *19*, 6201.

(16) Banga, D.; Jarayaju, N.; Sheridan, L.; Kim, Y. G.; Perdue, B.; Zhang, X.; Zhang, Q. H.; Stickney, J. *Langmuir* **2012**, *28*, 3024.

(17) Fedorova, E. A.; Maskaeva, L. N.; Tulenin, S. S.; Markov, V. F.; Kuznetsov, M. V.; Chufarov, A. Y. *Kondens. Sredy Mezhfaznye Granitsy* **2012**, *14*, 489.

(18) Jafarov, M. A.; Nasirov, E. F. *Proc. SPIE* **2012**, *8470*, 84700I/1.

(19) Ballikaya, S.; Chi, H.; Salvador, J. R.; Uher, C. *J. Mater. Chem. A* **2013**, *1*, 12478.

(20) Chen, S.-w.; Wu, H.-j.; Hsu, C.-w.; Chang, C.-I.; Chang, C.-f. *J. Taiwan Inst. Chem. Eng.* **2013**, *44*, 402.

(21) Hu, H.; Ge, X.; Deng, C.; Sun, M.; Xuan, H.; Zhang, K. *Asian J. Chem.* **2013**, *25*, 5516.

(22) Liu, S.; Zhang, Z.; Bao, J.; Lan, Y.; Tu, W.; Han, M.; Dai, Z. *J. Phys. Chem. C* **2013**, *117*, 15164.

(23) Tang, X.; Fu, F.; Zhang, H.; Ren, G.; Wuhan University of Technology, Peop. Rep. China . 2013, p 9pp.

(24) Yue, J.-L.; Sun, Q.; Fu, Z.-W. *Chem. Commun. (Cambridge, U. K.)* **2013**, *49*, 5868.

(25) Lincot, D. *Thin Solid Films* **2005**, *487*, 40.

(26) Pauporte, T.; Lincot, D. *Electrochimica Acta* **2000**, *45*, 3345.

(27) Kroger, F. A. *Journal of the Electrochemical Society* **1978**, *125*, 2028.

(28) Gregory, B. W.; Stickney, J. L. *Journal of Electroanalytical Chemistry* **1991**, *300*, 543.

(29) Gregory, B. W.; Suggs, D. W.; Stickney, J. L. *Journal of the Electrochemical Society* **1991**, *138*, 1279.

(30) Colletti, L. P.; Flowers, B. H.; Stickney, J. L. *Journal of the Electrochemical Society* **1998**, *145*, 1442.

(31) Colletti, L. P.; Stickney, J. L. *Journal of the Electrochemical Society* **1998**, *145*, 3594.

(32) Flowers, B. H.; Wade, T. L.; Garvey, J. W.; Lay, M.; Happek, U.; Stickney, J. L. *Journal of Electroanalytical Chemistry* **2002**, *524-525*, 273.

(33) Huang, B. M.; Colletti, L. P.; Gregory, B. W.; Anderson, J. L.; Stickney, J. L. *Journal of the Electrochemical Society* **1995**, *142*, 3007.

(34) Lay, M. D.; Stickney, J. L. *Journal of the Electrochemical Society* **2004**, *151*, C431.

(35) Venkatasamy, V.; Jayaraju, N.; Cox, S. M.; Thambidurai, C.; Happek, U.; Stickney, J. L. *J. Appl. Electrochem.* **2006**, *36*, 1223.

(36) Chandrasekar, M. S.; Pushpavanam, M. *Electrochimica Acta* **2008**, *53*, 3313.

(37) Xiao, F.; Hangarter, C.; Yoo, B.; Rheem, Y.; Lee, K. H.; Myung, N. V. *Electrochimica Acta* **2008**, *53*, 8103.

(38) Banga, D.; Lensch-Falk, J. L.; Medlin, D. L.; Stavila, V.; Yang, N. Y. C.; Robinson, D. B.; Sharma, P. A. *Crystal Growth & Design* **2012**, *12*, 1347.

(39) Lensch-Falk, J. L.; Banga, D.; Hopkins, P. E.; Robinson, D. B.; Stavila, V.; Sharma, P. A.; Medlin, D. L. *Thin Solid Films* **2012**, *520*, 6109.

(40) Davis, E. A.; Mott, N. F. *Philosophical Magazine* **1970**, *22*, 903.

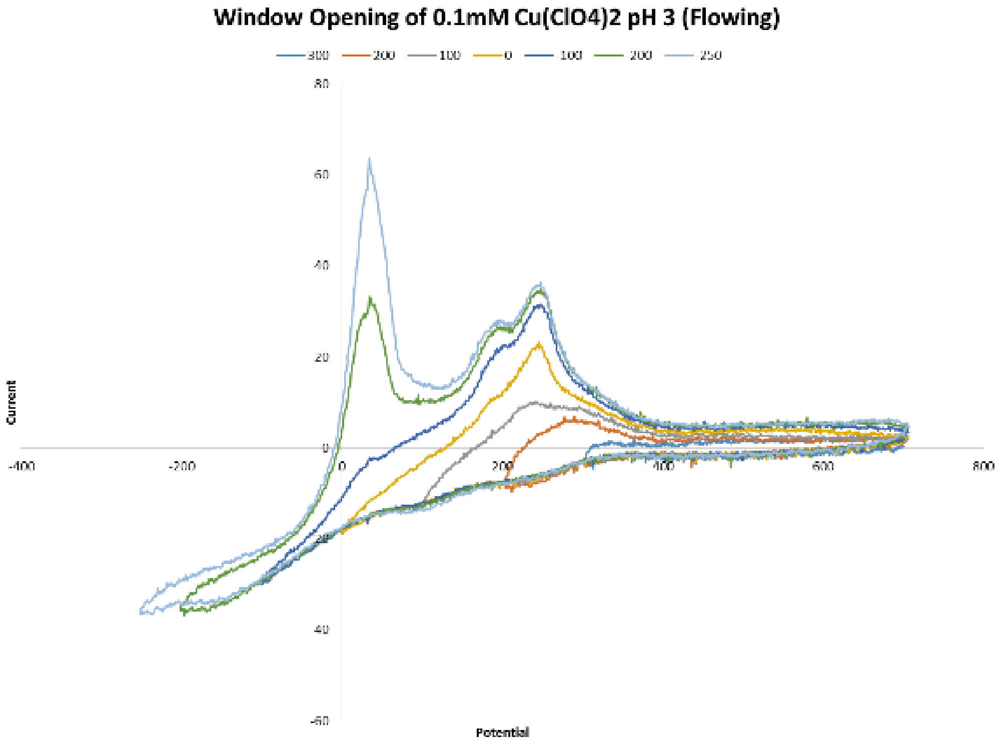

**Figure 8.1:** Cyclic voltammogram of 0.1mM Cu($ClO_4$)$_2$ pH 3 potentials vs Ag/AgCl scan rate 10 mV/sec flow rate 0.5mL/min electrode area 1.82 cm$^2$

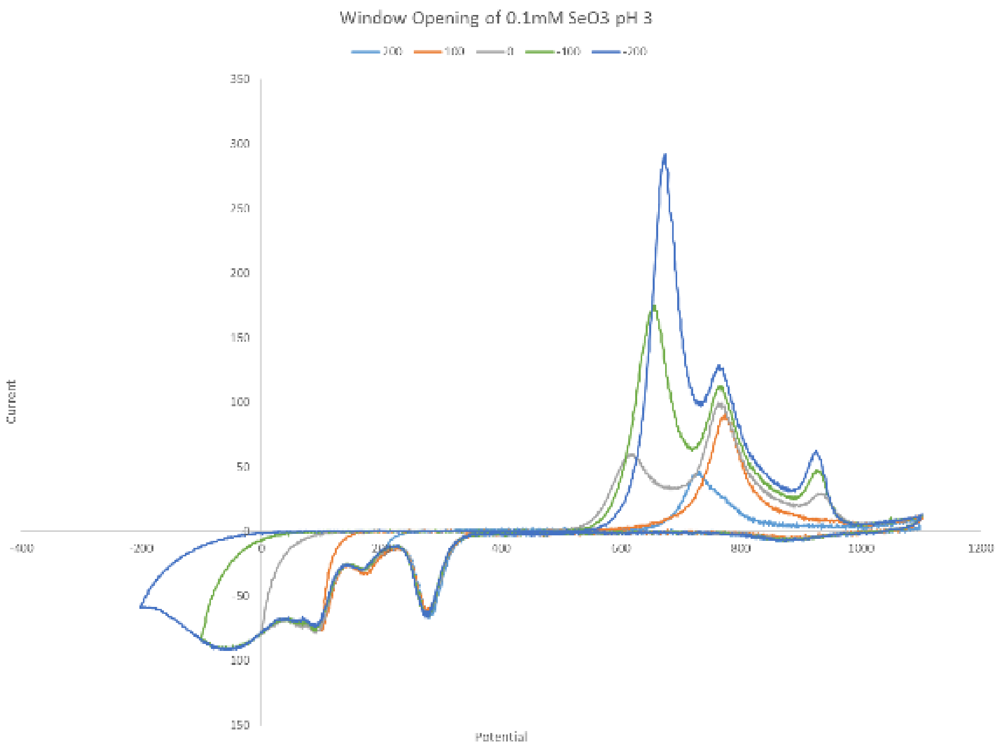

**Figure 8.2:** Cyclic voltammogram of 0.1mM SeO₂ pH 3 potentials vs Ag/AgCl scan rate 10 mV/sec flow rate 0.5mL/min electrode area 1.82 cm$^2$

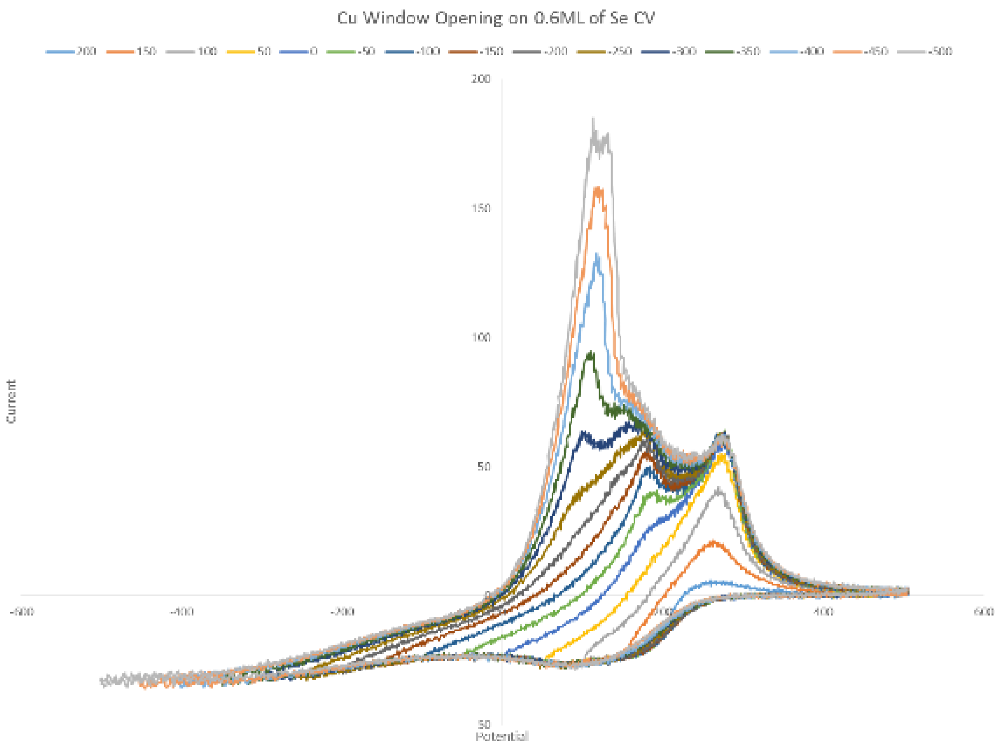

**Figure 8.3:** Cyclic voltammogram of 0.1mM $Cu(ClO_4)_2$ pH 3 on a Se monolayer. Potentials vs Ag/AgCl scan rate 10 mV/sec flow rate 0.5mL/min electrode area 1.82 $cm^2$

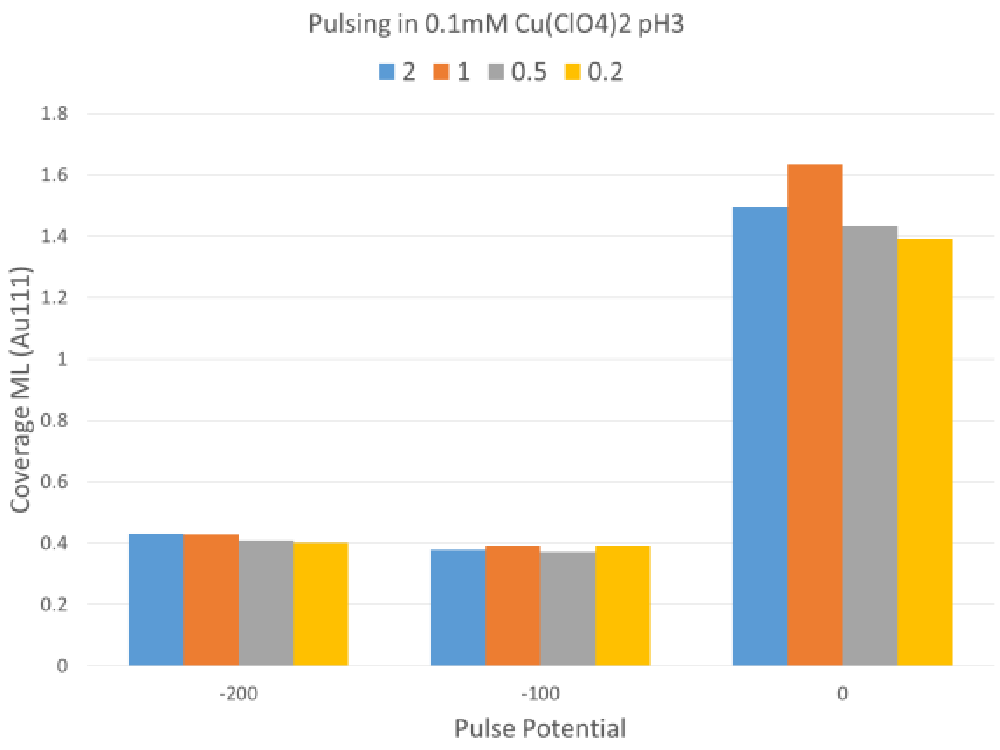

**Figure 8.4:** Cu pulsing studies

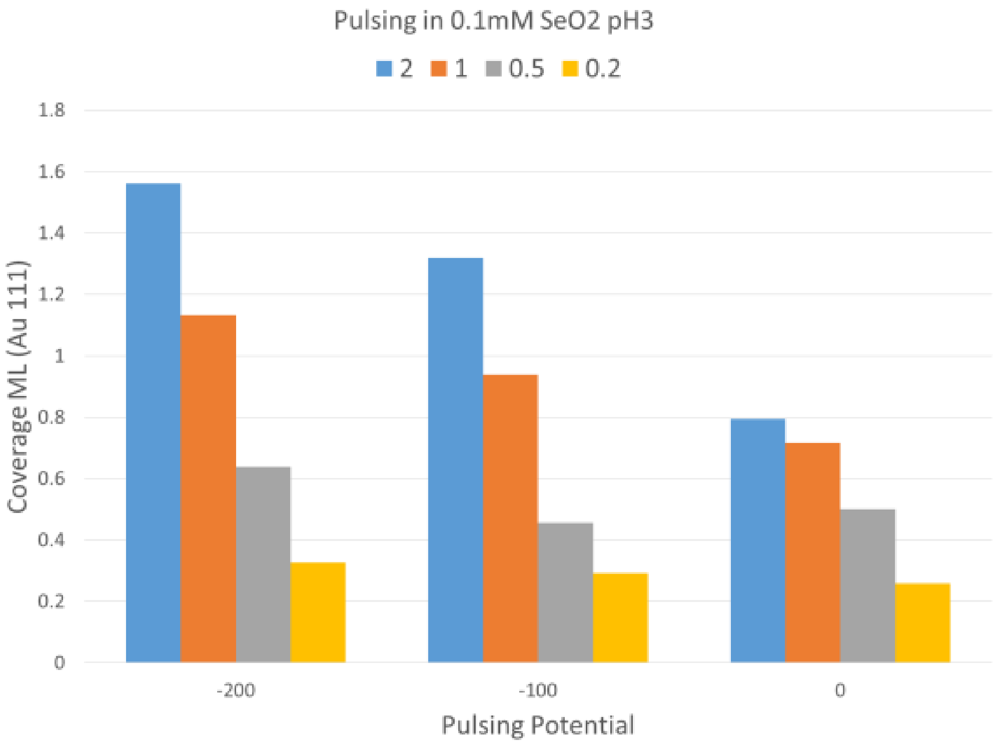

**Figure 8.5:** Se Pulsing Studies

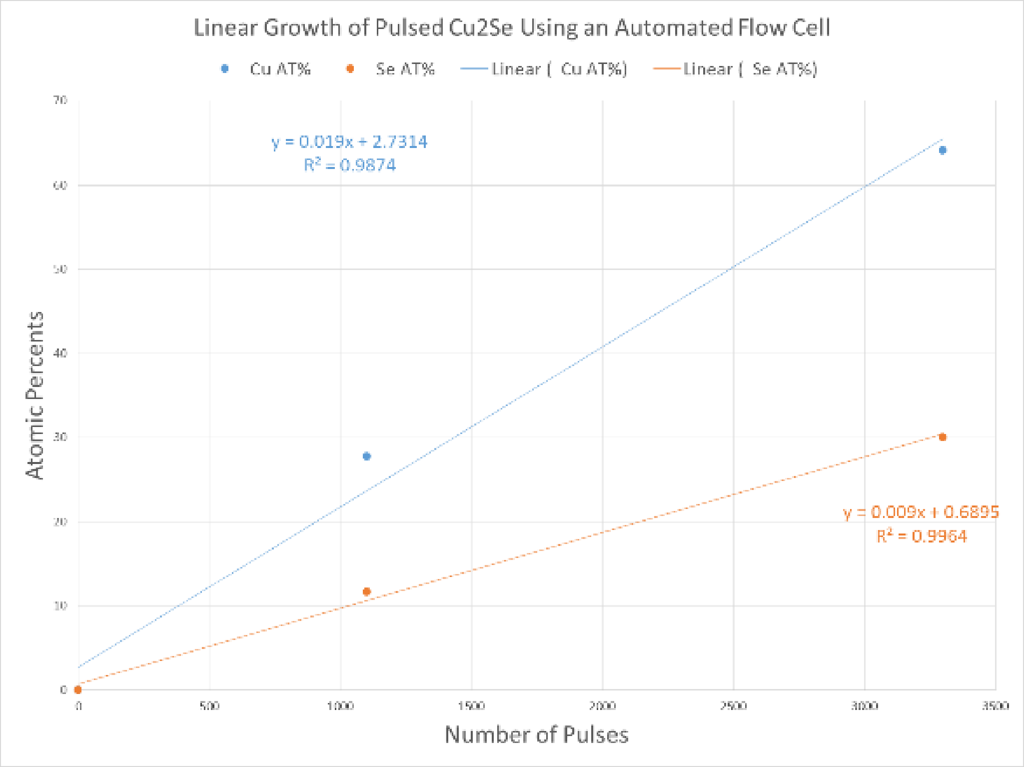

**Figure 8.6**: EPMA of $Cu_2Se$ as a function of the number of pulses

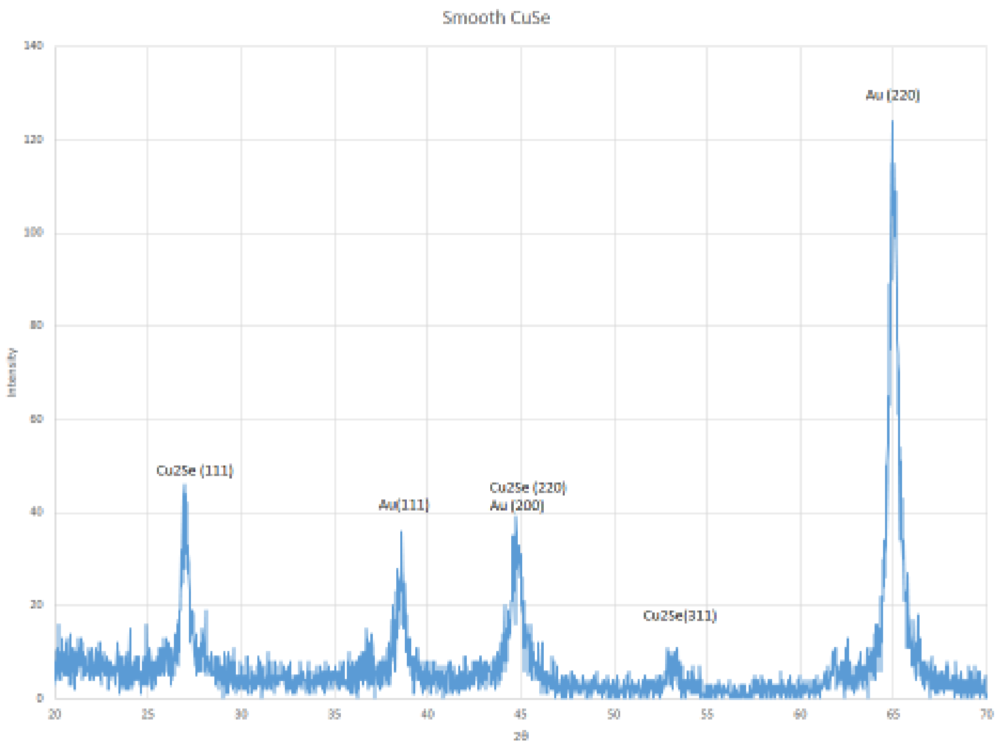

**Figure 8.7:** XRD of $Cu_2Se$ deposit on Au incident angle 0.5°.

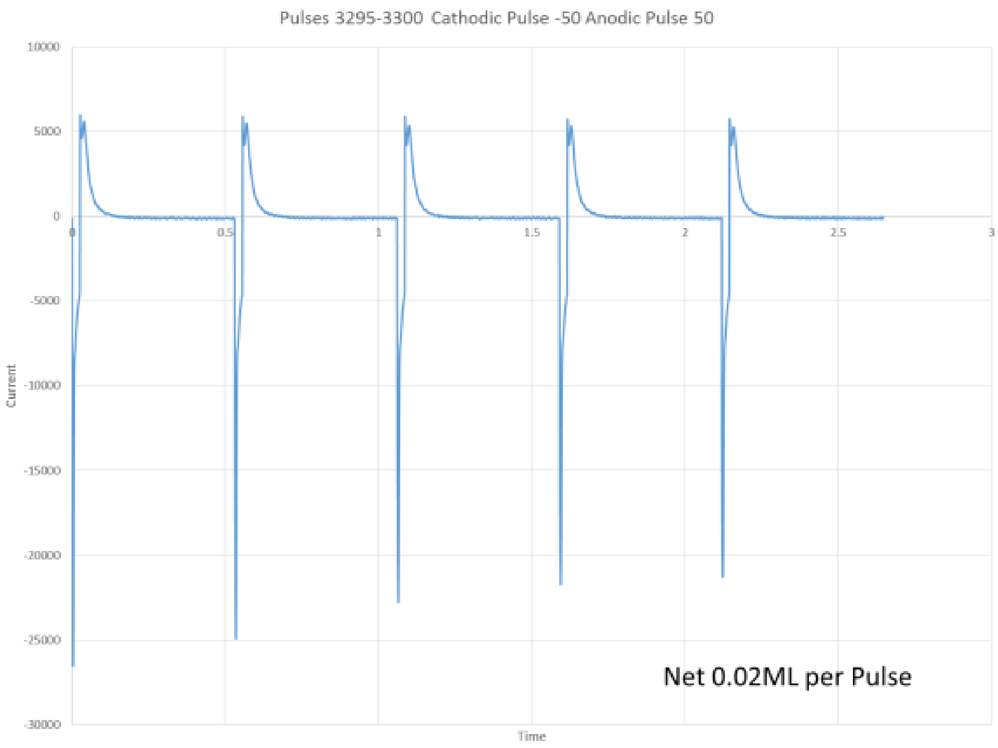

**Figure 8.8:** Current time trace of a $Cu_2Se$ pulsing sequence.

MSE = 45.665
Thickness # 1 = 74.78 ± 0.396 nm
n of Cauchy @ 632.8 nm = 1.90751

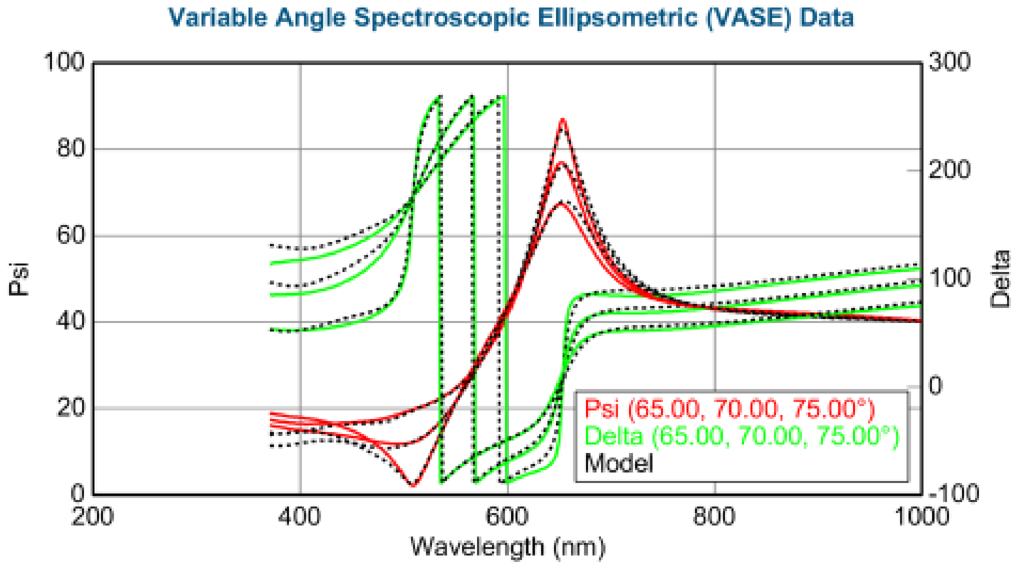

**Figure 8.9** SE data of $Cu_2Se$ deposit

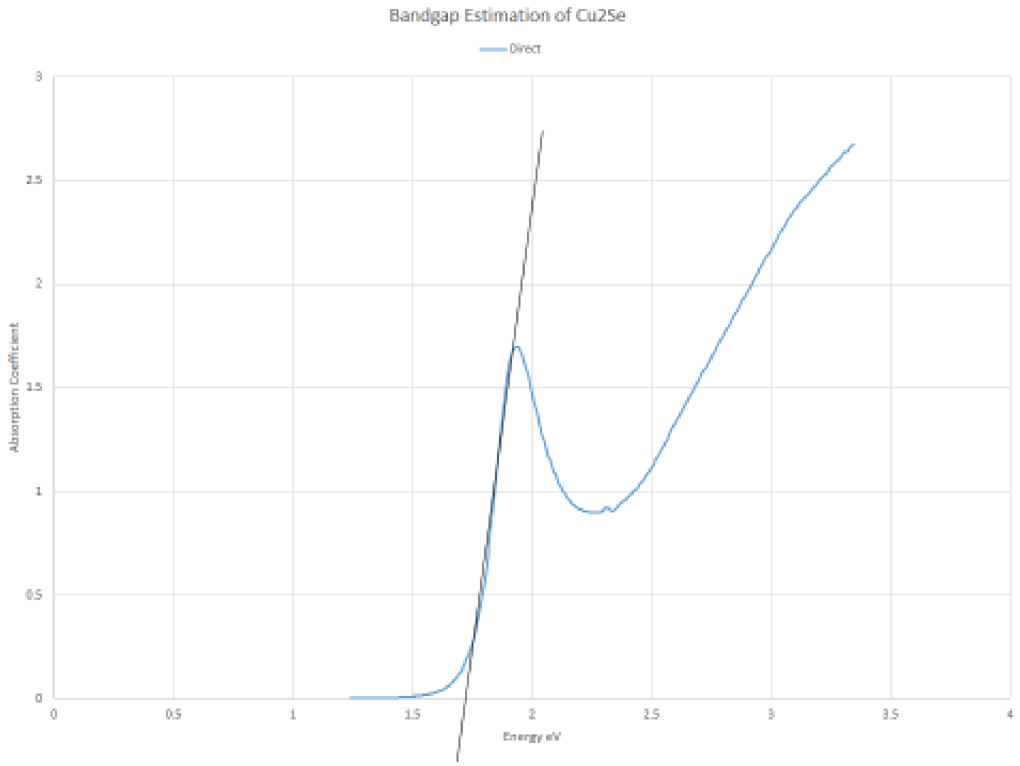

**Figure 8.10:** Bandgap estimation of $Cu_2Se$ assuming a direct bandgap

# CHAPTER 9

# CONCLUSIONS AND FUTURE WORK

The focus of this dissertation was the growth of photovoltaic materials by E-ALD. Chapter 2 examined the E-ALD growth of CdTe with different deposition chemistries. And subsequent analysis with various thin film techniques. Electron probe microanalysis (EPMA) results indicate that E-ALD CdTe is stoichiometric within the uncertainty of the instrument for all deposition chemistries. X-ray diffraction (XRD) results show that E-ALD grown CdTe has a strong preferred (111) orientation and deposits epitaxially onto a single crystal Au substrate. Spectroscopic ellipsometry (SE) results show that E-ALD CdTe has an index of refraction of 2.98 and the growth rate can be adjusted by adjusting the Te deposition potential. Both EPMA and Se show that the growth of E-ALD CdTe is linear with number of cycles run consistent with Frank-van der Merwe layer-by-layer growth. PEC results indicate that E-ALD grown CdTe is p-type, has an external quantum efficiency of 10% and has a direct bandgap of 1.5eV. In summation E-ALD is capable of growing a high quality CdTe deposit without the need of a post deposition anneal step

In Chapter 3 CdS deposits were fabricated and analyzed with different thin film characterization techniques. EPMA shows that the Cd/S ratio was 1.07, 1.10, and 1.05 for CBD, SILAR and ALD respectively. SILAR and E-ALD CdS grows crystalline while CBD does not. SE shows that E-ALD and SILAR grow at similar rates and produce deposits with the proper optical constants. Photoelectrochemical results show that the photoresponse for E-ALD grown CdS was the highest while CBD was the least photoactive and all deposits produce n-type CdS with a bandgap of 2.4 eV.  E-ALD and SILAR produce CdS deposits of almost identical quality this is probably because the growing mechanisms are very similar.

In Chapter 4 PV were fabricated in the substrate and superstrate configurations using E-ALD grown materials.  When devices were fabricated in the superstrate configuration, devices were delaminated from the glass most likely do to strain across the layers no matter the type of ITO or CdS used.  PV fabricated in the substrate achieve a maximum current density of 0.65 mA/cm$^2$ when exposed to light; however appear to suffer from shunts which lowered the open circuit voltage.  Work on these defects is underway.  Despite these shortcoming a PV was produced with a high current density with a 1/10 of the material used in current PV devices

Chapter 5 investigated the influence substrate chemistry plays on the deposition process. The substrates used in this study were Au, Ni, Cu, Ag, Ge, and Mo.  100 cycle deposits of E-ALD CdTe were grown onto each substrate and analyzed with EPMA, XRD and SE.  Results indicate that substrates that can oxidatively dissolve and produce ions (Ni Cu Ag) hinder the E-ALD deposition process and decrease the quality of the film grown.  It is proposed that competing compound formation reactions can occur when ions produced by the oxidative dissolution of the substrate are present with the E-ALD solution.  These reactions could potentially short circuit the E-ALD process in the early cycles.  Substrates that did not produce ions (Au Ge Mo) did not seem to affect the process and grew CdTe films of good quality, however, a surface pretreatment was required in some cases for successful electrodeposition.

In Chapter 6 the optimization of the E-ALD process on a Ni electrode was investigated. Three different growing chemistries were examined, acidic Te, acidic Te with stripping and basic Te, and examined to see what chemistries were compatible with a Ni electrode.  These deposits were examined with EPMA, SE and XRD.  EPMA results show variations in the stoichiometry with a Cd/Te ratio of 0.7, 0.8 0.9 for acidic, stripping and basic chemistries, this is most likely due to the influence of the Ni electrode, XRD shows all deposits produce crystalline CdTe with a strong preferred (111) orientation. SE results show differences in growth rates and quality for each deposition chemistry with the basic chemistry producing the best results. AFM and SEM results for E-ALD CdTe LPNE nanowires indicate that the nanowires produced are on average 200 nm in width which is inconsistent with an E-ALD process. The most probable cause for this discrepancy is diffusion of the electroactive species into and out of the trench. Insufficient rinsing may have caused a buildup of ions in the trench which promoted excess growth. It was demonstrated however that E-ALD CdTe can successfully be grown onto LPNE grown nanowires

Chapter 7 was a reevaluation of our previous work on germanium electrodeposition. New hypotheses were formulated using germanene as the model. These hypotheses were tested with STM and micro-Raman. STM results show the formation of large atomically flat terraces. When zooming in on one of the terraces an atomically resolved a Moiré pattern is produced. The Moiré pattern is consistent with the chair configuration of germanene. The bond distances calculated from the Moiré pattern are consistent with the bond distances predicted from the Ab initio calculations. Finally the samples were probed with micro-Raman which show a strong raman shift at 290 cm-1 which is consistent with the ab initio calculations. The new interpretation of the data implies the presence of electrodeposited germanene.

Chapter 8 presents the proof of concept work in the formation of $Cu_2Se$ by electrochemical pulse deposition. Results show that $Cu_{2.1}Se$ is the predominate species formed despite the sequence used. The slight Cu excess is most likely due to the excess of $Cu^{2+}$ ions created at the surface of the electrode during the anodic pulse which do not have time to completely diffuse away. XRD results indicate crystalline $Cu_2Se$ with a preferred (111) orientation. Excess selenium observed with the optical microscope is confirmed with XRD as well. SE results show an index of refraction of 1.9 as well as an average growth rate of 0.2mL per pulse and a direct bandgap of 1.7eV. The process appears to grow linearly with pulse number

Future work should progress down three major avenues. The first is an extension of Chapter 4. The E-ALD growth of CdS and CdTe have been optimized on a Au electrode. Au is an inert metal which implies it should not interfere with in electrodeposition, however, Au is not a suitable material for large scale PV production. The optimization of E-ALD chemistry should be extended to other metals. Mo is a popular back contact in CdS/CdTe PV because it is inexpensive, conducive and does not interdiffuse into the subsequent structures degrading their quality. Mo and other valve metals have a very thick surface oxide that needs to be removed in order to electrodeposit onto it. Investigating such treatments is an essential step for this chemistry. Another reason the optimization of E-ALD onto different materials could be important is the role E-ALD could play in the low cost fabrication of multijunction PV cells. Each junction would have a unique interface which would need special chemistry to grow the proper material. The optimization of E-ALD chemistries onto different materials is an important area of future work.

The next avenue to be developed is the formation of an E-ALD PV. There are many different combinations and permutations to be performed in this project, the different CdS deposition techniques paired with E-ALD CdTe, where and when to anneal, $CdCl_2$ treatments, substrate/superstrate configuration etc. The superstrate configuration should be reexamined. The ITO used in these may not have been of high enough quality which facilitated the delamination of the films. Thin Film Technologies (TFT) produces PV grade transparent conducting oxide substrates. Superstrate configuration PV should be investigated further using TFT ITO and FTO two of the major transparent conducting oxides used in CdS/CdTe based PV. Process control is an important topic that affects both methods of fabrication. The layers used in these studies are so thin that shunts can be easily formed. Practicing proper fabrication methods and using the NanoSEC cleanroom facility may assist in the proper fabrication of a PV

The final avenue to be discussed is the genesis of what is being called 3rd generation PV. The work presented in this dissertation is commonly referred to as 2nd generation or thin film PV. Thin film PV utilize ~2-3 μm of material for an absorber layer. It would take an E-ALD process 48 hours of continuous growth to achieve this thickness, needless to say that is too slow. In 3rd generation PV, however, the average absorber layer thickness is around 200 nm this is more reasonable for and E-ALD process. In 3rd generation PV the use of nanostructures is employed to increase efficiency of the PV while reducing the amount of material used. To do this a deposition method that can produce high quality deposits while conformally coating the nanostructure must be used. E-ALD is ideally suited for this purpose. The contribution E-ALD can make in the 3rd generation PV area is great. For this reason it is a very strong area for future work.